THESIS FOR THE DEGREE OF DOCTOR OF PHILOSOPHY (PHD)

Data integration from multi-omics approaches reveal inflammation dynamics upon muscle tissue injury and regeneration

by Nikolaos Giannakis, MSc

Supervisor: Professor Dr. Laszlo Nagy

UNIVERSITY OF DEBRECEN
DOCTORAL SCHOOL OF MOLECULAR, CELLULAR AND IMMUNE BIOLOGY

DEBRECEN, 2020

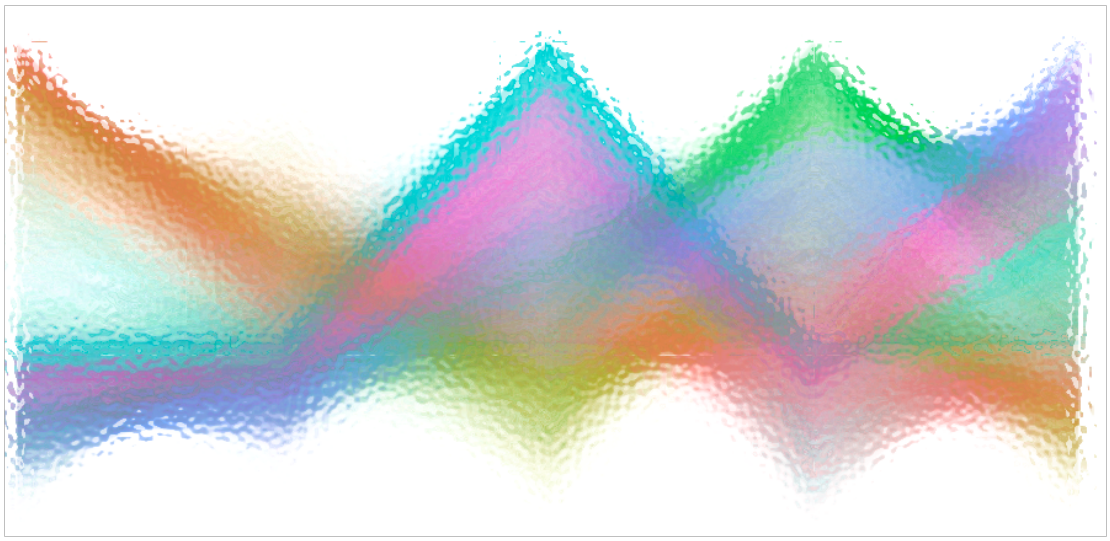

AESTHETICS OF INFLAMMATION DYNAMICS UPON MUSCLE TISSUE INJURY AND DURING REGENERATION BASED ON TRANSCRIPTOMIC DATA.

Contents

1. Abbreviations

API	Application program interface
AA	Arachidonic acid
ATAC-seq	Assay for transposase accessible chromatin with high-throughput sequencing
BMDM	Bone marrow-derived macrophage
BMT	Bone marrow transplantation
CER	Ceramide
COX	Cyclo-oxygenase
CPU	Central processing unit
CSA	Cross-sectional area
CTX	Cardiotoxin
DHA	Docosahexaenoic acid
ECI	Eccentric-contraction injury
EPA	Eicosapentaenoic acid
FACS	Fluorescence-activated cell sorting
F4/80	EGF-like module-containing mucin-like hormone receptor 1(EMR1)
GAST	Gastrocnemius
GPR18	G protein-coupled Receptor 18
GO	Gene ontology
MRM	Multiple reaction monitoring
LC-MS/MS	Liquid chromatography tandem mass spectrometry
LPC	Lysophosphatidylcholine
LY6C	lymphocyte antigen 6 complex, locus C
PC	Phosphatidylcholine
PCA	Principal component analysis
PE	Phosphatidylethanolamine
PI	Phosphatidylinositol
PUFA	Polyunsaturated fatty acid
RvD2	Resolvin D2

SM	Sphingomyelin
SPM	Specialised pro-resolving mediator
TA	Tibialis anterior
TAG	Triacylglycerol
2-DG	2-deoxy-D-glucose

2. Introduction

i) Overview of inflammation

Inflammation is the way the immune system responds to harmful stimuli, which includes toxic compounds, pathogens, damaged cells or irradiation (Medzhitov, 2008), and through its action the injurious stimuli is removed, while the healing process is initiated (Ferrero-Miliani et al., 2007). Consequently, it can be stated that inflammation can act as a defense mechanism, which is fundamental to health (Nathan, 2010). Usually, inflammatory responses involve an orchestrated sequence of molecular and cellular reactions that effectively reduce threating infections or injuries (Chen et al., 2018). This procedure efficiently contributes to recovery, but when unsuppressed can lead to chronic pathological conditions (Zhou et al., 2016). Main characteristics of inflammation at tissue level include tissue malfunction, redness, pain, heat and swelling, which arise due to immune and vascular responses locally (Takeuchi, 2010). At the site of inflammation, increases in vascular permeability, recruitment of immune cells and release of mediators that act as inflammatory signals, are the main microcirculatory procedures that occur (Chertov et al., 2000). Etiologies of inflammation include both infectious and non-infectious agents. Non-infectious agents include physical factors that cause inflammation (burn, foreign bodies, frostbite, physical injury, ionizing radiation), chemical factors (toxins, alcohol, chemical irritants, nickel and other trace elements) and biological factors such as damaged cells. Various bacteria, viruses and other microorganisms can be considered infectious factors. Briefly, an inflammatory response starts with a chemical signaling cascade that is followed by recruitment of leukocytes, that upon activation are the main producers of cytokines, causing an active inflammatory event (Jabbour et al., 2009). As stated previously, an inflammatory response is a process that involves a tightly regulated sequence of events that is mediated by signaling molecules. The first step in this process is the recognition of the trauma or infectious agent, which is achieved through the exposure and detection of pathogen-associated molecular patterns (PAMPs), which can initialize the cascade of molecular events by

activating receptors of the germline (Pattern Recognition receptors) both in cell subsets of the immune and non-immune cell repertoire (graphical scheme 1a) (Brusselle & Bracke, 2014; Gudkov & Komarova, 2016). Some of these receptors are capable of identifying endogenous alarming signals after tissue injury and damage, the so called danger-associated molecular patterns (DAMPs). Part of the Pattern recognition receptor (PPR) family of receptors are the C-type lectin receptors (CLRs), the NOD-like receptors (NODs), the retinoic acid-inducible gene-like receptors (RLRs) and the Toll-like receptors (TLRs) (Takeuchi, 2010). Myeloid differentiation factor-88 (MyD88) together with TLRs act as an intermediate for the delivery of PAMPs and DAMPs (graphical scheme 1b). Activation of TLRs promotes the stimulation of inflammatory pathways such as the MAPK pathway, the NF-kB pathway, the JAK-STAT pathway and the translocation to the nucleus of transcription factors such as the interferon regulatory factor 3 (IRF3) or the activator protein-1 (AP-1) (Adib-Conquy & Cavaillon, 2007; Rubartelli & Lotze, 2007).

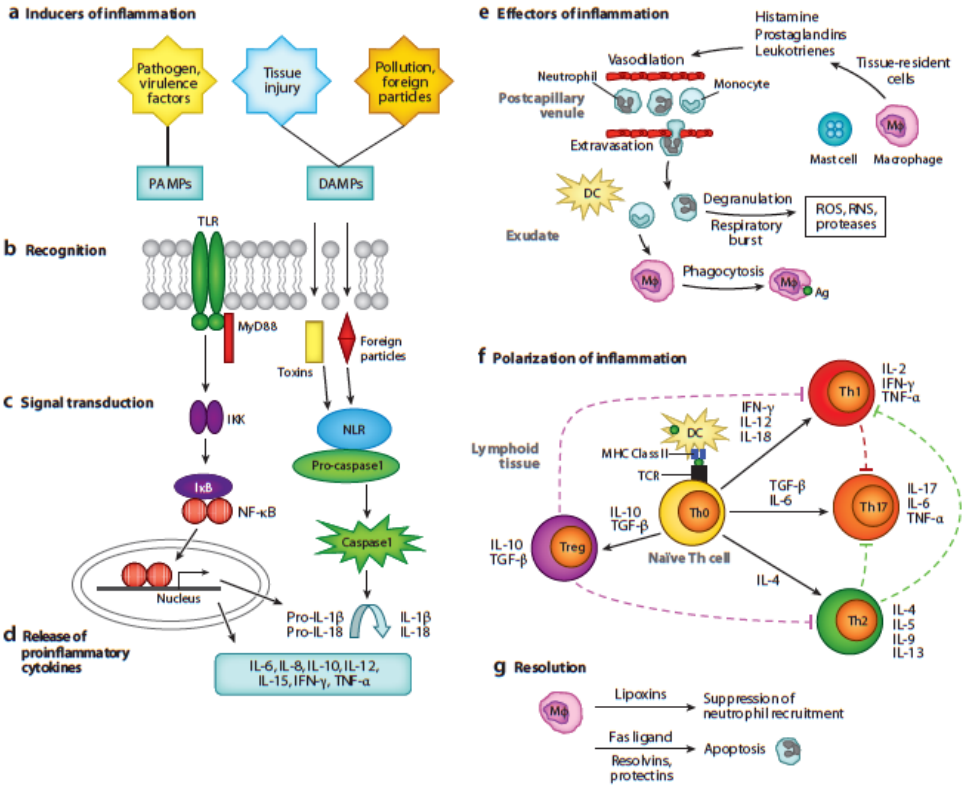

Graphical scheme 1: Events of the inflammatory cascade. (a) Inducers of inflammation. **(b)** Recognition of PAMPs and DAMPs from TLRs. **(c)** Signal transduction through MyD88. **(d)** Collection of

important pro-inflammatory chemokines and cytokines. **(e)** Effector cells of inflammation and their influx at the site of the inflammatory event as response to signal transducing mediators. **(f)** Polarization of inflammation through cells of the lymphoid cell repertoire. **(g)** Role of macrophages (MFs) in the resolution of inflammation. (Ashley, 2012)

Upon ligand identification, Toll-like receptors induce the activation of NF-kB pathway (nuclear factor kappa-light-chain-enhancer of activated B cells), releasing it from the IkB protein that binds it in inactivate conditions, allowing the translocation of the transcription factor to the nucleus, where it binds to target genes and upregulates their expression (graphical scheme 1c). NF-kB pathway is closely related to the regulation of expression of pro-inflammatory cytokines such as tumor necrosis factor-alpha (TNF-a), interleukin-1-beta (IL1-b), interferon gamma (IFN-g), interleukin 6 (IL6) and others (graphical scheme 1d), and also to the contraction of immune cells at the site of inflammation (Basak et al., 2007; Pasparakis et al., 2006). Another pathway that gets activated is the MAPK pathway, which involves the action of threonine/serine kinases in response to mitogens, cytokine storm, and stress via osmosis (Chertov et al., 2000). MAPK proteins affect the regulation of cell apoptosis, differentiation and proliferation (Kaminska, 2005; Pearson et al., 2001). Stimulation, induction and activation of MAPKs, Erk1/2 kinases and JNK kinases drive the downstream activation of p38 transcription factor through phosphorylation, launching the inflammatory response (Raingeaud et al., 1996). Another signaling pathway that orchestrates the regulation of inflammatory genes is the JAK-STAT pathway. It engages a diversified group of molecules (interferons, cytokines and growth factors) in signaling processes that involve transcription factors , which govern gene expression. More specifically, when JAKs get induced by ligand molecules , phosphorylate one another , driving the creation of STAT protein docking sites. There, STATs are dimerized (O'Shea et al., 2015) and translocate to the nucleus, where they downstream upregulate the expression and the secretion of inflammatory cytokines and receptors ((Ivashkiv & Hu, 2003; Walker & Smith, 2005).

Pro-inflammatory cytokines cooperatively with chemokines act as attractants, and promote the enrollment at the affected site of monocytes and neutrophils (graphical scheme 1e). The latter, through degranulation, release chemicals from their granules and proteinases, for elimination of pathogens. Additionally, macrophages contribute complementary to neutrophils at the site of the affected tissue (Nathan, 2002).

Of high importance is the tight regulation of innate immune responses by the adaptive immune system, which if optimized well can be crucial for mitigating fitness cost of infection (Ashley et al., 2012). Lymphocytes are key components of the adaptive immune system, affecting the polarization of inflammation (graphical scheme 1f). T-helper 0 (Th0) lymphocytes (with no prior exposure to an antigen) upon stimulation can differentiate to regulatory or effector adaptive immune system‘s cell types. Differentiated effector T-helper cell populations include Th1 lymphocytes (considered pro-inflammatory), Th2 lymphocytes (considered anti-inflammatory), Th17 lymphocytes, while Tregs are lymphocytes with regulatory capacities (Abbas et al., 1996; Anthony et al., 2007). Th1 cells facilitate immune responses against parasites , mainly by secreting IFNg (interferon-gamma), which is a cytokine having antiviral and immunoregulatory capacities, boosting further the differentiation of undifferentiated Th cells to a Th1 phenotype. Contrary to Th1 cells, Th2 lymphocytes are vital for handling helminth infections, in B-cell proliferation, to regulate immune responses to allergens and in antibody-mediated (humoral) immunity. They produce interleukins with anti-inflammatory role such as IL-4, IL-5, and IL-10, which promote further differentiation to Th2 cells, stimulate the alternative polarization of macrophages to a reparative phenotype and help in the decline of the production of pro-inflammatory cytokines. It becomes obvious the importance of the optimization of the ratio of Th1 to Th2 mediated responses, which are mutually antagonistic, although they can act simultaneously, to promote pathogen clearance with lowest destruction of the host’s tissue (Graham, 2002; Mosmann & Coffman, 1989) Th17 helper lymphocyte cells are involved in the clearance of extracellular microparasites, whose elimination is not

handled by the aforementioned Th cell groups (Korn et al., 2009). Regulatory T cells by releasing IL-10 and TGFb diminish Th1 and Th2 immune responses through the immunosuppressive action of these two cytokines , and tissue's destruction can be downplayed. Inferentially, Tregs are crucial for the abolishment of effector actions of T cells, NK cells and B cells (Sakaguchi et al., 2010). The final stage of inflammation involves its resolution (graphical scheme 1g), which will be discussed in higher extent at the muscle tissue injury and regeneration section.

To separate between distinct classes of inflammation, it is vital to consider its proportionate fitness cost to the host , as both itself and its *sequelae* differ temporally and spatially (Medzhitov et al., 2012). A significant aspect when handling a tissue injury or a pathogen, that highly affects an immune response, is the location of it. Inflammation starts in a localized area, and upon severe wound or infection can be become systemic (spread to the periphery). The switch of an immune response from a localized area to the periphery is pricey for the host both to produce it and to sustain it. Elevated inflammatory levels in the absence of infection can become detrimental leading to unsuitable pathologies that include autoimmune and other inflammatory diseases, while in the presence of pathogens clearly favors the host (Sorci & Faivre, 2009). Another crucial aspect is the time course of inflammation. While acute inflammatory responses come early upon injurious stimuli and rapidly resolve after its elimination, chronic and persistent inflammatory conditions promote the appearance of cell types, which associate with a variety of pathophysiological diseases (Hotamisligil, 2006; Medzhitov, 2008). Importantly, the magnitude of inflammation is crucial when calculating fitness costs. A costless response can be incomplete and underactive, while redundant inflammation has detrimental effects, driving severe pathologies. Taking into consideration all these aspects (location, magnitude and timing), ranking of costs is created, based on which the host decides for best strategy to eliminate an infection or to repair the tissue after injury (Raberg et al., 2007).

ii) Muscle tissue injury and regeneration

a) Tissue injury and immune response

Muscle tissue constitutes a large fraction of the total body mass, and due to its superficial location, it is easily damaged or traumatized. Tissue's damage can be caused by a plethora of factors that include toxin deposition, freezing, exercise, burns or acute trauma (Tidbal, 2017). It was only recently that scientists from different backgrounds provided information on the high level of coordination between biological processes that mechanistically relate muscle tissue's injury and regeneration. Several cell types that include myogenic precursor cells (MPs), immune cells, fibroblasts, mesenchymal cells and neural tissue's cells work together to retrieve previous muscle architecture and function after injury or harmful stimuli.

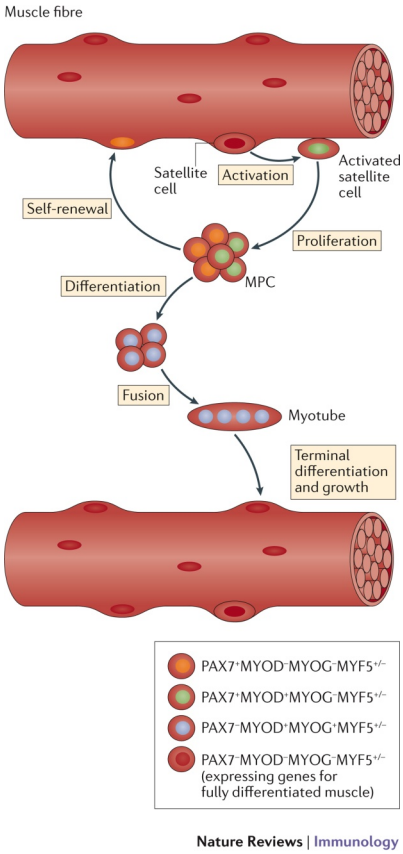

Graphical scheme 2: Satellite cells activation, proliferation and differentiation during muscle's regeneration (Tidball, 2017)

Indispensable for tissue's restoration are the myogenic precursor cells, known also as satellite cells, which are located on the surface of adult muscle fibers. Upon injury, quiescent satellite cells ($PAX7^+MYOD^-MYOG^-$) get rapidly activated and start to proliferate. The daughter cells stemming from the division of satellite cells can either continue to differentiate ($PAX7^+MYOD^+MYOG^-$) or return to the previous state to replenish the satellite cell reservoir ($PAX^+MYOD^-MYOG^-$). Later, activated satellite cells after post-mitotic cleavage ($PAX^-MYOD^+MYOG^+$) are able to fuse and create long, cylindrical multinucleated myotubes, which is followed by their growth. Consequently, terminally differentiated myotubes, fuse together to form initially nancent and later mature muscle fibers, as shown in the graphical scheme 2. It has been shown that satellite cell deletion causes impairment in

the regeneration of the tissue (Lepper et al., 2011; Murphy et al., 2011; Sambasivan et al., 2011) and NUMB protein's ablation (protein that regulates the asymmetrical cleavage between daughter cells after satellite cells' activation and proliferation) reduces the number of myogenic progenitors causing impaired regeneration. The latter, highlights the need of a reserve precursor cell population for notable muscle tissue's restoration (George et al., 2013).

It has been found that in a healthy adult murine limb muscle there are about 1000 leukocytes per mm^3 (Martinez et al., 2010; Villalta et al., 2014). The leukocyte population consists of neutrophils, eosinophils, cytotoxic T cells, T regulatory cells, but the vast majority comprises from monocytes and macrophages that reside next to the blood's vessels or in the connective tissue (Brigette & al., 2010; Honda et al., 1990). After injury, the quiescent resident macrophages escape quiescence and get activated (Krippendorf & Riley, 1993). They release chemoattractants such as the CC-chemokine ligand 2 (CCL2) or the CXC-chemokine ligand 1 (CXCL1) that promote the neutrophil influx at the site of the damaged muscle (Brigette & al., 2010). Neutrophil invasion is a generic response to trauma. Their numbers peak 24 hours after damage, and get eliminated rapidly right after (Belcastro et al., 1996; Fielding et al., 1993; Lu et al., 2011; Montironi et al., 2008). After the neutrophil influx, circulating monocytes and macrophages enter to the site of injury, which is enhanced in pro-inflammatory compounds such as tumor necrosis factor (TNF) and interferon γ (IFNγ) (Cheng et al., 2008; Collins & Grounds, 2001; Wang et al., 2014; Warren et al., 2002). The pro-inflammatory cytokines activate macrophages to a pro-inflammatory M1-like phenotype, while M2-like macrophages are associated with inflammation's resolution, muscle tissue's repair, restoration and recovered functionality (Locati et al., 2013; Mills, 2015; Mills et al., 2000). The role of signaling through these inflammation-related cytokines is quite important for the initiation of events that will lead to the return of tissue to homeostasis. Specifically, the receptor of IFN binds to myogenic progenitors causing the activation of the Janus kinase JAK-STAT1 pathway causing an up-regulation at the levels of CIITA.

CIITA (MHC class II trans-activator) is activating the EZH2 protein of the Polycomb Group 2, that facilitates the phosphorylation at the PRE of the promoters of genes related to MPC differentiation and silences them (Tidbal, 2017). Additionally, TNF causes induction at the levels of NOTCH (transmembrane receptor), which down-regulates MYOD (myoblast determination protein 1), and MYOG (myogenin), causing an induction in proliferation of MPCs and impairing their differentiation. This supports tissue repair by expanding the MPC populations needed for facilitation of muscle's architecture restoration.

On the other hand, resolving cytokines such as the TGFb and the IL-10 up-regulate AMPK (AMP-activated protein kinase) that down regulates TNF, therefore, causing a switch from a pro-inflammatory to a pro-resolving phenotype. Interestingly, at the same timeframe (resolution phase), p38 mitogen-activated protein kinase gets activated and through the Polycomb 2 repressive pathway, represses the expression of PAX7, and therefore, enhances activated satellite cells differentiation by impairing their proliferation. At this phase of transition to the terminal differentiation, the population of phagocytic pro-inflammatory macrophages is highly replaced with macrophages caring a pro-resolving signature (graphical scheme 3). CD163 positive cells (related to the resolving MF phenotype) constitute the dominant cell population at the stage of terminal differentiation and growth. CD163 is a transmembranic glycoprotein, which is down regulated by TNF, while IL-10 induces its expression. It strongly binds to hemoglobin- haptoglobin complexes, facilitating their internalization and degradation (Kristiansen et al., 2001; Shaer & Gadegbeku, 2001). This is of high importance as elevated hemoglobin levels after hemolysis induce tissue

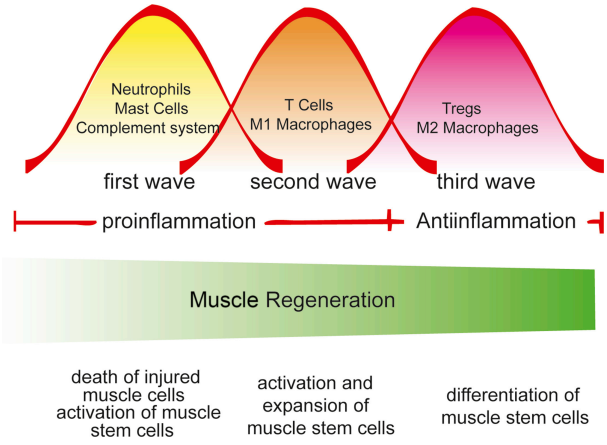

Graphical scheme 3: Immune cell levels are related to muscle regeneration (Yang, 2018)

damage (Moestrup & Moller, 2004).

Apart from immune cells of myeloid origin, lymphoid cells also play catalytic roles in regulating muscle regeneration. It has been found that $CD4^+$, $CD8^+$ lymphocytes' levels are induced in injured muscles (McLennan, 1996). Additionally, T_{reg} cell depletion, by affecting the normal transition from pro-inflammatory to anti-inflammatory/ pro-resolving macrophages, impairs repair and down regulates the expression of key myogenic components (Burzyn et al., 2013).

As presented above, leukocytes act on MPCs by directly influencing their gene expression, or they instruct the generation of a myogenic environment by permissive interactions on $PAX7^+$ cells.

Another important cell population that directly affects regeneration are the fibro-adipogenic progenitors (FAPs) (muscle resident mesenchymal cells), which are strongly regulated by the actions of immune cells, especially macrophages. Following the expression pattern of macrophages and satellite cells, fibro-adipogenic progenitor production is induced straight after injury, and peaks at day 3 post trauma (Joe et al., 2010), returning to baseline levels by day 14. It is the crosstalk between FAP cells and macrophages that facilitates the assembly of the extracellular matrix scaffold that is crucial for muscle regeneration. Eosinophils produce IL-4, which possibly increases FAP proliferation to a phagocytic phenotype, while FAPs elimination and apoptosis is due to the action of TNF from inflammatory (M1-like) macrophages. Interestingly, the fibrogenic phenotype of FAPs is driven mainly by resolving macrophages (M2-like), which by releasing TGFβ, block the TNF-driven induction of FAP apoptosis leading to their increase and differentiation (Lemos et al., 2015). This supports the deposition of connective tissue, which is fundamental for a thorough structural and functional recovery of the tissue. As fibrogenic cells produce the connective tissue needed (collagen I, IV) for ECM (extra-cellular matrix) accumulation, they can promote disease states of the cells and possibly fibrosis, if not controlled successfully.

b) Models of muscle tissue injury and repair

Acute muscle injuries are considered an interesting scheme to explore the cooperation between the immune system and muscle tissue's restoration mainly because seizure of the tissue damage is predictable and the time course of initiation of inflammation and resolution during regeneration is very well defined. Between a wide spectrum of models that induce damage, the constructive processes are analogous one to each other, or at least they appear to be in high resemblance. In some models the muscle tissue appears to shrink, while at the end of the regeneration process it returns back to baseline levels. The damage there is quite trivial, causing necrosis of only a small fraction of the damaged tissue (Krippendorf & Riley, 1993) In a model of intense exercise, a big part of myofibers undergo structural damage (Lieber et al., 1996). On the other hand, models that induce the freezing of the muscle are much more severe (Warren, 2005). The most widely used models to study muscle tissue injury and regeneration include the deposition of snake toxins to the site, which lead to an extensive damage, nearly to all myofibers (Arnold et al., 2007; Mounier et al., 2013). Nonetheless, novel observations on the inflammatory response after injury have reported differences between models. For instance, it has been found that the number of neutrophils persists in high amounts for a great amount of days after injury after cardiotoxin (CTX) injection, while after barium chloride ($Bacl_2$) or notexin (NTX) injection their levels decline immediately (Hardy et al., 2016). Additionally, the same has been shown for the models of modified loading or exercise-induced injury (Krippendorf & Riley, 1993; Tidbal & Wehling-Henricks, 2007). The magnitude of injury highly relates to the dissimilarity between models, and it is known that there is quicker resolution of inflammation after CTX injury, in comparison to injury after $Bacl_2$ or NTX (see table 1) (Hardy et al., 2016), pinpointing qualitative dissimilarities among the models in the time course of inflammation and resolution of it. The answer may depend on unquestioned contrasts caused by the toxins, that may not only cause an injury but also influence inflammatory cells, and how the immune system responds to them. For instance, like in other snake venoms that include phospholipase A2, the same

is happening for cardiotoxin and notexin. This enzyme has the potential to cause lysis on the cell membrane of the muscle cells, trigger neutrophil influx, has high anticoagulant capacity and is hemolytic, inducing the activation of immune cells such as macrophages and the degranulation of mast cells (Gutierrez & Lomonte, 2004; Teixeira et al., 2003; Zuliani et al., 2005).

<table>
<tr><th>Category</th><th>Injury model</th><th>Injury agent</th><th>Mechanism of myofiber damage</th></tr>
<tr><td rowspan="3">Chemical injuries</td><td rowspan="2">Biological toxin</td><td>Cardiotoxin (CTX)</td><td rowspan="2">Calcium influx in to myofiber's cytoplasm. Mitochondrial swelling, and lysis of mitochondrial matrix.</td></tr>
<tr><td>Notexin (NTX)</td></tr>
<tr><td>Other chemicals</td><td>Barium chloride (BaCl2)</td><td>Alters myofiber permeability.</td></tr>
<tr><td rowspan="2">Physical injuries</td><td colspan="2">Freezing injury</td><td>Death of all types of cells in the affected region.</td></tr>
<tr><td colspan="2">Exercise-induced injury</td><td>Immune response to mechanical stress.</td></tr>
</table>

Table 1: Models of muscle tissue injury in mice

iii) Lipids in inflammation

a) Lipidomics to study metabolism

Lipids constitute a big family of biomolecules with diverse cellular functions. They can be used as membrane components, for energy storage and as signaling molecules. Additionally, some of them have other special functions, that enable them to be used as antioxidants (plasmalogen), co-factors for lipid synthesis (phosphatidylcholine as a substrate for phosphatidylethanolamine synthesis) and they are crucial in mitochondrial respiration (cardiolipin) (X. Han, 2016). The majority of eukaryotic lipids can be divided in four big lipid metabolic networks, that include the glycerophospholipids, the sphingolipids, the glycerolipids and the non- esterified fatty acids (NEFAs). Additionally, another distinct lipid network is the one of oxysterols that are highly involved in signaling (Griffiths, 2009). Sphingolipids are crucial compounds, found in the cell membrane, but they also participate in key cellular functions. Sphingolipid metabolism's imbalances are associated with lysosomal storage disorders (Selvaraj et al., 2015). They are increased in lipid rafts, and possible alterations in their levels affect the raft composition, causing changes and elevated levels of ceramides (products of the sphingolipid metabolism) can cause lipotoxicity, affecting insulin metabolism and causing insulin resistance (Chaurasia & Summers, 2015). Glycerophospholipids, such as diacylglycerols and triacylglycerols, can be markers of lipotoxicity when increased, and are highly correlated with disorders such as insulin resistance (Unger & Scherer, 2010). The most abundant lipid species in cell membranes are the glycerophospholipids. They can be divided in different classes based on the head group involved in their structure.

Changes in the glycerophospholipid metabolic network affect important functions in cellular level (Bogdanov et al., 2014; Feillet-Coudray et al., 2014; Hishikawa et al.; Mayr, 2015; Pinot, 2014). Additionally, differences in lipid composition of the membrane may affect functions that include the fission, the vesicle transport and the fusion (McMahon & Boucrot, 2015). Phospholipase's A_2 activation leads to increase at the levels of lysoglycerophospholipids, which is associated with inflammation and lipotoxicity (Neuschwander-Tetri,

2010). In addition, ion transport may be affected by changes in the homeostasis of the glycerophospholipid network (McMahon, 2015). Non-esterified fatty acids in high concentrations are indicators of pathological states such as the metabolic syndrome.

b) Lipid mediators in inflammation and its resolution

As described previously, inflammation consists of two phases, namely initiation and resolution. Resolution is an active process highly orchestrated by metabolites that have the capacity to mediate it. In order for a metabolite to be considered a lipid mediator, it should be expressed in sufficient amounts to elicit its biological actions. Lipid mediators are a big family of biosynthesized lipids that participate either in the initiation or during the resolution of the immune response. Highly known lipid mediator families are the following: (i) Prostaglandins, (ii) Leukotrienes, (iii) Lipoxins, (iv) Resolvins, (v) Protectins and (vi) Maresins. During the initiation of inflammation leukocytes, more specifically neutrophils, are the first responders and move along with chemotactic gradients to the inflamed tissue. It has been found that Leukotriene B4 (LTB4) as a chemoattractant (Malawista et al., 2008), while members of the prostaglandin family (PGE2 and PGI2) affect the vasculature and enhance the blood flow (Flower, 2006).

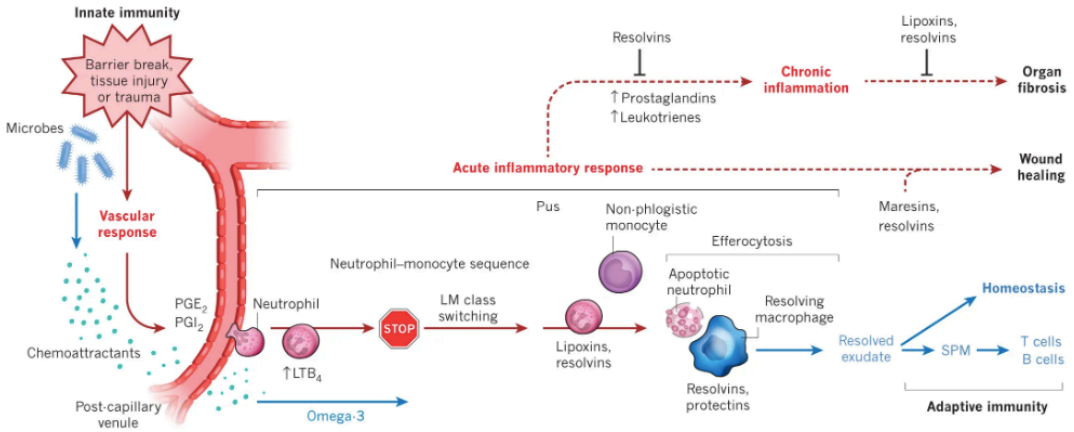

Graphical scheme 4: Lipid mediators in the initiation of the inflammation response, during resolution and their outcomes (Serhan, 2014).

Together with other cytokines, chemokines and complement components (5a and 3b), they trigger the neutrophil influx to the site of injury to eliminate the damage caused by invaders (Dinarello et al., 2012; Maderna & Godson, 2009; Serhan & Savill, 2005; Tabas & Glass, 2013). Initiation of inflammation is followed by cessation of neutrophil migration to the site of injury and

macrophage clearance of apoptotic cells and debris (Serhan & Savill, 2005). These procedures are highly related to resolution and are mediated mainly through lipoxins, resolvins and other resolving exudates, which constitute the family of the specialized pro-resolving lipid mediators (SPMs). As can be seen clearly in graphical scheme 4, the acute inflammatory response is important for the repair of the tissue and to eradicate the harmful stimuli.

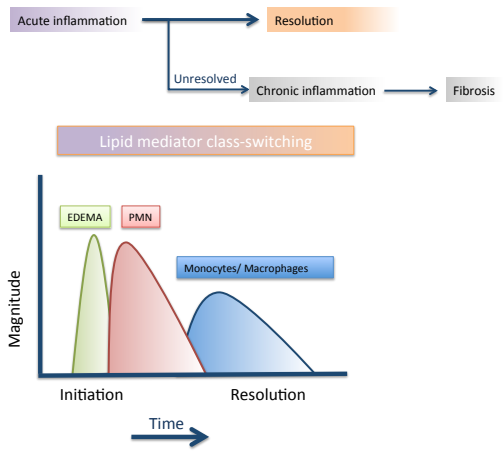

Graphical scheme 5: Time course of an acute inflammatory response.

Together with a successful complete resolution, the tissue returns to the previous homeostatic phase. Liquid chromatography with tandem mass spectrometry (LC-MS-MS) has enabled the identification of several lipid mediators and their temporal switch from high levels of leukotrienes and prostaglandins to high levels of lipoxins and other SPMs. This process is known as lipid mediator class switching and is crucial for regeneration after tissue injury or harmful stimuli. This lipid mediator class switching (graphical scheme 5) from metabolites of the eicosanoid metabolism to SPM production signals the termination of the acute inflammatory response, which is followed by the non-phlogistic monocytes' recruitment at the site. These repair macrophages eliminate the apoptotic neutrophils, in a process highly orchestrated by resolvins and protectins. This clearance is indispensable for restoration of the normal tissue's homeostasis and architecture. Following these changes, pro-inflammatory molecules such us cytokines get eliminated, while debris and apoptotic cells are removed. Deteriorated resolution leads to chronic inflammation (graphic schemes 4&5), and later to organ fibrosis.

Serhan (2016) described SPMs as molecules that have the potential to lower the duration and the magnitude of the inflammatory response and trigger wound healing processes. Through their actions SPMs have the potential to

increase survival and wound healing. The positive effect of SPMs in different pathological conditions is closely related to their receptors (G-protein coupled receptors). RvE1 binds to BLT1, antagonizing LTB4 , and therefore, promotes neutrophil apoptosis (Ohira et al., 2010). RvD1 binds to both murine and human GPR32 (also called ALX/FPR2), mediating the up-regulation of miR-208 and IL-10 (anti-inflammatory interleukin) or the down-regulation of miR-2019 and LTB4, by the action of lipoxygenase 5 (Fredman et al., 2012). Resolvin's D2 receptor, GPR18 (Chiang et al., 2015), mediates the resolution from infection and organ protection.

Exogenous delivery of SPMs has been found, in several mouse models, to be helpful either in the cessation of neutrophils from the site of injury or in clearance of debris and apoptotic cells, and therefore, accelerates the recovery to a homeostatic state. For example, LXA_4, has been found to be protective in CLP-induced sepsis, impairing inflammation , by limiting the pro-inflammatory mediators through the NF-kB pathway in macrophages (Walker et al., 2011). Moreover, RvD1 and RvD2 enhance dermal healing, limiting neutrophil influx at the site of injury, and trigger the re-epithelization of the tissue (Menon, 2012). It becomes obvious that SPM treatment has the potential to drive resolution, and the identification of the actions of SPMs sets a new terrain of research in muscle tissue injury and regeneration.

iv) Omics technologies to study diseased systems

"Omics" is a term that suggests an extensive assessment of a collection of biomolecules. The very first "omics" category to emerge, genomics, concentrated on the examination of entire genomes, contrary to genetics that investigated individual genes or gene variants. Genomic analyses served as an effective experimental scheme to globally assess distinct gene variants that affect monogenic or complex diseases (Hasin et al., 2017). The "omics" scientific area has been largely driven by advancements in technology, which can facilitate cost-effective, high-throughput studies of biomolecules. After this, a lot of new omics technologies got established, which are efficient in cross-examining the linkage between groups of transcripts, proteins and other biomolecules, in respect to the genome. Briefly, omics technologies in response to the genome, epigenome, transcriptome, proteome, metabolome and lipidome have been described, named "genomics", "epigenomics", "transcriptomics", "proteomics", "metabolomics" and "lipidomics", respectively. Genomics pay attention in identifying genetic variants associated with disease and therefore, with inflammation. The first and most widely used approach, GWAS (GWAS catalog https://www.ebi.ac.uk/gwas/home) is able to identify genetic variants for multiple complex diseases, based on genetic markers after genotyping of a variety of individuals. Epigenomics, as a field of studies, refers to the depiction of modifications in DNA or proteins, genome-wide. More specifically, modifications, such as DNA methylation, applies to the identification of methyl groups added to specific nucleotide bases, such as cytosine and adenine. This process, the addition of methyl groups, relies on DNA methyltransferases (DNMTs) and is associated with repression of associated genes, in promoters, in transposable elements and in the gene body of highly transcribed genes. The most used approach to detect methylation patterns in DNA is bisulfite sequencing (Tang, 2019). Another type of epigenomic modification, acetylation, refers to the addition of acetyl group in the tails of histones, and it can have positive or negative effects in the transcription of associated genes. Additionally, chromatin openness/

accessibility studies, based on ATAC-seq (Buenrostro et al., 2015) or DNase-seq (Chen et al., 2018), reveal the exposed/ nucleosome free regions to transcription factors to facilitate transcription. Transcriptomics (Ozsolak & Milos, 2011; Wang et al., 2009) identify the presence of transcripts genome-wide, either by quantitatively examining the levels of transcripts or qualitatively identifying novel splicing and RNA editing sites. Transcriptomic studies in a high extent reveal information about the transcription between healthy/ diseased tissues (Arnes et al., 2016; Gupta et al., 2010; Ishii et al., 2006; Schmitz et al., 2016), differences in development of cells (Yao et al., 2016) or about the status of non-coding RNAs and how they are associated to inflammation (Schmitz et al., 2016). Proteomics, as a method, is used for quantification of protein transcripts, their changes and interactions. The last fields to emerge in the omics categories, due to the difficulty to identify and discriminate small biomolecules, metabolomics and lipidomics , can give insights in metabolic function of cells and tissues, and together with modern modeling techniques can examine the metabolic influx in inflamed tissues (Dettmer et al., 2011; Dunn et al., 2011; Joyce & Palsson, 2006; Madsen et al., 2006; Patti et al., 2012; Steuer, 2006).

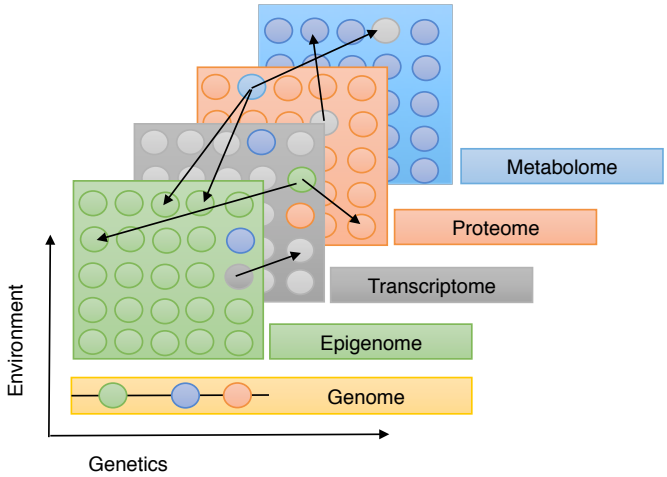

Graphical scheme 6: Different levels of omics data, and the interactions between molecules of distinct data layers.

Recently, multi-omics approaches are used to associate different levels of information, from etiology of a diseased state to the functional consequences it may has (graphical scheme 6) (Civelek & Lusis, 2014). A big range of processes can be used to associate data across numerous levels of omics,

but the most regularly used relate to correlation identification or co-mapping. Consequently, if two layers of data partake a mutual driver, they will show a high level of correlation between them. The ways to integrate various omics data can be divided into three main groups. Firstly, the genome approach, where the initial focus of the analysis is on the genome, identifies these genes that contribute to disease. Once the causative variants of a disease have been identified, other omics data can be used to establish the downstream synergy of factors or pathways that are affected. Interestingly, (Claussnitzer et al., 2015), focusing on the FTO locus, that is highly related to obesity, by comparing more than 100 cell type chromatin state maps, and by performing Hi-C (Han et al., 2018) interaction analyses, identified two genes that highly relate to obesity in adipose tissue. Secondly, the phenotype-first approach, focuses on the correlation between various systems that are related to a particular phenotype. These levels of information can be associated in relevant pathways to further understand how different entities affect disease development. In a study from Gjoneska et al. (2015), an integration between epigenomic and transcriptomic data showed how a variety of epigenetic modifications affect chromatin states. The last approach focuses on the involvement of different factors such as the diet, the weight, the gender and other measurable entities, in disease. By exploring the effect of 25 different diets across 800 mice, scientists identified how these affect health and longevity (Solon-Biet et al., 2014). Lately, new advancements in technology have made it possible to examine the epigenomic and transcriptomic profile in single cells. These approaches – single cell RNA-seq and single cell ATAC-seq and methylome single cell-seq - show and highlight in high resolution cellular differences and give insights to better understand the role of an individual cell in context to its microenvironment (Eberwine et al., 2014). As the writers say “Sequencing from single cells suggest a more complex ecology of heterogeneous cell states that together produce emergent system-level function. These technologies together with other omics methods can give an insight about the etiology of disease or tissue development in complex biological systems. For example, Moignard et al. (2013) identified the

transcriptional networks that govern blood stem and progenitor cells. Moreover, single cell technologies can be used to identify the cells that correspond to the high heterogeneity in cancer (Gonzalez-Silva et al., 2020; Halbritter et al., 2019).

v) Bioinformatic challenges in integration of biological datasets

As described previously, recent advancements in technology have led to the establishment of novel experimental set-ups to study biological systems. The outcome of these set-ups carries the information in blocks of “big data” that need to be analyzed to decipher the biological meaning, which they carry. A variety of challenges is associated with the analyses of biological big data and they will be described here. The generation of an excessive amount of data has led to the need of attentive methods for management and organization. Specifically, in the level of national and international initiatives, data should be stored and be accessible for all. Data incorporation and annotation from distinct sequencing technologies emerge and have to be available to scientists and easy to access. High amounts of data result in repository problems as tremendous amounts of CPU have to be used. Additionally, heterogeneous data formats define a technical need for data reformatting in order for them to be used and analyzed to reveal the biological information. Bioinformaticians should carry diverse practical skill sets to complete data analysis-related tasks. There is a high need in data preprocessing and quality measurements, data transformation and filtering, application of machine learning and statistical evaluation. Moreover, bioinformaticians have to be able to use specific tools for data visualization and report. In order to integrate data, usage of APIs, databases and flat files is required. Apart from the use of tools, data analysis relies in the ability of the scientist to program, write code that is reusable, efficient and well documented. To perform these tasks, somebody has to use sequencing alignment tools such as Bowtie (Langmead, 2010), or HISAT (Kim et al., 2015), tools for handling high throughput data (Li et al., 2009), get gene datasets from databases such as Ensemble (Hunt et al., 2018; Zerbino et al., 2018). It becomes clear that a bioinformatician, must have knowledge of biology in terms of molecular biology, genetics, immunology and others, knowledge of high-throughput sequencing technologies and computational genomics or other omics categories, database management skills for queries in relational and non-relational databases, know techniques for data mining and be able to perform clustering

or decision trees analyses and be able to use one or more programming languages such as R and Python.

vi) Mathematical and statistical interlude

In this section, mathematical and statistical terms, approaches and algorithms that are used in this study, will be highlighted and briefly explained.

Clustering

Genes that function together often exhibit direct or inverse correlated expression. The simplest method for identifying those modules and connections is by clustering the genes to identify groups of genes whose expression is similar across the set of samples.

Hierarchical clustering

The commonly used hierarchical clustering technique agglomeratively sorts genes based on the similarity of their expression, producing a tree that can be cut into clusters. For each pair of genes *i* and *j*, hierarchical clustering computes a distance metric *Dij*; then, starting with each gene as its own "cluster," iteratively merges clusters based on the smallest *Dij* between them.

k-means clustering

The algorithm iteratively finds points that define the centers of globular clusters: starting with a user–specified number of clusters *k*, it selects *k* genes at random as starting centroids, and clusters all the genes based on the centroid to which they are closest. For each of the resulting *k* clusters, new centers are computed based on the mean expression of the genes assigned to that cluster. The genes are reclustered with respect to the new centroids, and the process is repeated until the clustering assignments converge.

Dimensionality reduction

Because the number of genes assayed is vast, it is often of interest to find a small number of representative patterns that describe most of the variation observed in the data and on which the gene expression may be modeled, rather than dealing with the whole dataset. This can be done by reducing the levels of the information in less dimensions.

Principal component analysis

The simplest and best–known dimension reduction technique is Principal Component Analysis (PCA) , which transforms a set of observations of possibly correlated variables (e.g., gene expression measurements) into a new set of variables, called the principal components (PCs), which are constructed such that the PCs are completely independent of each other. The transformation is defined such that the first principal component lies along the direction of greatest variation in the data, accounting for as much of the overall variation in the gene expression between samples as possible.

Mathematically, the principal components are the eigenvectors of the covariance matrix; the associated eigenvalues indicate the amount of variance along each component.

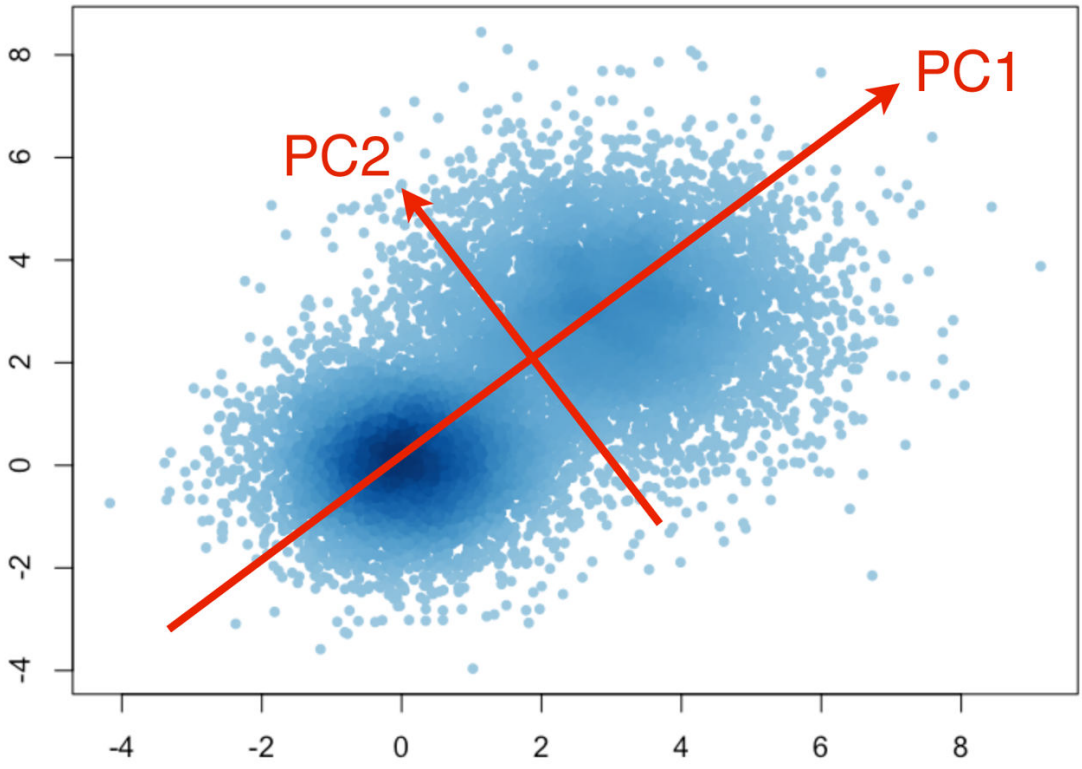

Representation of a PCA plot based on the two principal components (PC1 and PC2). Here to note that PC1 is always perpendicular to the PC2

The principal components are defined such the first principal component (PC1) lies along the direction of greatest variation and each succeeding component (in two dimensions, only PC2) is defined to lie in an orthogonal

direction with the highest variance. Geometrically, the PCA space is a rotation of the original axes.

Machine learning

Machine learning (ML) is the scientific study of algorithms and statistical models that computer systems use to perform a specific task without using explicit instructions, relying on patterns and inference instead. It is seen as a subset of artificial intelligence. Machine learning algorithms build a mathematical model based on sample data, known as "training data", in order to make predictions or decisions without being explicitly programmed to perform the task.

Random forests

The Random Forests algorithm is a decision–tree-based classifier that permits multiple types of data to be mixed *a priori*, enabling its use as an integrative predictor. Decision trees are a conceptually simple supervised classifier. At each step, a variable and threshold is chosen to optimally partition the samples based on known labels. The decision rules may operate on continuous or categorical variables. The partitioning continues until either all nodes are pure, or all variables have been used. Once the rules are established based on labeled samples (i.e., the tree is trained), the rules may be used to classify a new sample of unknown status.

2) Materials and Methods

Ethical approval

All animal experiments were carried out in accordance with guidelines prescribed by the Institutional Animal Care and Use Committee at Sanford Burnham Prebys Medical Discovery Institute and University of Debrecen, School of Medicine following Hungarian (license no.: 21/2011/DEMÁB) and European regulations.

Mice

Wild type BoyJ (B6.SJL-Ptprca Pepcb /BoyJ, stock number 002014) and C57BL/6J male control mice were obtained from the Jackson Laboratories and bred under specific-pathogen free (SPF) conditions.

Acute cardiotoxin (CTX) muscle injury

Mice were anaesthetized with isoflurane (adjusted flow rate or concentration to 1.5%) and 50 μl of cardiotoxin ($12x10^{-6}$ M in PBS) (Latoxan) was injected in the tibialis anterior (TA) muscle (Guardiola et al., 2017). Muscles were recovered for flow cytometry analysis at day 4 post-injury or for muscle histology and IHC-Fr at days 0, 1, 2, 4 and 8 post-injury.

Histological analysis of muscle regeneration

Muscles were removed and snap frozen in nitrogen-chilled isopentane (–160 °C), then 8-μm-thick cryosections were cut and stained with H&E. For each histological analysis, at least five slides (per condition) were selected where the total regenerative region inside the CTX-injured tibialis anterior muscle was at least 70%. For each tibialis anterior muscle, myofibers in the entire injured area were counted and measured. H&E muscle sections were scanned with Mirax digital slide scanner and the CSA was measured with HALO software (Indica Labs). CSAs for these samples are reported in μm^2.

Eccentric Contraction-Induced Muscle Damage

Animals were maintained in a surgical plane of anesthesia (3-5% isoflurane delivered in 100% O_2) for the duration of procedure. Anesthetized mice are placed on a warm heating pad and their hind limbs are removed of hair using fine electric hair clippers. A two-minute rest was given to the animal while under anesthesia to allow muscles to return to normal function after tetanus. The hind limb was restrained at the knee firmly with a clamp to ensure that the animal's knee does not move, and the foot strapped to a footplate/force transducer with a dual motor-arm attached (Aurora Scientific). Two 30g needle platinum electrodes were inserted intramuscularly into the thigh of the right leg, then the sciatic nerve was stimulated by an electric pulse of 100Hz at 200usec pulse width at 2.5mA and 25V for 0.4 seconds. While the muscle is under contraction, the motorized footplate applies an eccentric rotational torque, causing micro-trauma and a resultant force deficit to muscle fibers. This protocol was repeated for forty repetitions to create a significant and physiologically relevant injury to the muscle. The experimental mice were then allowed to recover for a period of anywhere from 1-14 days and followed for muscle contraction force recovery after injury. After which, they were sacrificed, and muscle tissue was collected.

Bone Marrow Transplantation (BMT) and delayed model of muscle regeneration

Recipient congenic BoyJ mice (7 weeks old) are irradiated with 11 Gy using a Theratron 780C cobalt unit for the ablation of the recipient bone marrow. During irradiation one of the hindlimbs was shielded as described previously[35] (Patsalos et al., 2017). Following the irradiation, isolated bone marrow cells (in sterile RPMI-1640 medium) flushed out the femur; tibia and humerus from donor C57Bl/6J mice were transplanted into the recipient mice by retro-orbital injection ($20x10^6$ BM cells per mice). This experimental BMT CD45 congenic model allowed for the discrimination of donor, competitor and host contribution in hematopoiesis and repopulation efficiency of donor cells (congenic mice with CD45.1 versus CD45.2). The CD45.1 and CD45.2 contribution is then

detected by flow cytometry usually 8-12 weeks following the BMT. In short, a cut at the tail tip of the mice provided a drop of blood that was placed into 0.5 ml PBS + 1% FBS + 10 U/ml Heparin buffer (samples kept on ice). The cells were directly stained by 2 µl mouse anti-mouse CD45.2-FITC (clone 104) and 2 µl rat anti-mouse GR1-PE (clone RB6-8C5) antibodies (BD Pharmingen) and incubated on ice for 30 min. After 2 washes with ice-cold PBS/FBS/Heparin buffer we resuspended the cells in 0.5-1 ml FACS Lysing solution (BD Cat #349202). We incubated for 5 min at RT then centrifuged the cells (400g, 5 min, 4°C). We ran the double stained samples on FACS (BD FACS Calibur) and determined the ratio of donor cells. The repopulation is usually over 90% gated on the granulocyte fraction. Two months following the BMT the animals were TA-injured with CTX as described above. For *in vivo* RvD2 treatments, mice where treated with either 4 *µ*g/kg RvD2 (Cayman Chemical; item #: 10007279) or saline at day 2 and 3 post CTX injury. All irradiation experiments were performed under anesthesia in cohorts of 12 animals per experiment.

Immunohistochemistry

Tissue sections were fixed and permeabilized in ice cold acetone for 5 min and blocked for 30 minutes at 20 °C (room temperature) in PBS containing 2 % bovine serum albumin (BSA). Tissues were stained for 1 h at room temperature using a primary antibody diluted in 2 % BSA. The primary antibodies used for immunofluorescence were rabbit anti-Desmin (Abcam 32362) at a dilution 1/200 and rat anti-F4/80 (Abcam 6640) at a dilution 1/200. In all cases, the primary antibody was detected using secondary antibodies (dilution 1/200) conjugated to FITC (JIR 703-095-155) or Cy3 JIR (711-165-152). The nuclei were counter stained with 0.1-1 µg/ml Hoechst. Fluorescent microscopy was performed using Carl Zeiss Axio Imager Z2 microscope equipped with lasers at 488, 568 and 633 nm. Figures were analyzed and assembled using Fiji and Illustrator CS5 (Adobe).

In vivo muscle force measurement

To determine the effect of RvD2 on muscle function, we performed force measurements in the murine model of delayed regeneration, as described above. In these experiments, mice were treated with RvD2 at day 3 post-injury. For this, mice were first anesthetized with 3% vaporized isoflurane mixed with O_2. Mice were then positioned under a heat lamp to maintain the body temperature at 37 °C. Knees of the animals were secured to a fixed steel post, and their feet were taped to the platform to prevent movement from the contraction of other muscle groups. Electrical stimulations were applied across two needle electrodes placed through the skin just above the knee and beneath the tibialis anterior muscle to stimulate the tibial nerve. In all measurements, we used 0.1-ms pulses at a predetermined supramaximal stimulation voltage. Tibialis anterior muscles were stimulated with a single 0.1-ms pulse for twitch force measurements and a train of 150 Hz for 0.3-s pulses for tetanic force measurements. A 2-min rest was given to the animal while under anesthesia to allow muscles to return to normal function after tetanus. We performed five twitch and then five tetanic measurements on each muscle, with 2–3 min of recovery between each measurement. For recording the muscle force measurements, we used the 610A Dynamic Muscle Control software from Aurora Scientific.

In vivo small animal FLI imaging using 2-DG

To determine whether RvD2 modulates inflammation in vivo, we performed imaging of 2-DG uptake in the delayed model of regeneration (see above). For this, mice were treated with RvD2 at day 3 post-CTX injury. During the light cycle to minimize muscle activity, BoyJ chimeric mice were intravenously injected with 10 nmol of XenoLight RediJect 2-DG 750 probe (Perkin Elmer) or control 750 dye (in 0.2 ml volume) and imaged at 3 h with IVIS Spectrum (Ex745 nm/Em820 nm). Specifically, 3 h after 2-DG injection animals were anesthetized by 3% isoflurane with a dedicated small animal anesthesia device and whole body FLI scans were acquired using the IVIS Spectrum system (Caliper LifeSciences). To prevent movement, the animals were fixed to the mouse chamber and positioned in the center of field of view. We

acquired FLI using a 3-s exposure with field of view of 6.5. Digital images were recorded and analyzed using Living Image v.4.7.2 software (IVIS Imaging Systems). We analyzed images with a consistent region of interest placed over each hind limb to calculate a fluorescence signal. We calculated the fluorescence signal in average radiance efficiency $((p\,s^{-1}\,cm^{-2}\,sr^{-1})/(\mu W\,cm^{-2}))$.

Isolation of macrophages from CTX injured skeletal muscle

TA muscles from CTX-injured animals were isolated and fascia of the TA was removed. Muscles were then dissociated in RPMI containing 0.2% collagenase B (Roche Diagnostics GmbH) at 37°C for 1 hour and filtered through a 100 μm and a 40 μm filter. $CD45^+$ cells were isolated using magnetic sorting (Miltenyi Biotec). For FACS, macrophages were treated with Fcγ receptor blocking antibodies and with 10% normal rat serum: normal mouse serum 1:1 mix, then stained with a combination of PE-conjugated anti-Ly6C antibody (HK1.4, eBioscience), APC-conjugated F4/80 antibody (BM8, eBioscience) and FITC-conjugated Ly6G antibody (1A8, Biolegend). $Ly6C^{high}$ F4/80low macrophages, $Ly6C^{low}$ $F4/80^{high}$ macrophages and $Ly6G^{high}$ $Ly6C^{int}$ F4/80- neutrophils were quantified. In each experiment, compared samples were processed in parallel to minimize experimental variation. Cells were analyzed on a BD FACSAria III sorter and data analysis was performed using BD FACSDIVA and FlowJo V10 software.

Shotgun lipidomics

Muscle samples were collected from mice and were pulverized into a fine powder using a stainless steel biopulverizer at the temperature of liquid nitrogen. The tissue powders of 10 to 20 mg were weighed and homogenized in 0.5 mL 10x diluted PBS in 2.0 ml cryogenic vials (Corning Life Sciences, Tewksbury, MA) by using a digital sonifier (Branson 450, Danbury, CT). Protein assay on the homogenates was performed using a bicinchoninic acid protein assay kit (Thermo Scientific, Rockford, IL) with bovine serum albumin as standards. The rest of homogenate was accurately transferred into a

disposable glass culture test tube, and a mixture of lipid internal standards was added prior to lipid extraction for quantification of all reported lipid species. Lipid extraction was performed by using a modified Bligh and Dyer procedure as described previously (M. Wang & Han, 2014). Individual lipid extracts were resuspended into a volume of 100 µL of chloroform/methanol (1:1, v/v) per mg of protein and flushed with nitrogen, capped, and stored at –20 °C for lipid analysis. For ESI direct infusion analysis, lipid extracts were further diluted to a final concentration of ~500 fmol/µL, and the mass spectrometric analysis was performed on a QqQ mass spectrometer (Thermo TSQ QUANTIVA, San Jose, CA) equipped with an automated nanospray device (TriVersa NanoMate, Advion Bioscience Ltd., Ithaca, NY). Identification and quantification of lipid molecular species were performed using an automated software program (Wang et al., 2014; Wang et al., 2016; Yang et al., 2009) Data were normalized per mg of protein.

Lipid mediator identification and quantitation by liquid chromatography-tandem mass spectrometry

Samples of muscle tissue (TA) or flow-sorted leukocyte populations isolated from muscle of mice exposed to CTX were subjected to solid phase extraction followed by a targeted liquid chromatography-tandem mass spectrometry (LC-MS/MS) analysis. For muscle samples, tissue was minced with scissors in ice-cold methanol containing deuterated internal standards and stored at -80°C. For leukocyte samples, cells were isolated from CTX-treated muscle then flow sorted and plated in phenol red-free and serum-free medium. The cells and medium were then combined with two volumes of ice-cold methanol and deuterated internal standards were added. Samples were then stored at -80°C. Deuterated internal standards (d_5-RvD2, d_4-LTB_4, d_8-5-HETE, d_4-PGE_2 and d_5-LXA_4; Cayman Chemical) were used to assess extraction recovery and quantification. Samples were centrifuged (3,000 rpm) and supernatants were then subjected to solid phase extraction (SPE) and LC-MS/MS analysis, as described here (Dalli, Colas, Walker, & Serhan, 2018; Dalli & Serhan, 2018; English, Norris, Hodges, Dartt, & Serhan, 2017). In short, acidified water (pH

3.5 with HCl) was added to samples immediately prior to SPE using C18 column chromatography. Lipid mediators were eluted in the methyl formate fraction, the solvent was evaporated under a gentle stream of N_2 gas and the sample were then resuspended in methanol:water (50:50). Samples were then injected using a high-performance liquid chromatograph (HPLC, Shimadzu) coupled to a QTrap5500 mass spectrometer (AB Sciex) operating in negative ionization mode. Individual lipid mediators were identified using specific multiple reaction monitoring (MRM) transitions, information-dependent acquisition and enhanced product ion scanning. Identification was based on matching retention time with authentic standards, MRM transitions and 6 diagnostic MS/MS fragmentation ions. Quantitation of mediators was then normalized to the extraction recovery of the deuterated internal standards and calibration curves of external standards for each individual mediator. Once each individual lipid mediator was quantitated, lipid mediator profiles for each sample were constructed. These profiles were then subjected to further analyses using two statistical software platforms. Using the Metaboanalyst online tool (Xia et al., 2015), the data first underwent a missing value imputation in which half the minimum positive value was inserted for compounds that were not detected in all samples. The data were then log transformed and autoscaled. Once these preliminary functions were completed, hierarchical cluster analysis using Euclidean distance measure and Ward's clustering algorithm was performed followed by partial least squares-discriminant analysis. In some cases, lipid mediator profiles were also subjected to interaction network pathway analysis using the Cytoscape online platform (Shannon et al., 2003).

Isolation and *in vitro* differentiation of macrophages from murine bone marrow

Bone marrow was flushed from the tibiae and femurs of 8-10 week old male C57BL/6J mice using a 25 gauge needle and DMEM media (ATCC) containing 10% FBS, 20 mM HEPES and 1% penicillin/streptomycin. Once isolated, the bone marrow was plated in this medium supplemented with 10

ng/ml M-CSF (macrophage colony-stimulating factor; Sigma). On day four of differentiation, the media was replenished with fresh media (containing M-CSF). After seven days, the cells were liberated using a cell scraper centrifuged and re-plated in media lacking M-CSF. After 24 hours, cells were exposed to 10 nM RvD2 (Cayman Chemical) for four hours then collected in Buffer RLT (Qiagen) with 10 μl/ml 2-mercaptoethanol.

ATAC-seq

ATAC-seq was carried out with minor modification as described in Buenrostro et al. (2013). A total of 20,000 cells was sorted in ice-cold PBS. Nuclei were isolated with ATAC lysis buffer (10 mM Tris–HCl [pH7.4], 10 mM NaCl, 3 mM MgCl2, 0.1% IGEPAL) and were used for tagmentation, using Nextera DNA Library Preparation Kit (Illumina), from two to three biological replicates. After tagmentation, DNA was purified with MinElute PCR Purification Kit (QIAGEN). Tagmented DNA was amplified with Kapa Hifi HotStart Kit (Kapa Biosystems) using 9 PCR cycles. Amplified libraries were purified again with MinElute PCR Purification Kit. Fragment distribution of libraries was assessed with an Agilent Bioanalyzer, and libraries were sequenced on a HiSeq 2500 platform.

Mapping and normalization of ATAC-seq

Three replicates of the muscle-derived Ly-6C^{high} MFs of day 1 and Ly-6C^{high} and Ly-6C^{low} MFs of days 2 and 4 upon muscle injury were used for the ATAC-seq experiments (20,000 sorted cells per sample). The primary analysis of ATAC-seq–derived raw sequence reads includes the following steps: alignment to the mm10 mouse genome assembly was done by the BWA tool (33), and BAM files were created by SAMTools (Li et al., 2009). Signals (peaks) were predicted by MACS2 (Zhang et al., 2008), artifacts were removed according to the blacklist of ENCODE (Consortium, 2012) and filtered for further analysis by removing low mapping quality reads (MAPQ score ,10), duplicated reads, and reads located in blacklisted regions. All regions derived from at least any two samples were united within 0.5 kb, and those summits having the highest MACS2 peak score in any sample were

assigned to each region. Promoter-distal regions were selected excluding the transcription start site (TSS)+/20.5 kb regions according to the mouse GRCm38.p1 (mm10) annotation version. In total, we identified 57,409 peaks from muscle-derived MF samples. Tag directories used by HOMER in the following steps were generated with a 120-nt fragment length with makeTagDirectory (Heinz et al., 2010). Genome coverage (bedgraph and.tdf) files were generated by makeUCSCfile.pl (HOMER) and igvtools, respectively, and used for visualization with Integrative Genomics Viewer (IGV) (Thorvaldsdottir et al., 2013) Coverage values were further normalized by the upper decile value detected in the consensus regions for each sample to minimize the intersample variance.

Differential chromatin accessibility analysis

To identify the open chromatin regions involved in muscle-derived MF differentiation, we compared the two end-point cell populations of this process: day 1 Ly-6Chigh versus day 4 Ly-6Clow. DiffBind v2.6.6 (Stark and Brown, 2011) was used to identify differentially opened regions, with DESeq2 (method = DBA_DESEQ2, bFullLibrarySize = FALSE) An ATAC-seq region was defined as differentially changed if the peak showed | log2 fold change | . 1.5 and a false discovery rate–corrected p value ,0.05. For K-means clustering, we used the previously defined differentially opened chromatin regions. Briefly, we counted the normalized read counts of all samples across the differential sites with the HOMER annotatePeaks.pl program (Heinz et al., 2010). Sample values for each peak were scaled and used as an input for K-means clustering in R. Clusters were visualized in R.

RNA isolation

Total RNA was isolated with TRIZOL reagent according to the manufacturer's recommendation. 20ug glycogen (Ambion) was added as carrier for RNA ethanol precipitation.

RNA sequencing (RNA-Seq) library preparation

cDNA library for RNA-Seq was generated from 100ng-400ng total RNA using TruSeq RNA Sample Preparation Kit (Illumina, San Diego, CA, USA) according to the manufacturer's protocol. Briefly poly-A tailed RNA molecules were pulled down with poly-T oligo attached magnetic beads. Following purification, mRNA was fragmented with divalent cations at 85C, and then cDNA was generated by random primers and SuperScript II enzyme (Life Technologies). Second strand synthesis was performed followed by end repair, single `A` base addition and ligation of barcode indexed adaptors to the DNA fragments. Adapter specific PCRs were performed to generate sequencing libraries. Libraries were size selected with E-Gel EX 2% agarose gels (Life Technologies) and purified by QIAquick Gel Extraction Kit (Qiagen). Libraries were sequenced on HiSeq 2500 instrument. Three biological replicates were sequenced for each population.

RNA-seq analysis

Tophat2 (Kim et al., 2013) was used to align the reads to the mm10 mouse assembly. Further downstream analysis of the aligned reads was performed using the StrandNGS software, Version 2.8, Build 230243. © Strand Life Sciences, Bangalore, India .There, normalization of the raw read counts was performed using the DeSeq2 method (Love, Huber, & Anders, 2014). 1-way ANOVA and Tukey's post hoc test was performed for the normalized counts of untreated/ RvD2 treated for 4 hours BMDMs, and also of the sorted and isolated neutrophils of Day 1, Ly6C^{high} and Ly6C^{low} macrophages of days 2 and 4, post CTX. Changes in genes with Fold Change > 1.5 and p-value < 0,05, were considered to be statistically significant and the genes differentially expressed. Heatmaps were drawn using the R package pheatmap.

Gene ontology analysis

Lists of differentially expressed genes (p value<0.05 and FC>2) were analyzed using Panther tool (http://www.geneontology.org/) and the GO Enrichment Analysis to create a gene ontology (GO). GOs with p values <0.05 were selected and results were presented according to their $\log_{10}$ p value.

Statistical analysis

All experiments were performed using at least three biological replicates. Student's *t*-tests and 2-way ANOVA analyses were performed in GraphPad Prism 6 and $P<0.05$ was considered significant ($P<0.05$=*, $P<0.01$=**, $P<0.001$=***, $P<0.0001$=****). Mean and SEM values are shown in graphs.

Data availability

Shotgun lipidomics and targeted lipidomics raw data are provided upon reasonable request. The accession codes for the RNA-seq data reported in this study are SRP145076 (SRA) and GSE114291 (GEO). They have been assigned to Bioproject PRJNA466152. ATAC-seq data can be found under the accession code GSE129393 (GEO).

3) Hypothesis and aims

Macrophages constitute a fraction of myeloid immune cells that shape the regeneration process from the initiation of inflammation to its resolution, leading to a successful healing of the tissue, and by our approach we hypothesized that novel pathways and molecules governing tissue's repair, could be revealed. For this reason, in this study we want to identify how structural lipids are changing after muscle tissue injury with cardiotoxin (CTX) and during regeneration in tibialis anterior muscle (TA muscle) in mice. We further try to decipher the role of PUFA-derived lipid mediators, which have been shown to be important in starting the inflammation phase of the immune response and in mediating the resolution of it using a targeted metabololipidomic approach after CTX. This model and its uniformity make it exceptionally convenient to assess the effect of specific cell types and lipid mediators and their involvement in every phase of injury and tibialis anterior muscle tissue's restoration. Along with this approach, we try to discover and determine the changes in the lipidome in a more pathophysiologically relevant model of muscle tissue injury and regeneration and also to determine if obstruction of the production of the bioactive lipid mediator molecules could affect the inflammation dynamics in regard to the infiltrating immune cell subtypes. Our next goal is to define cellular sources of lipid mediators in inflamed muscle tissue and to further highlight the contribution of these cells in shaping the epigenome during the same time-course using ATAC-seq analyses. To further elucidate the gene expression dynamics upon sterile muscle tissue injury, RNA-seq analyses are performed on isolated Ly6C^{high} (at days 1, 2 and 4) and Ly6C^{low} (at days 2 and 4) immune cell subsets. Finally, we assess the effect of lipid mediators in macrophage-dependent muscle tissue's repair, focusing on a specific biomolecule.

4) Results

i) PUFAs and mobilization from phospholipid pools

An unbiased shotgun-lipidomics experimental approach was used to discover in which way the structural lipids change after a cardiotoxin-induced acute sterile injury in tibialis anterior muscle (TA muscle) in mice. This type of injury stimulates a systematic inflammatory and resolving/regenerative response (Hardy et al., 2016). Morphometry together with Hematoxylin and eosin (H&E) was used for histological analysis in order to reveal the advance of inflammation and regeneration of the muscle fibers. Based on this analysis before the CTX-induced injury (day 0) and after CTX-induced injury (day 8), a well restored muscle architecture can be documented by day 8. Although there is a complete regeneration of the tissue, the myofibers that have been regenerated show a central micronuclei and are smaller, suggesting that the differentiation of the myofibers is recent (fig. 1a). Myofiber cross-sectional area (CSA) repartition is shown for the uninjured and 8 days after injury muscle tissue (fig. 1b). If the uninjured tissue is compared to the regenerated tissue, the cumulative CSA distribution is shifted to the left for the later. In addition, the average CSA repartition decreases significantly for the regenerated tissue (day 8), meaning that the regenerated myofibers are smaller. In this lipidomic analysis, the following days were chosen : 0, 1, 2, 4, 8, as timepoints, because they represent considerable changes in the process of inflammation and muscle regeneration.

Multi-dimensional mass spectrometry MS-based shotgun lipidomics was used to quantify the total lipid content of murine tibialis anterior skeletal muscle (see Methods). The following lipid classes were quantified: glycerolipids, ceramides, sphingolipids and glycerophospholipids, and their lipid content was expressed as a percentage of the total identified lipidome (fig. 1c). Phosphatidylinositol (PI), phosphatidylcholine (PC) and phosphatidylethanolamine (PE) were the most abundant lipid classes before the cardiotoxin injury (day 0) (13.5%, 19.3% and 39.6%, respectively).

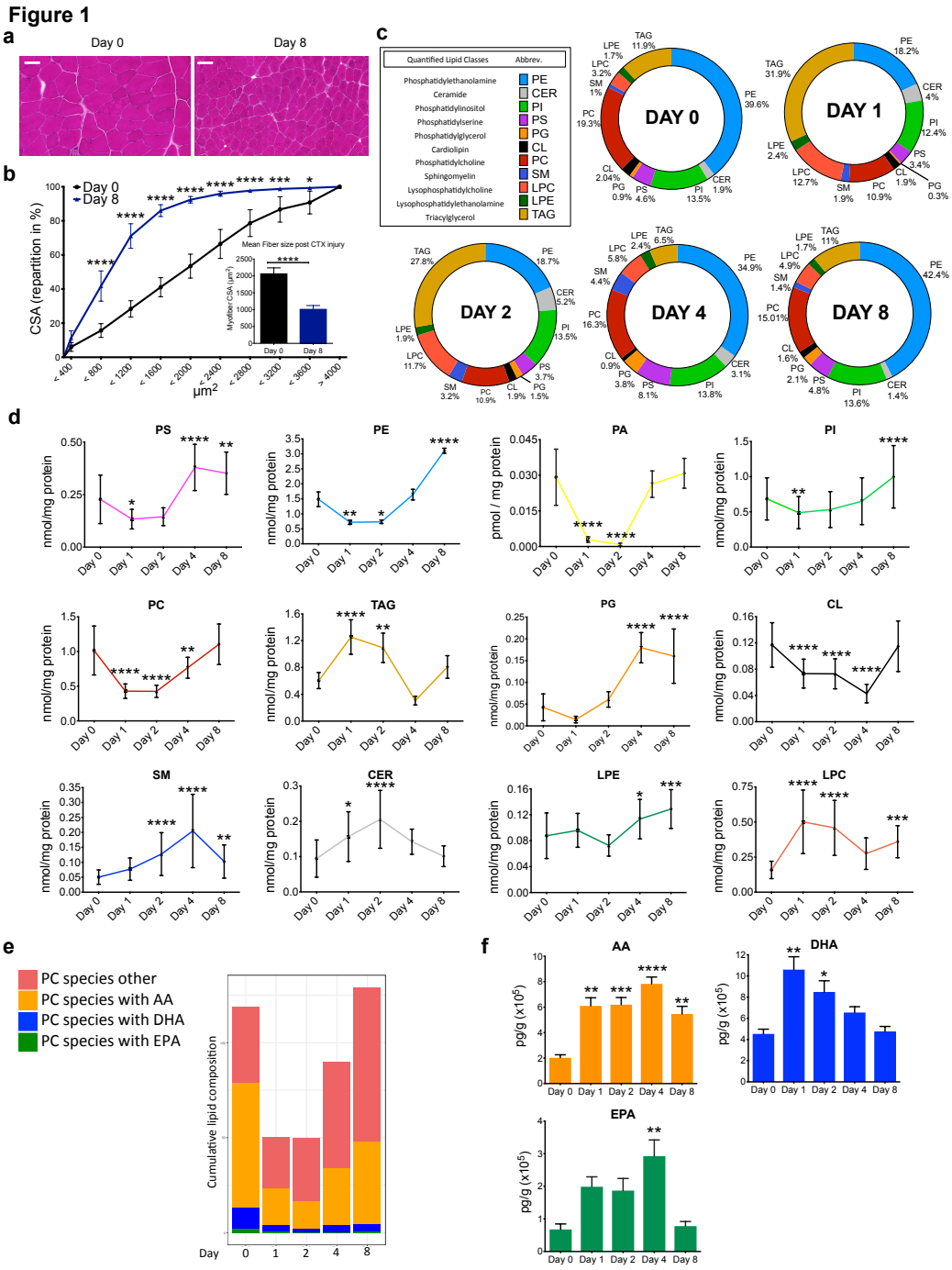

Figure 1. Temporal regulation of structural and signaling lipids during the time course of tissue regeneration after sterile muscle injury. (**a**) Representative images of H&E-stained TA muscles at days 0 and 8 after CTX-induced injury. Scale bars are 100 µm. (**b**) Fiber size repartition of uninjured and regenerating muscle at day 8 post CTX injury. Mean fiber CSA is shown in the inset. (**c**) Relative distribution of lipid classes at selected time points after CTX, expressed as percentages. Their color code and abbreviations are shown as inset (**d**) Quantification of each lipid class as measured at 5 different time points after CTX. p<0.05=*, p<0.01=**, p<0.001=***, p<0.0001=**** (Dunnett's multiple comparison test in two-way ANOVA). Data are shown as mean ± SEM and n=3 for each time point. (**e**) Bar graph showing the cumulative lipid composition of four distinct groups of phosphatidyl choline (PC) species at selected time points (days 0, 1, 2, 4 and 8 after CTX). The four groups consist of PC species

containing Arachidonic Acid (AA), Docosahexaenoic Acid (DHA), Eicosapentaenoic Acid (EPA) or other PUFA chains at the *sn*-2 position of PC. (**f**) Bar graphs showing the levels of AA, EPA and DHA lipid species at selected time points (days 0, 1, 2, 4 and 8) after CTX (right panel). p<0.05=*, p<0.01=**, p<0.001=***, p<0.0001=**** (Dunnett's multiple comparison test in one-way ANOVA). Data are shown as mean ± SEM and n=3 for each time point.

The lysophosphatidyl species only exhibited a small portion of the identified lipid content in uninjured tibialis anterior skeletal muscle. During the inflammation (days 1 and 2) there was a change in the lipid composition of the muscle due to injury. PC and PE species decreased, and this was coupled with a simultaneous increase in lysophosphatidylcholine (LPC) and triacylglycerol (TAG) (fig. 1d). The levels of PE and PC increased at day 4 and begun to return to baseline levels by day 8, when there is restoration of the damaged muscle tissue. On the other hand, the levels of ceramide (CER) and sphingomyelin (SM) were increased at days 2 and 4, before returning to baseline levels at day 8. There was an obvious inverted association between LPC and PC, and for this we determined the PUFA composition, which is esterified to the sn-2 position of the PC. The majority of the PC species consisted of arachidonic acid (AA), and of eicosapentaenoic acid (EPA) and docosahexaenoic acid (DHA). Enzymes such as the phospholipase A_2 (PLA_2) (Dennis & Norris, 2015) release the esterified phospholipids after cellular activation. We hypothesized that liberation of the PUFAs could be the reason of the decreased PC species levels. As a result, the levels of the free EPA, DHA and AA were elevated in an inverse manner compared to the PC after injury and during the regeneration time course, returning to standard levels at day 8. These combined data, collectively, show that there is PUFA liberation after phospholipid remodeling and this is determined dynamically after acute muscle injury and regeneration of the murine tissue.

ii) Lipid mediator class switching during regeneration

Based on the inverse correlation between the free arachidonic acid (AA), docosahexaenoic acid (DHA) and eicosapentaenoic acid (EPA) and the Phosphatidylcholine (PC) lipid species, we made the hypothesis that they are

selectively liberated and there is a further downstream conversion to bioactive lipid mediators during inflammation and repair after the cardiotoxin injury. The role of the PUFA-derived lipid mediators is important in starting the inflammation phase of the immune response and in mediating the resolution of it. A targeted metabololipidomic approach (liquid chromatography-tandem mass spectrometry (LC-MS/MS) was used to analyze the lipid mediator metabolome at day 0 (uninjured tissue) and days 1, 2, 4 and 8 after cardiotoxin injury, similarly to the previous time course. Multiple reaction monitoring (MRM) was used to identify the main pro-inflammatory and resolving lipid mediators, such as prostaglandins/ leukotrienes and maresins/ protectins/ lipoxins/ resolvins, respectively. In figure 2a, MRM chromatograms for chosen lipids, are shown, together with MS/MS spectra for lipoxin B4 (LXB_4) and resolvin D2 (RvD_2) (fig. 2b). Lipid mediators we divided in five general classes and their input to the total lipid mediator pool was counted for every day of the examined time course. By doing this, we were able to identify the global monitored changes of the species after injury and till the regeneration of the tissue. Pro-inflammatory lipid mediator classes were highly produced at days 1 and 2 (inflammatory phase), while specialized pro-resolving lipid classes were identified mainly at days 2 to 8.

Figure 2

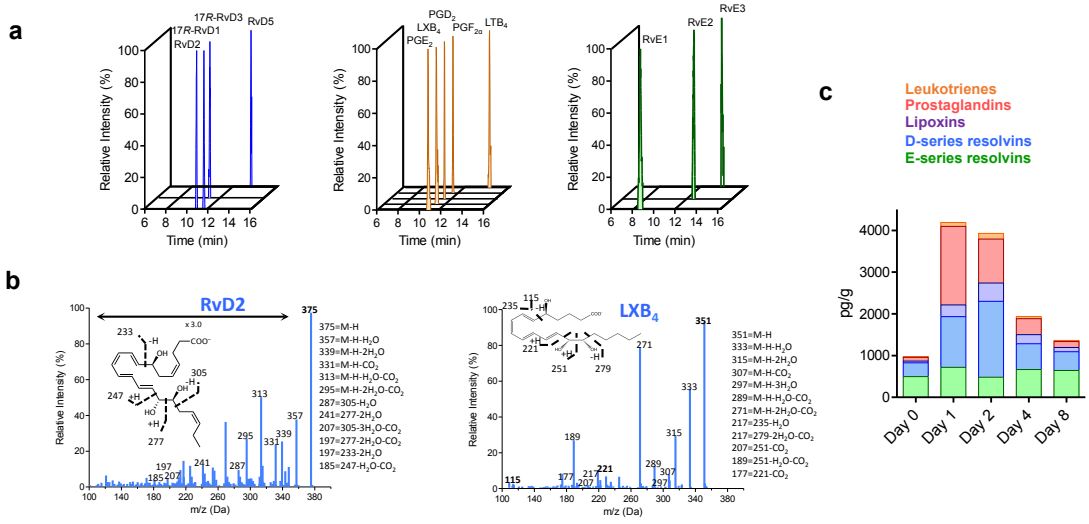

Figure 2

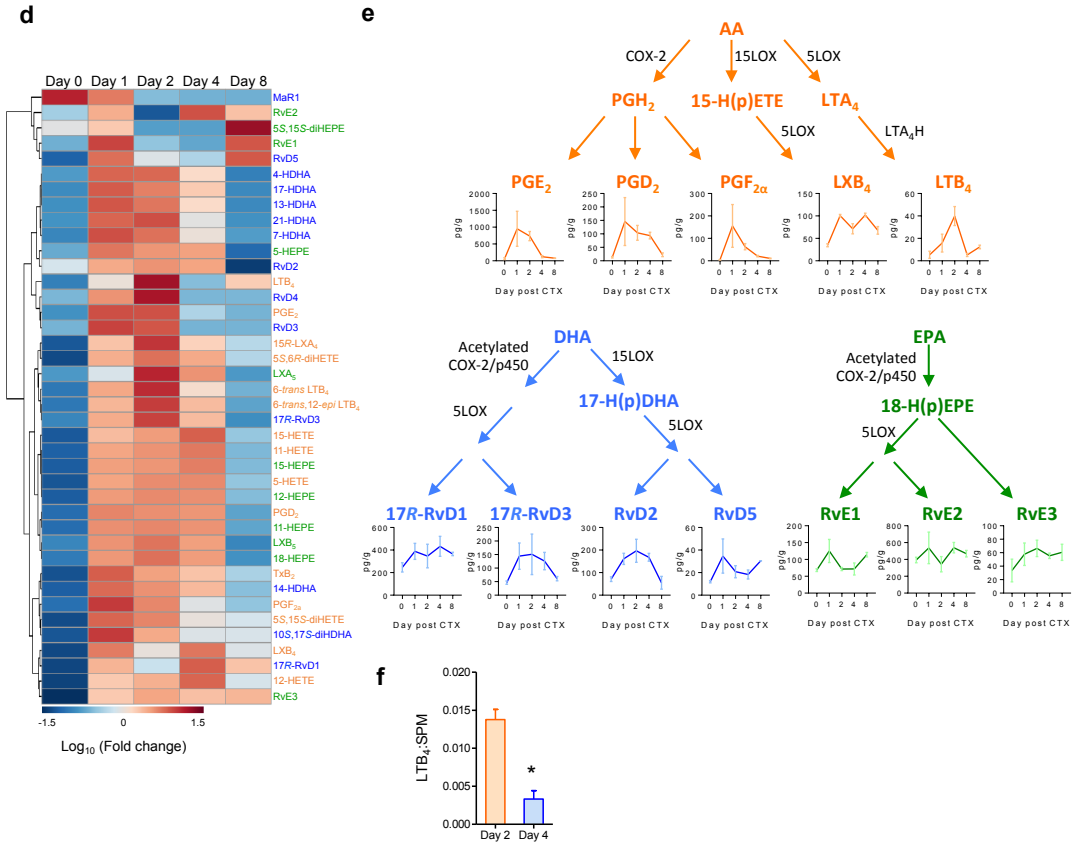

Figure 2. PUFA-derived lipid mediator profiles of TA muscle are temporally regulated following CTX-muscle injury. (**a**) Representative multiple reaction monitoring (MRM) chromatograms of bioactive lipid mediators derived from DHA (blue), AA (orange) and EPA (green). (**b**) Representative MS/MS spectra of RvD2 and LXB_4 with their diagnostic ion assignments and structures shown as inset. (**c**) Stacked histogram showing the cumulative levels of each specific class of lipid mediators at the indicated day after CTX exposure. Constituent members for each group are: Leukotrienes—LTB_4, Δ6-*trans*-LTB_4, Δ6-*trans*,12-*epi*-LTB_4; Prostaglandins—PGD_2, PGE_2, $PGF_{2\alpha}$, TxB_2; Lipoxins—15*R*-LXA_4, LXB_4, LXA_5, LXB_5; D-series resolvins—17*R*-RvD1, RvD2, 17*R*-RvD3, RvD4, RvD5; E-series resolvins—RvE1, RvE2, RvE3. (**d**) Heatmap displaying the relative abundance of individual lipid mediators at the indicated day post CTX. Each column represents the average of n=3 at the indicated time point. The text color of each lipid mediator indicates the PUFA from which it is derived (AA—orange, DHA—blue, EPA—green). (**e**) Levels of selected AA (orange)-, DHA (blue)-, and EPA (green)-derived lipid mediators displayed in their biosynthetic pathways. (**f**) Ratio of LTB_4 to total SPM (15*R*-LXA_4, LXB_4, LXA_5, LXB_5, 17*R*-RvD1, RvD2, 17*R*-RvD3, RvD4, RvD5, 10*S*,17*S*-diHDHA, MaR1, RvE1, RvE2, RvE3) at indicated days post-CTX. *p<0.05 (two-tailed unpaired Student's *t*-test). Data are mean ± SEM. and n = 3 per time point.

Examining the similarity of the capacity of each broad lipid class to the whole lipidome at days 0 and 8, we could argue that the tissue's state is quite similar (fig. 2c). The heatmap of figure 2d shows how each lipid mediator changes

after muscle tissue injury and regeneration. Most of the lipid mediators showed an increase at days 1 and 2. SPMs such as resolvins RvE2, RvE1, RvD5, RvD2, and RvE3, and lipoxin B_4 sustained their elevated levels, in contrast to pro-inflammatory lipids such as prostaglandin E_2 (PGE_2), prostaglandin F_2 (PGF_2) and leukotriene B_4 (LTB_4) who were down-regulated after this increase (days 4 and 8). By mapping the absolute values of selected lipids (fig. 2e) in their biosynthetic pathways over the muscle regeneration time course, this trend was even more evident. For example, resolvins (RvD2, 17*R*-RvD1, RvE3) and lipoxin B_4 had elevated levels at day 4 , while leukotriene B4, which was increased at day 2, declined rapidly by day 4. The ratio of leukotriene B4 to the cumulative amount of pro-resolving lipid mediators can be used as marker of inflammation. By comparing this ratio at days 2 and 4 (fig. 2f), becomes evident the turn of the lipid mediator production from pro-inflammatory to their resolving counterparts. Collectively, these data suggest a dynamic switch in lipid mediator classes from inflammatory to resolving species during the restoration of muscle tissue's architecture after cardiotoxin injury.

iii) Lipid mediator profiling upon exercise injury

Cardiotoxin causes myolysis of the fibers of the complete injured area coupled by inflammation and tissue restoration through repair mechanisms *ad integrum* (Hardy et al., 2016). CTX-injury model and its uniformity make it exceptionally convenient to assess the effect of specific cell types and lipid mediators and their involvement in every phase of injury and tibialis anterior muscle tissue restoration. Along with this approach, we tried to identify and determine the changes in the lipidome in a more pathophysiologically relevant model of muscle tissue injury and regeneration.

This model is an adaptation of the eccentric-contraction injury model (ECI) (Childers, 2011) in mice. It represents a less serious injury, but the inflammatory and regenerative response highly resembles the cardiotoxin induced injury model. As it is shown in figure 3a the infiltration of $CD45^+$ myeloid cells and the dynamics of neutrophil, inflammatory and reparative

macrophage accumulation is analogous to the accumulation of these cells in the muscle tissue after CTX injury (fig. 2b-d).

Figure 3

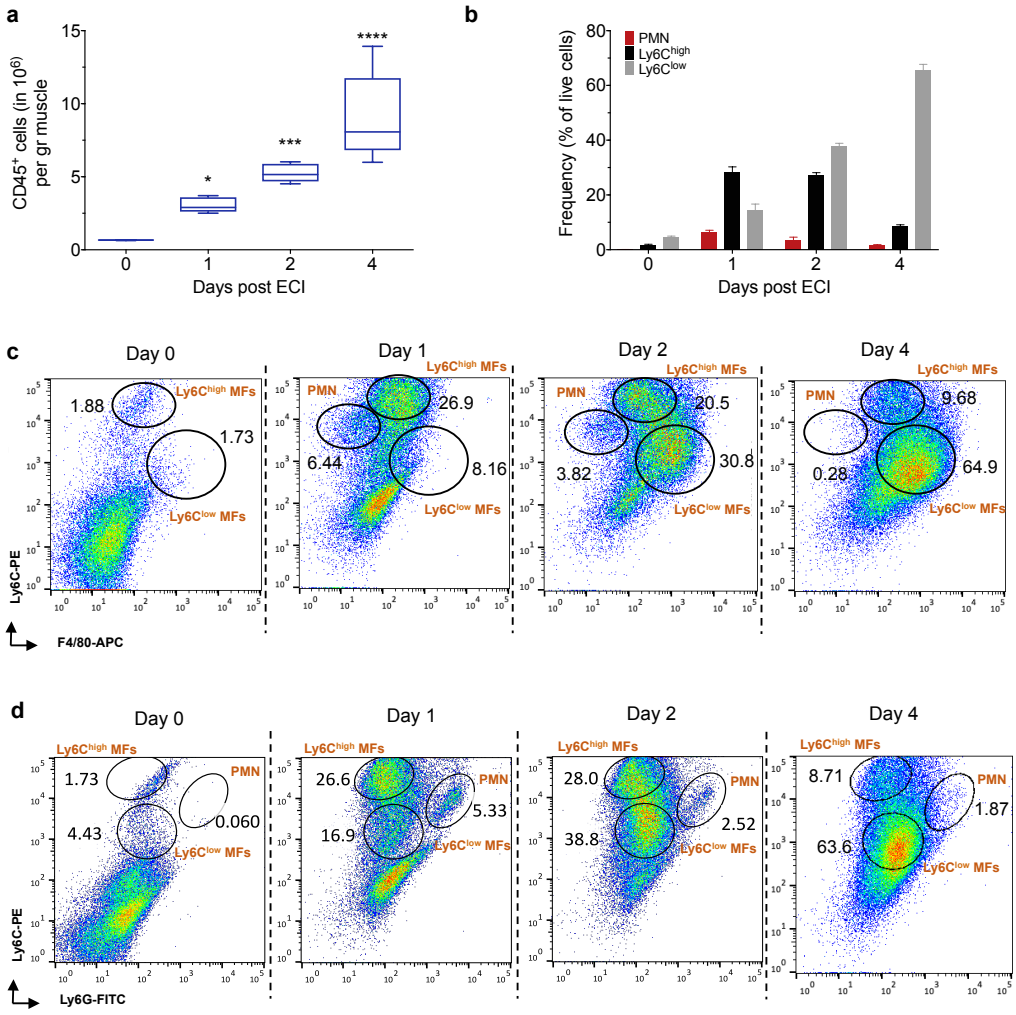

Figure 3. Leukocyte differential profile in muscle of mice undergoing eccentric exercise-induced muscle injury. (**a**) Absolute number of $CD45^+$ cells isolated from GAST muscles at indicated timepoints following eccentric contraction induced injury (ECI). p<0.05=*, p<0.001=***, p<0.0001=**** (Sidak's multiple comparisons test in two-way ANOVA). Data are shown as mean ± SEM, n = 3 mice per group. (**b**) Percentage of PMNs, inflammatory ($Ly6C^{high}$ $F4/80^{low}$) and repair ($Ly6C^{low}$ $F4/80^{high}$) macrophages at indicated timepoints following eccentric exercise-induced (ECI) injury. (**c**) and (**d**) Representative flow cytometry pseudocolor density plots (with 2 alternative gatings) of PMNs, inflammatory and repair macrophages at indicated timepoints post ECI injury. Insets shows representative percentages of each gated population.

By using interaction network pathway analysis to image alterations in global lipid mediator metabolome from AA, EPA and DHA, we compared days 0 and 1 after injury in both CTX and ECI models (fig. 4a and 4b, respectively). This

analysis integrates pathway relationships with lipid mediator abundance and fold-change vs. baseline (day 0). The identified lipid mediator species and their direction of change were greatly steady between the two models. However, the degree of change of some lipid mediators (designated by the fold-change scale) was higher in the CTX model (fig. 4). In both models, the first day upon injury, there was an induction in AA-derived prostaglandins (PGE_2, PGD_2), leukotriene (LTB_4) and lipoxins (LXB_4, 15R-LXA_4). Thus, EPA- and DHA-derived SPMs such us RvD_2, RvE_3 and RvD_5 were increased in comparison to baseline levels, in both models. There were also elevated levels for 17-HDHA (D-series resolvin biosynthetic marker) and 18-HEPE (E-series resolvin biosynthetic pathway marker). By examining the individual lipid mediator levels of pro-inflammatory (LTB_4, PGF_2) to resolving exudates (LXB_4, RvD_4, and RvE_3), an inverse relationship become visible between them (fig. 4c). Interestingly, in the more pathophysiological ECI model, there was a slower transition from inflammation to resolution, as leukotriene's B4 levels remained elevated by day 4.

Figure 4

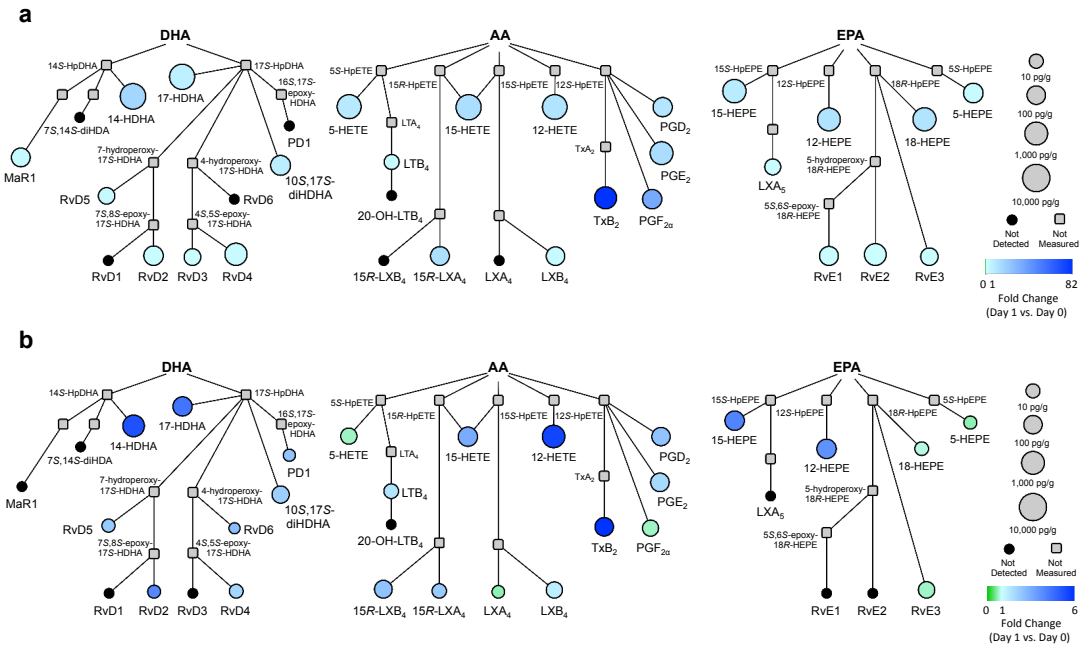

Figure 4

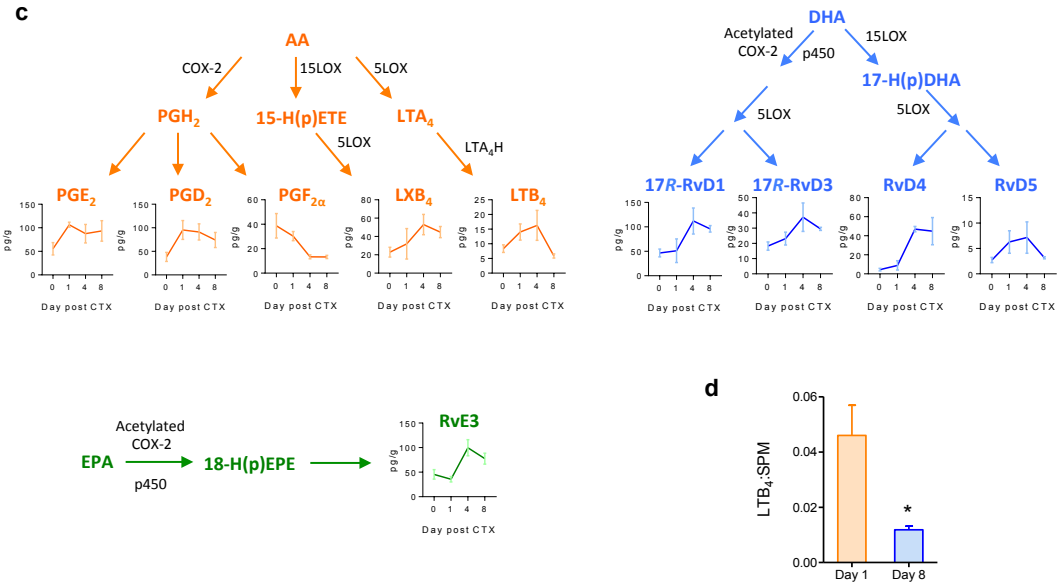

Figure 4. Changes in PUFA metabolomes are conserved across pharmacological and physiological models of skeletal muscle injury. (**a**, **b**) Interaction network pathway analyses of the docosahexaenoic (DHA), arachidonic (AA) and eicospentaenoic (EPA) acid bioactive metabolomes in TA muscle after CTX (**a**) or eccentric exercise-induced injury (**b**). The networks depict both the relative changes of each lipid mediator at day 1 compared to day 0 (color of circle) and the absolute abundance of the mediators at day 1 (size of circle). Compounds that were not detected in the analysis are shown in black, while those that were not included in the analysis are shown in grey. n = 3 per group per time point. (**c**) Quantification of selected lipid mediators from the AA, DHA and EPA bioactive metabolomes depicted in their biosynthetic pathways. (**d**) Ratio of LTB_4 to total SPM (LXA_4, 15*R*-LXA_4, LXB_4, 15*R*-LXB_4, 17*R*-RvD1, RvD2, 17*R*-RvD3, RvD4, RvD5, RvD6, PD1, 17*R*-PD1, 10*S*,17*S*-diHDHA, MaR2, RvE3) at days 1 and 8 post eccentric exercise injury. *p<0.05 (two-tailed unpaired Student's *t*-test). Data are mean ± SEM. and n = 3 per time point.

To further decipher the switch from a pro-inflammatory lipid state to a resolving one, we plotted the ratio of LTB4 to the total amount of specialized pro-resolving lipid mediators at two different time points (days 1 and 8). The levels of the ratio were high at day 1 and greatly declined at day 8, indicating an effective regeneration process. Consequently, changes in the lipid mediator metabolome were apparent in both models, showing a switch from inflammation to resolution, even though the later was visible in the latest time point in the ECI model (day 8), compared to CTX's day 4 (fig. 2f).

iv) Lipid mediator signatures of innate immune cell subsets during muscle injury and regeneration.

Although it is known that leukocytes constitute both biogenic sources and cellular targets of lipids, specifically of lipid mediators, the distinct lipid mediator repertoire of immune cell groups after injury has not been carefully examined. For this reason, we aimed to characterize cellular sources of these biomolecules in inflamed tibialis anterior muscle after cardiotoxin injection. By performing immunofluorescence assays at days 0, 1, 2, 4 and 8 upon muscle tissue injury, we were able to highlight the complete destruction of the tissue's architecture (desmin^{+}; red) together with a synchronous progressive accumulation of macrophages (F4/80^{+}; green) (fig. 5a).

Macrophage infiltration was seen at days 1 and 2, peaking by day 4, while with the restoration of muscle's architecture restoration, the immune cells were largely disappeared. Data from flow cytometry showed an obvious dynamic temporal profile of innate immune cells (neutrophils; fig. 5c, macrophages; figure 5d) upon tissue destruction and during regeneration, in line with previous observations (Varga et al., 2016) . More specifically, Ly6G^{+} neutrophils' accumulation reached its peak at day 1 post CTX injury, declined at day 2 before its rapid clearance by day 4, indicating a switch from the inflammatory to the resolution phase (figure 5b, c). On the other hand, F4/80^{+} Ly6C^{high} macrophages started accumulating at day 1, reaching their maximum at day 2 after muscle tissue's injury, declining in numbers by day 4, before being cleared from the site at day 6. F4/80^{+} Ly6C^{low} macrophages emerged at day 2, keeping elevated levels at days 4-6 (figure 5b, d), suggesting an important role in coordinating the resolution phase of inflammation.

Figure 5

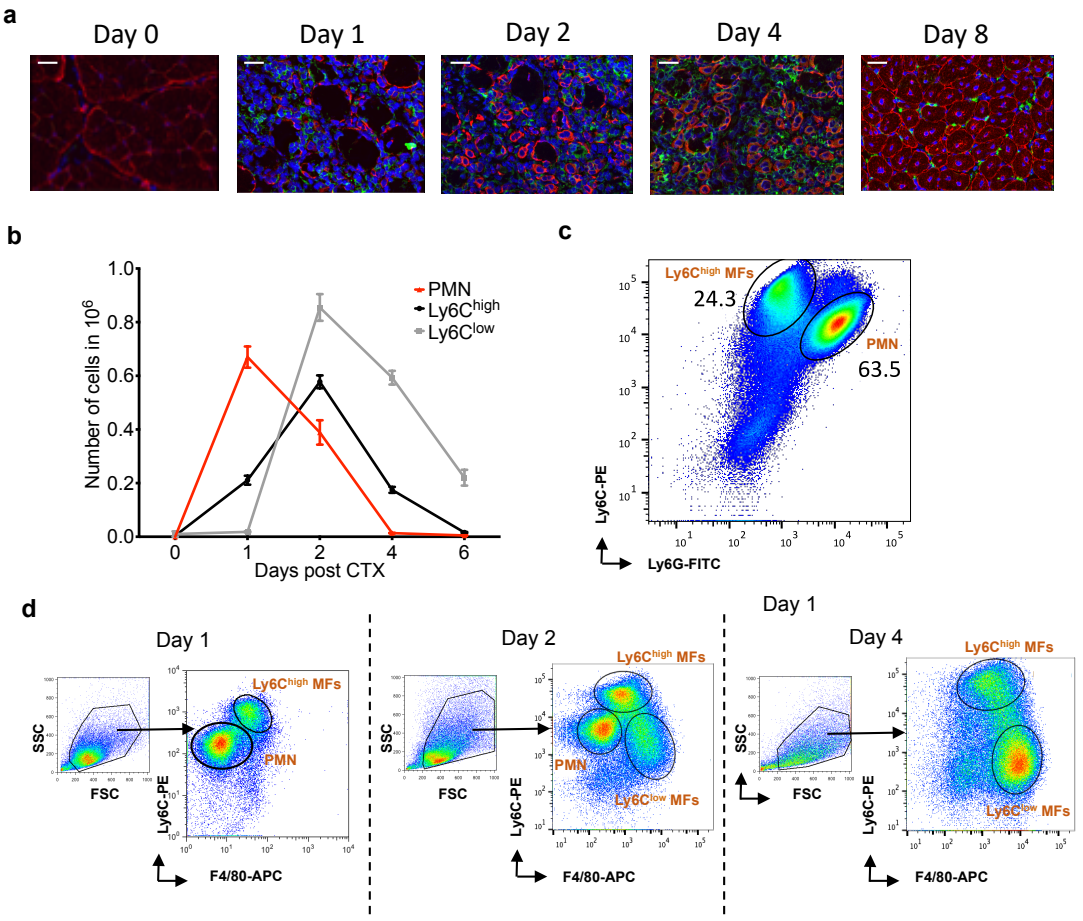

Figure 5. Time course of innate immune cells upon cardiotoxin-induced muscle tissue injury. (**a**) Immunohistochemistry assay of desmin (red), F4/80 macrophages (green) and nuclei (blue) at days 0, 1, 2, 4 and 8 after injury. For days 1-4 scale bars indicate 100 μm, while for days 0, 8 indicate 50 μm. (**b**) Line plot showing the number of infiltrating neutrophils ($CD45^+$ $Ly6G^{high}$ $Ly6C^{int}$ $F4/80^-$), inflammatory macrophages ($CD45^+$ $Ly6C^{high}$ $Ly6G^{low}$ $F4/80^{low}$), and repair macrophages ($CD45^+$ $Ly6C^{low}$ $Ly6G^-$ $F4/80^{high}$) in murine muscle at the marked day upon CTX injury (n=8 muscles/group). (**c**) FACS gating strategy of infiltrating neutrophils at day 1 after injury in murine tibialis anterior muscle. Insets correspond to their number expressed as a percentage of each gated population. (**d**) FACS gating strategy of infiltrating macrophages at days 1, 2 and 4 after injury in murine tibialis anterior muscle. Insets correspond to their number expressed as a percentage of each gated population.

By isolating distinct immune cell populations (neutrophils, $Ly6C^{high}$ and $Ly6C^{low}$ macrophages) through FACS (fluorescence activated cell sorting) (figure 5c, d), we determined their lipid mediator composition profile through LC-MS/MS (liquid chromatography tandem mass spectrometry) at days 1,2 and 4 upon injury. Figure 6a shows the relative abundance of individual

species of lipid mediators after hierarchical clustering, similarly to the analysis performed for the whole muscle tissue (figure 2d). There was notable high expression of AA-derived pro-inflammatory lipid mediators such as PDF_{2a}, PGE_2, LTB_4 and TxB_2 from polymorphonuclear neutrophils of day 1 compared to the macrophage subsets of days 2 and 4. Additionally, the same lipid compounds together with RvD3 exudates, 6-trans- LTB_4 and 7S, 12-trans Mar1 were highly up regulated in $Ly6C^{high}$ macrophages of day 1 compared to their macrophage counterparts. Even if there were some resolving exudates (RvD3 and Mar1) produced by neutrophils, the vast majority of SPMs was produced in relatively higher amounts from macrophages. A noticeable SPM cluster (RvD5, RvD6, RvE3, RvE2, MaR1, MaR2 and 15*R*-LXA_4) was witnessed in both macrophage populations of day 4. Interestingly, this SPM cluster seems to be highly down-regulated in macrophages of day 2 and neutrophils of day 1, at the inflammatory phase of the immune response to injury. Lipid mediator profile of macrophages of day 2 was in a high extent comparable, but with some key differences. For instance, $Ly6C^{low}$ macrophages of day 2 had a decreased production of pro-inflammatory exudates compared to $Ly6C^{high}$ macrophages of the same day. A striking difference was the decreased expression of RvD2, LxA_4, LxB_4 and RvD5 from $Ly6C^{high}$ compared to $Ly6C^{low}$ macrophages of day 2. To assign correlations between the global lipid mediator profile to different cell subsets of the inflammation time-course, a supervised regression method was applied based on a linear classification model, explaining more than 68% of the variance based on the principal components 1 and 2 . More specifically, through partial least squares-discriminant analysis (PLS-DA), we discovered that there was a partial overlap between neutrophils of day 1 and macrophage subsets ($Ly6C^{high}$ and $Ly6C^{low}$) of day 2 (fig. 6b). Contrary to this, both day 4 macrophage populations displayed a pronounced partition and clustered separately into their distinct classes based on their Ly6C protein marker.

Figure 6

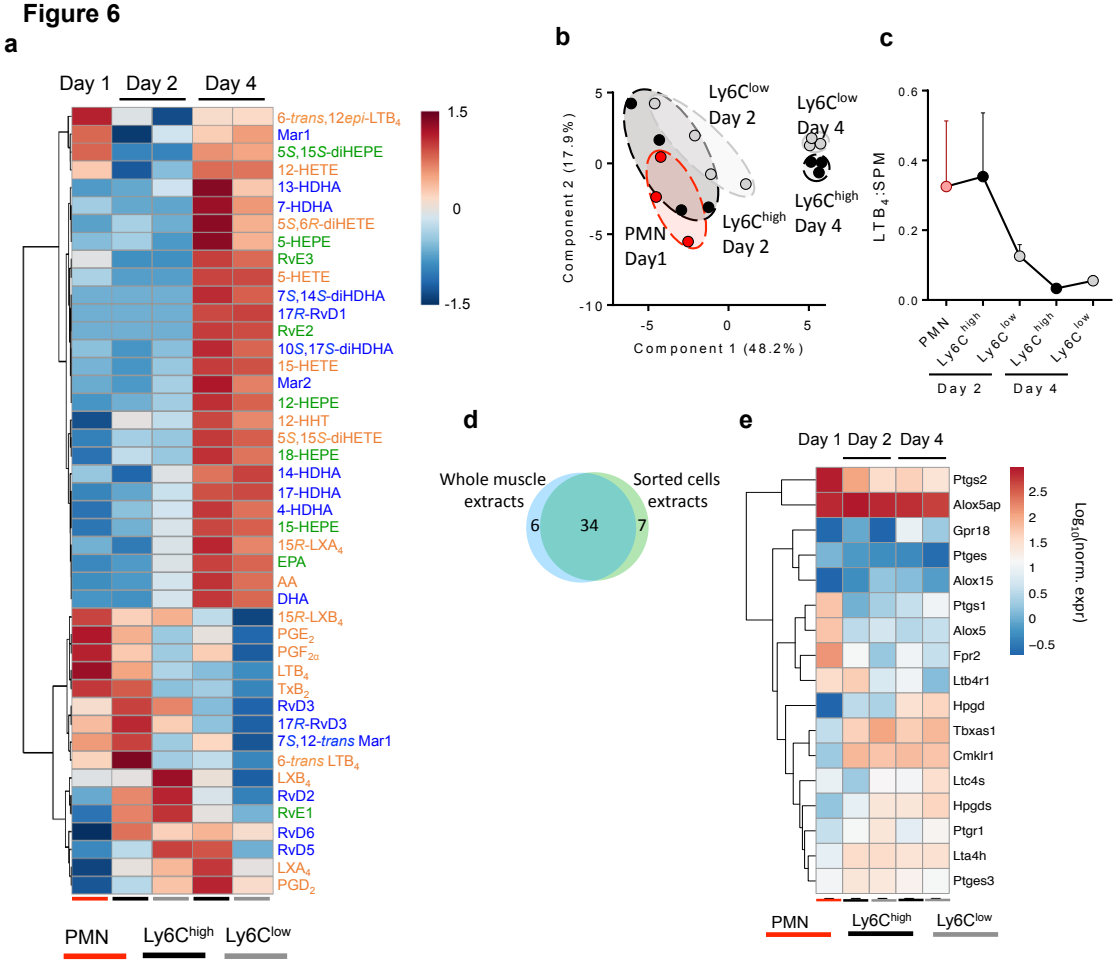

Figure 6. Lipid mediator content, transcriptomic expression of their receptors and of key enzymes in AA-, DHA- and EPA-metabolism are representative of innate immune cell types after muscle tissue injury and during regeneration. (a) Heatmap showing the relative expression of lipid mediators produced from neutrophils and macrophage populations (Ly6C^{high} and Ly6C^{low}) at the indicated day post injury. **(b)** 2-dimensional score plot of the PLS-DA presents the distinct sample clusters, in relation to the global lipid mediator profile and the leukocyte cell subsets at the indicated day post injury. **(c)** Ratio of LTB_4 to total SPM (15*R*-LXA_4, LXB_4, LXA_5, LXB_5, 17*R*-RvD1, RvD2, 17*R*-RvD3, RvD4, RvD5, 10*S*,17*S*-diHDHA, MaR1, RvE1, RvE2, RvE3) at the indicated day post injury. **(d)** Integration of the identified lipid mediator pool from whole muscle extracts (blue) and distinct immune cells (green), presented as a Venn diagram. (e) Heatmap showing the relative abundance of selected genes (lipid mediator receptors – signal transducers in lipid metabolism) using hierarchical clustering analysis based on Ward's clustering algorithm and Euclidean distance as a measure. Data are mean ± SEM. and n = 3 per time point

By calculating the LTB_4 to the sum of SPMs ratio as an indicator of inflammation , we sought to understand the state of the cell based on their lipid mediator profile, as described previously. The ratio was elevated in neutrophils of day 1 and Ly6C^{high} macrophages of day 2 when compared to

the macrophage populations of day 4 (fig. 6c). At Ly6C^{low} cells of day 2, the ratio gets reduced, reaching its lowest values at macrophages of day 4. This is indicative of a switch from a pro-inflammatory phase to resolution and tissue regeneration. Venn diagram of figure 6d shows that 34 of the lipid mediators were common between the two datasets, while 7, that include RvD6, LXA4, 15R-LXA4 and Mar2, were found only in sorted immune cell subsets. Finally, 6 lipid mediators, that include the specialized pro-resolving lipid mediators LxA_5, LxB_5 and RvD4, were not assigned to individual immune cell subsets, suggesting that they are probably produced by alternate cellular sources. RNA-seq analysis on isolated leukocyte populations was performed at days 1,2 and 4 after CTX-induced injury. Heatmap (fig. 6e) shows the relative abundance of biosynthetic enzymes of lipid mediators, together with the expression profile of their receptors. Cyclooxygenases 1 and 2 (*Ptgs1* and *Ptgs2*, respectively as named in the heatmap) and prostaglandin synthase E (*Ptges*) are elevated in neutrophils of day 1 compared to both types of macrophages at days 2 and 4, which is expected as levels of PGE2 (prostanoid) were simultaneously higher in neutrophils compared to other cell types (figure 6a). Hematopoietic prostaglandin synthase D (*Hpdgs*) , which is a key enzyme in the conversion of arachidonic acid to downstream prostaglandin D2 was relatively elevated in macrophage populations compared to day 1 neutrophils, agreeing with the elevated levels of prostaglandin D2 in Ly6C^{high} and LY6C^{low} macrophages of days 2 and 4. Leukotriene biosynthetic pathway is regulated by the expression of arachidonate lipoxygenase 5 (*Alox5*) and arachidonate 5-lipoxygenase protein (*Alox5ap*), whose levels are higher in PMNs, albeit the expression of *Alox5ap* keeps getting expressed in macrophages at days 2 and 4. *Ltb4r1*, leukotriene's receptor's relative expression was elevated in neutrophils of day 1 and Ly6C^{high} macrophages of day 2, while leukotriene A4 hydrolase (*Lta4h*) keeps elevated levels in both macrophage subsets at days 2 and 4 compared to neutrophils of day 1. Most of the SPM's biosynthetic pathways require the collaboration of *Alox5* and arachidonate lipoxygenase 15 (*Alox15*). Contrary to *Alox5*, *Alox15* is expressed higher in macrophage populations at days 2 and 4

relatively to neutrophils of day 1. *Fpr2*, intracellular receptor of RvD1 and LXA_4, expressed throughout the whole time-course but relatively higher in neutrophils, denoting the effector action, these 2 lipid mediators have in limiting the PMN infiltration at the site of active inflammation. Contrary, resolvin's D2 receptor, *Gpr18* (Chiang et al., 2015), shows an up-regulation in day 4 $Ly6C^{high}$ macrophages, compared to the other cell types in previous days but also compared to $Ly6C^{low}$ macrophages of day 4, indicating a role in resolution of active inflammation.

v) Effect of Ibuprofen on lipid mediators after injury.

Our next goal was to determine if obstruction of the production of the bioactive lipid mediator molecules could affect the inflammation dynamics in regard to the infiltrating immune cell subtypes. To interfere with their orderly and dynamic production, we performed CTX-injury in murine muscle while treating them with a generally used anti-inflammatory non-steroidal drug, ibuprofen (IBP) (fig. 7a). More precisely, ibuprofen was administered at days 0 (together with cardiotoxin), 1, 2 and 3. Samples were harvested for lipidomic analyses at the end of day 1, 2 and 4, while FACS analysis was performed on samples collected at the end of day 2 and 4. IBP treatment highly inhibited the production of COX-derived pro-inflammatory lipid mediator molecules (PGF_{2a}, PGE_2, PGD_2 and TxB_2) 28 hours after its administration, as expected (fig. 7b). At day 2 , IBP caused a dysregulated production of lipid mediators, up-regulating pro-inflammatory molecules, while it down-regulated specialized pro-resolving molecules such as RvD_3, RvD_4 and 15R-LxB_4 (light green circles. FC<1). At day 4, all the identified lipid mediators were increased in absolute numbers (size of the circle) and up-regulated after IBP treatment compared to untreated mice (fig. 7c). Interestingly, treatment with IBP didn't influence the number of infiltrating $CD45^+$ cells (fig. 7d) but affected the frequency of live cells (expressed as a percentage) in the comparisons between IBP treated and untreated mice, both at days 2 and 4 (fig. 7e-f).

Figure 7

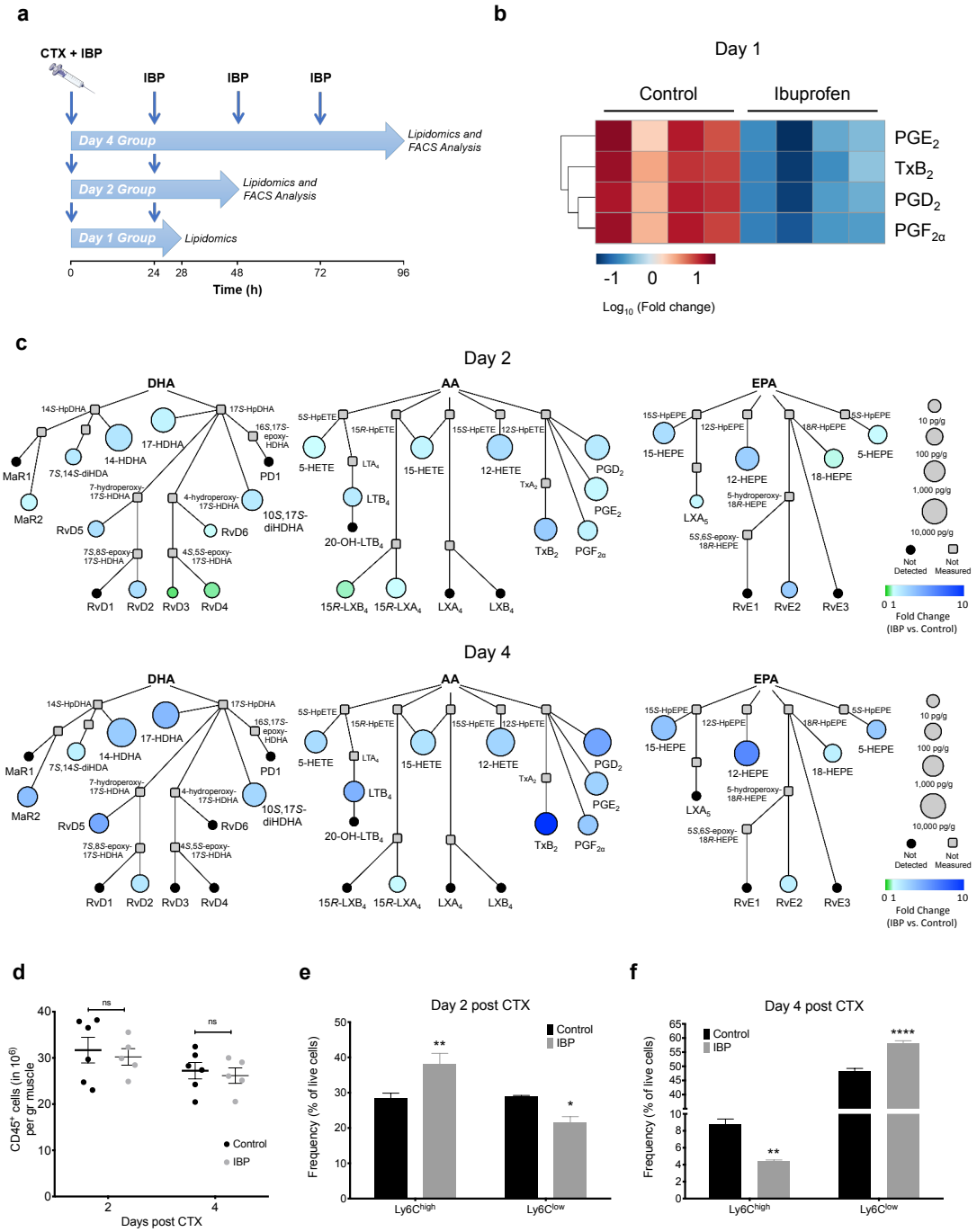

Figure 7: COX inhibition through ibuprofen alters the lipid profile and phenotype of macrophages following CTX injury. (a) Graphical representation of the working workflow and downstream lipid mediator identification and FACS analyses, after CTX-induced muscle injury and ibuprofen (IBP) treatment. **(b)** Heatmap displaying the $\log_{10}$ fold change relative abundance of pro-inflammatory lipid mediator molecules in tibialis anterior muscle at day 1 after cardiotoxin-induced muscle injury and ibuprofen (IBP) treatment. **(c)** Interaction network pathway analyses of the docosahexaenoic (DHA), arachidonic (AA) and eicospentaenoic (EPA) acid bioactive metabolomes in tibialis anterior muscle after CTX at days 2 (top) and 4 (bottom) in the comparison between ibuprofen (IBP) treated and untreated mice. **(d)** Absolute number of $CD45^+$ cells isolated from tibialis anterior

muscles at indicated timepoints following CTX-induced injury in untreated and ibuprofen (IBP) treated mice. **(e)** Percentage of inflammatory (Ly6C^{high} F4/80^{low}) and repair (Ly6C^{low} F4/80^{high}) macrophages at day 2 following CTX-induced injury in untreated and ibuprofen (IBP) treated mice. **(f)** Percentage of inflammatory (Ly6C^{high} F4/80^{low}) and repair (Ly6C^{low} F4/80^{high}) macrophages at day 4 following CTX-induced injury in untreated and ibuprofen (IBP) treated mice. p<0.05=*, p<0.01=**, p<0.0001=**** (Sidak's multiple comparisons test in two-way ANOVA). Data are shown as mean ± SEM, n = 5 mice per group.

These data serve as evidence of the impact a pharmacological substance can have in the production dynamics of the affected lipid mediators and macrophage subtype specification.

vi) ATAC-seq analyses reveal the remodeling of the muscle infiltrating epigenome.

To illuminate the contribution of myeloid immune cell subsets in shaping the epigenome during skeletal muscle tissue injury and regeneration, we took an unbiased genomic approach based on ATAC-seq (Array for Transposase-Accessible Chromatin) analysis.

Figure 8

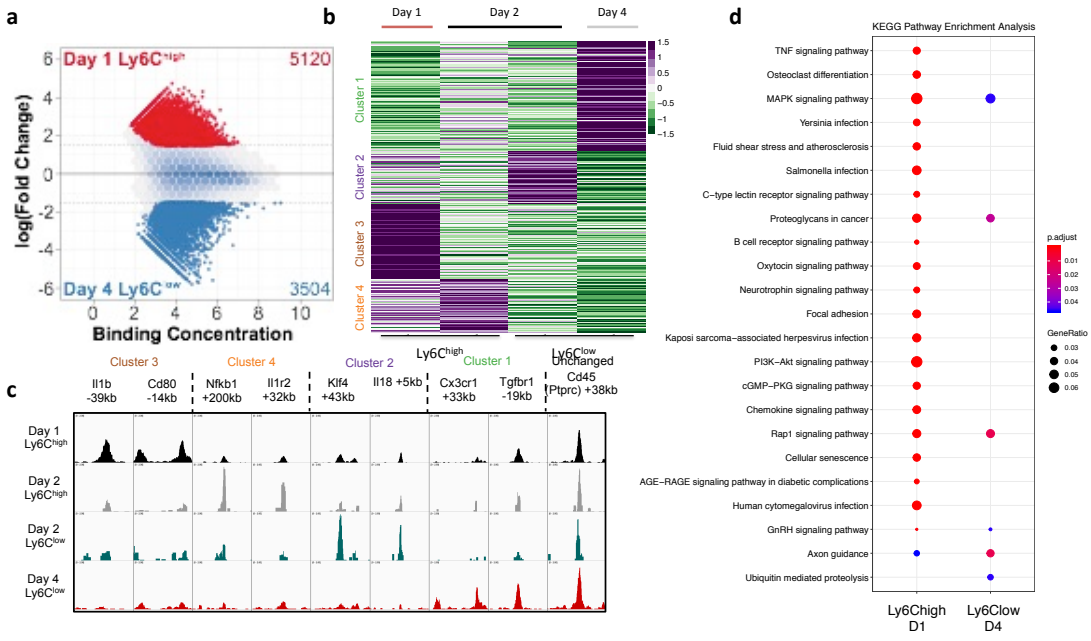

Figure 8: Chromatin accessibility landscape in isolated Ly6C^{high} and Ly6C^{low} macrophages. (a) Differential chromatin openness between pro-inflammatory Ly6C^{high} macrophages at day 1 post injury and Ly6C^{low} macrophages at day 4. Statistically significant changes (fold change (FC) >1.,5 and false discovery rate (FDR) < 0.05) are shown in the dot plot (log2FC versus average binding concentration). **(b)** Heatmap representation of 4 defined clusters with differential bound regions related to chromatin openness from the comparison between pro-inflammatory Ly6C^{high} macrophages at day 1 post injury

and Ly6C^{low} macrophages at day 4. K-means clustering was performed for 8624 differentially accessible sites (fold change >1.5 and FDR< 0.05). **(c)** IGV view of distal regions of well-known inflammatory and repair associated markers (two examples shown for each cluster) after ATAC-seq analysis. **(d)** Dot plot highlighting the functional categories found to be enriched in 5120 exclusively differentially bound regions of Ly6C^{high} macrophages at day 1 post injury and in 3504 exclusively differentially bound regions of Ly6C^{low} macrophages at day 4.

This approach allowed us to elucidate the chromatin accessibility upon tissue injury during the phenotypic switch from pro-inflammatory Ly6C^{high} macrophages to their reparative Ly6C^{low} macrophage counterparts. Our focus on the comparison between Ly6C^{high} macrophages of day 1 and Ly6C^{low} macrophages of day 4 showed that there was a cumulative composition of 8624 differentially bound sites, from which 5120 were up-regulated in the pro-inflammatory leukocytes of day 1 and 3504 were exclusively elevated and statistically significant for reparative macrophages of day 4 (fig. 8a). The dynamic kinetics of closed and open chromatin regions during inflammation were highlighted when these 8624 differentially bound sites were subjected to k-means cluster analysis. As can be seen in figure 8b (heatmap), cluster 3 is representative of macrophages of the highly inflammatory phase, right after CTX injury. Clusters 2 and 4 correspond to temporary-transient chromatin accessibility changes during the switch from a pro-inflammatory to a reparative phenotype, which is happening mainly at day 2 (both functionally diverse macrophage phenotypes exist at day 2). Cluster 1 is associated with highly induced chromatin regions of Ly6C^{low} macrophages of day 4. As can be shown in figure 8c, well established inflammatory markers such as Il1b, Cd80, Nfkb1 and Il1r2 were induced early (belong to clusters 3 and 4) and are characteristic for pro-inflammatory Ly6C^{high} macrophages, while repair associated markers (Klf4, Il18, and Tgfbr1) are elevated in clusters 1 and 2, which correspond to regions induced in Ly6C^{low} macrophages of days 4 and 2, respectively. KEGG pathway enrichment analysis for the differentially bound peaks from Ly6C^{high} macrophages of day 1 and Ly6C^{low} macrophages of day 4 (fig. 8d) showed that one intracellular signalling pathway activated during the phenotypic switch of macrophages is the mitogen-activated protein kinase (MAPK) pathway. Additionally, Rap1 signalling pathway was enriched. Rap1 is a ubiquitous protein that plays an essential role in the control of

metabolic processes, such as signal transduction from plasma membrane receptors, cytoskeleton rearrangements necessary for cell division, intracellular and substratum adhesion, as well as cell motility and leukocyte movements.

vii) Inflammation dynamics upon muscle tissue injury in mice based on transcriptomic data.

To further decipher the gene expression dynamics upon sterile muscle tissue injury, RNA-seq analyses were performed on isolated Ly6C^{high} (at days 1, 2 and 4) and Ly6C^{low} (at days 2 and 4) immune cell subsets (see fig. 5b,d for gating strategy) after CTX. To elucidate the kinetics of inflammation, transcriptomic profile of Ly6C^{high} macrophages at day 1 (highly inflammatory stage upon injury) was compared to the profile of Ly6C^{high} and Ly6C^{low} macrophage cell groups, both at days 2 and 4. Results of these comparisons, highlighting the differentially expressed genes , are shown below at table 2.

Differentially Expressed Genes (DEGs)	Ly6C^{high} Day 1 vs Ly6C^{high} Day 2	Ly6C^{high} Day 1 vs Ly6C^{high} Day 4	Ly6C^{high} Day 1 vs Ly6C^{low} Day 2	Ly6C^{high} Day 1 vs Ly6C^{low} Day 4
Up-regulated	607	3504	2829	3698
Down-regulated	501	1811	2191	2458
Sum of DEGs	1108	5315	5020	6156

Table 2: Number of differentially expressed genes at the indicated comparisons after DEseq analysis (explained in methods)

Several genes that are differentially expressed in the pairwise comparisons described above, are common between comparisons. To illuminate, unique tracks of genes (unique records), four way venn comparison was applied. As it shown at figure 9a, 8425 individual genes were found (sum of the different sections at the Venn diagram), the majority of which was common in the comparison Ly6C^{high} Day 1/ Ly6C^{low} Day 2 (green circle) to Ly6C^{high} Day 1/ Ly6C^{low} Day 4 (yellow circle) (intersection between these two circles gives a sum of 3733 genes). Interestingly, 29 genes were differentially expressed (up-, or down-regulated with absolute fold change > 1.5 and adjusted pvalue < 0.05) only in the comparison Ly6C^{high} Day 1/ Ly6C^{high} Day 2.

Figure 9

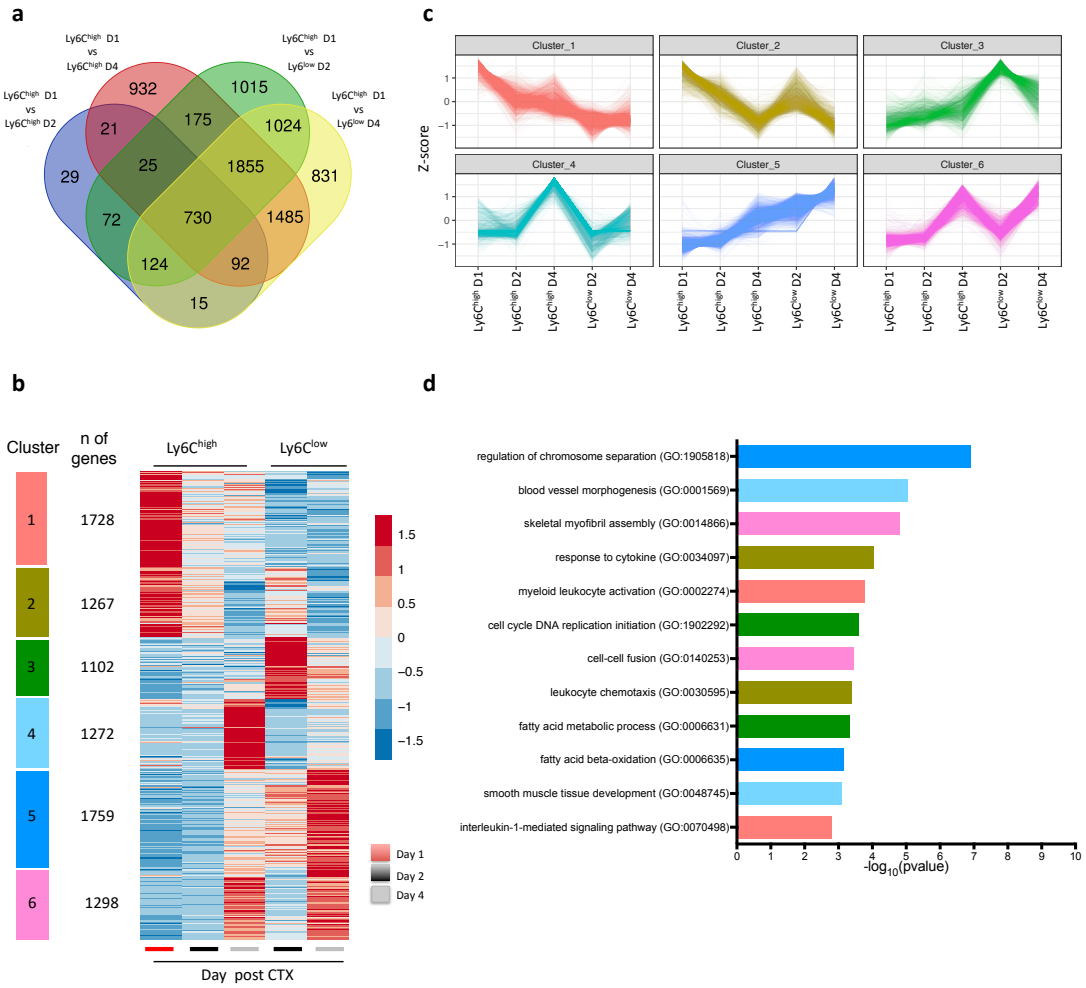

Figure 9: Transcriptomic data reveal the inflammation dynamics upon muscle tissue injury in mice (a) Venn diagram showing the intersection of differentially expressed genes in the following comparisons: Ly6C^{high} Day 1 vs Ly6C^{high} Day 2 (blue), Ly6C^{high} Day 1 vs Ly6C^{high} Day 4 (red), Ly6C^{high} Day 1 vs Ly6C^{low} Day 2 (green) and Ly6C^{high} Day 1 vs Ly6C^{low} Day 4 (yellow). **(b)** Heatmap representation of 6 defined clusters with differential expression values K-means clustering was performed for 8425 differentially expressed genes (fold change >1.5 and adjusted p-value< 0.05) Z-score of the expression values was used to visualize the dynamically changing expression pattern of immune cells after CTX injury. **(c)** Line plots displaying the centered and scaled expression values of the aforementioned genes. **(d)** Gene ontology analysis of differentially expressed genes based on selected terms (color coded based on which cluster the genes used for the gene set enrichment analysis belong) (absolute fold change threshold > 1.5 and Bonferroni corrected p-value < 0.05). Line plots show the negative $\log_{10}$ p-value.

Moreover, 932, 1015 and 831 were exclusively differentially expressed at the comparisons Ly6C^{high} Day 1/ Ly6C^{high} Day 4, Ly6C^{high} Day 1/ Ly6C^{low} Day 2 and Ly6C^{high} Day 1/ Ly6C^{low} Day 4, respectively. 8425 individual genes were

subjected to k-means clustering (k=6) based on their centered and scaled average expression values. Heatmap (fig. 9b) and line plots (fig. 9c) show the dynamically changing transcriptomic profile of immune cell subsets after CTX injury. Cluster 1 (salmon) is occupied by 1728 genes that correspond to Ly6C^{high} macrophages regardless the day upon injury, assigning them a specific transcriptional signature, while genes of cluster 2 (1267 genes – mustard) facilitate the immune response in earlier time points at the time course of tissue regeneration (days 1 and 2). In both clusters, expression of these genes is relatively higher for LyC^{high} macrophages of day 1. Cluster 3 (green) with 1102 genes is highly up-regulated in LyC^{low} macrophages of day 2, keeping high relative abundance based on the expression of these genes in Ly6C^{low} cell subsets of day 4. In cluster 4 (sky blue), 1272 genes are found to be especially up-regulated in Ly6C^{high} macrophages of day 2, while 1759 genes of cluster 5 (deep blue) correspond to Ly6C^{high} macrophages of day 2 and reparative Ly6C^{low} macrophages. Interestingly, cluster 6 (violet), has 1298 genes, whose relative abundance is higher in LyC^{low} immune cells subsets, assigning them a specific transcriptional signature. Gene set enrichment analysis was performed for the genes participating in each identified cluster to highlight the functional categories in which they belong. Selected terms that were found to be enriched and statistically significant after Bonferroni correction are shown (fig. 9d - color coded based on their assigned cluster). It can be seen that cluster 1 (salmon) is enriched in terms related to myeloid leukocyte activation and IL-1 mediated signaling. Genes associated with myeloid leukocyte activation include *Tlr2* and *Tlr4* (Toll-like receptors 2 and 4), *Fpr2* (formyl peptide receptor 2) and *Cxcl5* (C-X-C chemokine 5). Response to cytokine and leukocyte chemotaxis were enriched terms for genes participating at cluster 2, which is associated with Ly6C^{high} pro-inflammatory macrophages. Several chemokines are related to leukocyte chemotaxis (*Ccl2, Ccl6, Ccl7*), while apoptosis regulator *Bcl2* and C-X-C motif chemokine 2 (*Cxcl2*) are involved in response to cytokine. Enriched terms of genes belonging to cluster 3 include fatty acid metabolic process and cell cycle DNA replication. Cluster's 4 statistically significant terms include blood vessel

morphogenesis (*Col4a1, Tek, Cxcl12, Flt1, Ednra)* and muscle development (*Pdgfrb, Zfp950,Col3a1, Tshz3, Mylk*). Cluster 5, whose genes are associated with the reparative phase of inflammation, include terms such as fatty acid beta-oxidation and regulation of chromosome separation. Finally, cluster 6 is enriched in terms such as skeletal muscle myofibril assembly and cell-cell fusion. Muscle myofibril assembly includes genes such as myomesins 1, 2 and 3 (*Myom1, Myom2* and *Myom3*), titin (*Ttn*), alpha actin in skeletal muscle (*Acta1*) and leiomodin-3 (*Lmod3*).

viii) RvD2 induces specific macrophage gene expression changes.

Based on the analyses shown so far, it becomes obvious a potential effector activity of lipid mediators that it is coupled with changes in the muscle tissue injury and regeneration time course. Therefore, we decided to assess the effect of lipid mediators in macrophage-dependent muscle tissue's repair. We decided to focus on RvD2 for the following reasons: (1) it is a known potent regulator of resolution of inflammation (Serhan, 2014; Spite et al., 2009); (2) it is produced in a dynamic fashion primarily by repair type macrophages (see fig. 6a); (3) its receptor (*Gpr18*) was expressed in inflammatory macrophages, suggesting a role in inter-macrophage communication (see fig. 6e); and (4), it was present in both muscle injury models (see fig. 2d, 4a, 4b, and 6a). As has been described previously, RvD2 could act as a signaling molecule on macrophage immune cells by enhancing a process called efferocytosis (Glaudemans et al., 2013; Spite et al., 2009). Efferocytosis is an active process that involves the clearance of apoptotic cells by phagocytic cells such as macrophages (Glaudemans et al., 2013). It is undiscovered yet the way RvD2 influences gene expression programs in naïve macrophages. To this end, bone marrow derived macrophages (BMDMs) were isolated and treated with RvD2 for four hours (4h), while untreated BMDMs were used as control samples and compared to the first in regard to their transcriptomic profile using RNA-seq. Cumulatively, 751 genes appeared to be differentially expressed in the comparison between control to RvD2 treated samples (fold change (FC) >1.5; pval<0.05). From them 310 were upregulated in the

untreated BMDMs, while 441 were found to be upregulated in the RvD2 treated samples. Heatmap at figure 10a displays the top 120 differentially expressed genes based on the highest absolute fold change differences in the comparison between the two conditions.

Figure 10

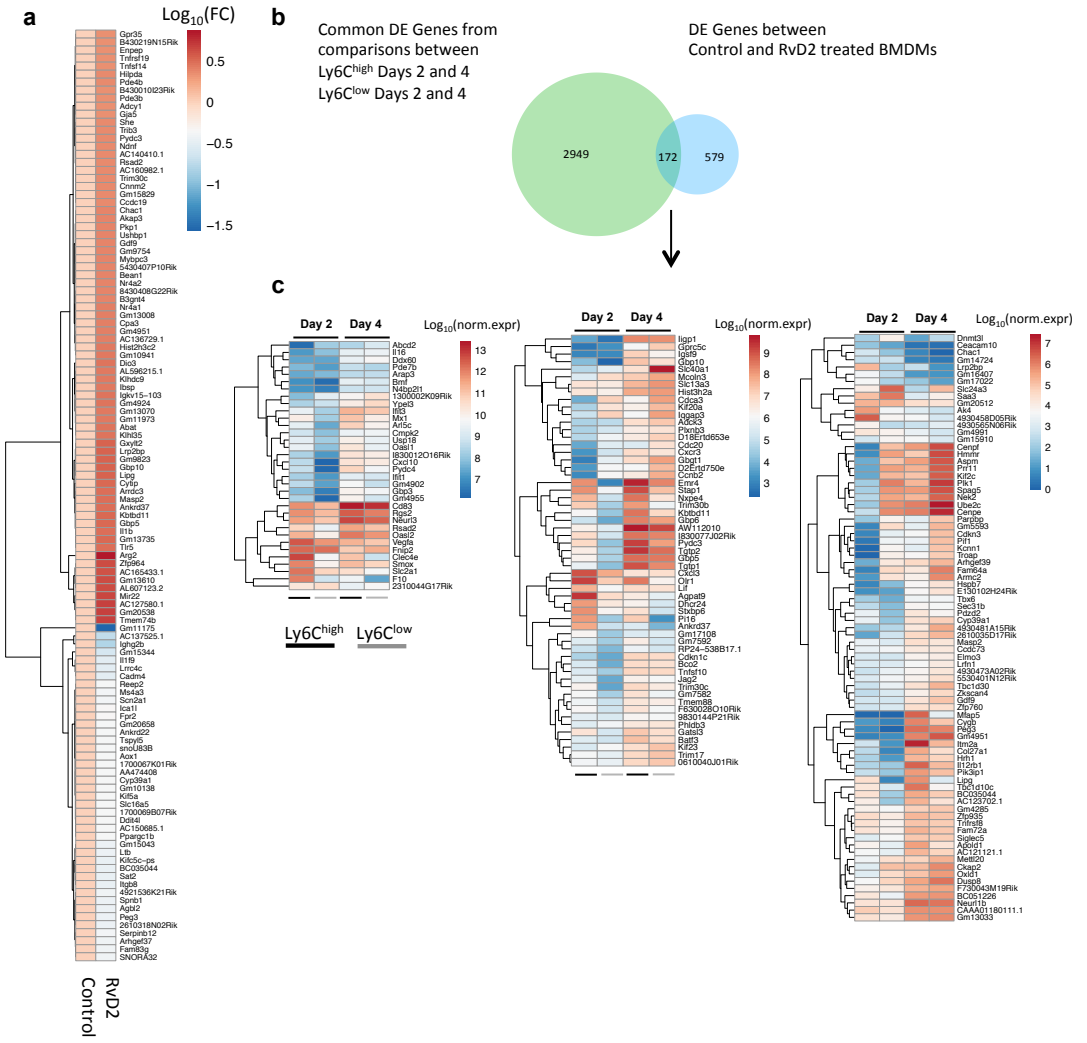

Figure 10. RvD2 generates a sui generis transcriptomic profile in bone marrow derived macrophages (BMDMs), which resembles the transcriptomic changes during the progress from inflammation to resolution after muscle injury and during regeneration. (a) Heatmap displaying the top 120 differentially expressed genes in control versus RvD2 treated BMDMs. For visualization purposes fold change is shown in $\log_{10}$ scale. **(b)** Integration of the differentially expressed genes (DE) found in the comparison between control/ RvD2 treated samples with the common differentially expressed (DE) genes during the transition from day 2 to day 4. 172 genes were found to be part of the intersection between the indicated groups, as shown in the Venn diagram. **(c)** Heatmaps displaying the $\log_{10}$ normalized of the 172 common differentially expressed genes in the following datasets: control-RvD2 vs. $Ly6C^{high/low}$ at days 2/4. Hierarchical clustering analysis was applied based on Ward's clustering algorithm and Euclidean distance as a measure

Regulators of transcription (*Nr4a1, Nr4a2),* genes that participate in arginine metabolism (Arg2), host defense (*Tlr5, Masp2, Gbp10, Gbp5, Rsad2*) and G-protein/ cAMP signaling (*Pde4b , Adcy1, Akap3, Gpr35*, *Arrdc3*) were found to be up regulated after RvD2 treatment. Gene ontology enrichment analysis was performed for the differentially expressed genes between control and RvD2 treated BMDMs. As shown in figure 11a, several functional categories (GO terms) were found to be enriched and statistically significant. These term include pathways related to response to a molecule of bacterial origin (up regulated: *Gbp6, Tlr2, Ticam2, Cmpk2, Stap1, Cd14),* movement of a subcellular component (up regulated: *Enpep, Ccdc40, Wnt11;* down regulated: *Elmo3*, *P2ry1, Kif22, Kif23, Celsr2, Cdk5r1*), and chemotaxis (up regulated: *Cxcl3, Cxcr4, Cxcl10, Nr4a3, Vegf, Gab1;* down regulated: *Kif5a, Plxnb3, Robo1).* Collectively, these results indicate that RvD2 generates a *sui generis* transcriptional signature in naïve macrophages.

Figure 11

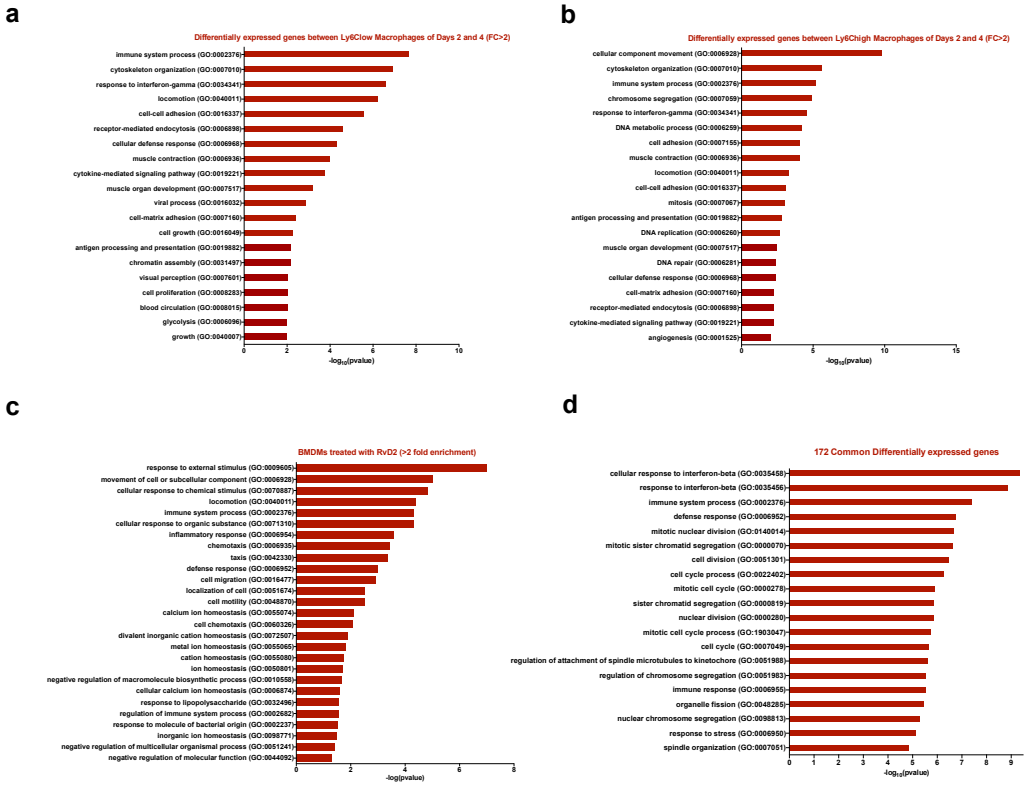

Figure 11: Gene ontology analysis of differentially expressed genes in Ly6C^{high} macrophage subsets compared with RvD2-treated macrophages. (a) Gene ontology (GO) analysis of the genes that are differentially expressed in control and RvD2 treated BMDMs. Fold enrichment threshold was set at >2. (**b**) Gene ontology (GO) analysis of the genes that are differentially expressed in Ly6C^{high} macrophages at days 2 and 4 post CTX. Fold enrichment threshold was set at >2. The data were annotated to Panther GO-Slim Biological Process. Fisher's Exact with FDR multiple test correction was performed for the submitted data. (**c**) GO analysis of the genes that are differentially expressed in Ly6C^{low} macrophages at days 2 and 4 post CTX. Fold enrichment threshold was set at >2. The data were annotated to Panther GO-Slim Biological Process. Fisher's Exact with FDR multiple test correction was performed for the submitted data. (**d**) GO analysis of the differentially expressed genes identified through the GeneVenn software during the integration of the genes modulated by RvD2 in bone marrow-derived macrophages and the genes modulated during the inflammatory (Ly6C^{high}) to repair (Ly6C^{low}) transition during CTX-induced muscle injury. Fold enrichment threshold was set at >2.

Next, we integrated the changes discovered after RvD2 treatment of BMDMs with the transcriptional changes occurring in Ly6C^{high} and Ly6C^{low} macrophage immune subsets, when their profile at day 2 is compared with their profile at day 4 upon muscle tissue injury, during the switch from inflammation to resolution of it, performing RNA-seq analysis. More specifically, we highlighted the changes between Ly6C^{high} macrophages of day 2 and Ly6C^{high} macrophages of day 4, and Ly6C^{low} macrophages of day 2 and Ly6C^{low} macrophages of day 4. Firstly, from the comparison between the Ly6C^{high} entities of days 2 and 4, we identified 5021 differentially expressed genes (1689 and 3332 and upregulated genes, respectively). The comparison between the Ly6C^{low} entities of days 2 and 4, showed 4966 differentially expressed genes (1893 and 3073 and upregulated genes, respectively). Gene ontology enrichment analysis of the 5021 differentially expressed genes shows that they participate in functional categories associated with cell adhesion, muscle organ development, locomotion and cytoskeleton organization (fig. 11b). Gene ontology enrichment analysis of the 4966 differentially expressed genes indicates that they are part of functional categories related to similar categories to the aforementioned (muscle organ development, locomotion and cytoskeleton organization), but also in terms related to cell-cell adhesion, cell proliferation and blood circulation(fig. 11c). Gene Venn software (Mehdi Pirooznia, 2007) was used to integrate the

resolvin D2 modulated genes to the genes that are expressed differentially during the transition from inflammation (day 2) to resolution (day 4). Figure 10b (Venn diagram) shows that 172 genes were common, while heatmaps of figure 10c, display their normalized expression profile. Resolvin D2 caused an upregulation in a lot of genes (*Arap3, Cxcl10, Gbp3, Il16, Abcd2, Vegfa, Mx1, Cd83, Rgs2, Usp18, Pydc4*) that were very highly expressed in macrophages of day 2 compared to macrophages of day 4. Analogous gene cluster similarities were shown in those with more moderate overall expression but that were highly induced selectively in both Ly6C^{high} and Ly6C^{low} macrophages at day 4 (*Pydc3, Gbp6, Gbp5, Elmo3, Hist3h2a, Gdf9, Kbtbd11, Slc13a3*). Gene set enrichment analysis of the 172 common differentially expressed genes highlighted their participation in functional categories related to cell division, mitotic cell cycle, response to stress and defense responses (fig. 11d). We can now conclude that resolvin D2 generated a specific transcriptional signature, which is similar to the macrophage transcriptional phenotype at the first stages of the resolution (day 4/ reparative phase) upon muscle tissue injury and regeneration.

ix) RvD2 is an effector of macrophage subtype specification.

After seeing that RvD2 is mainly produced at later stages, during the resolution phase of the inflammation time-course and that it generates a specific transcriptional signature, when used as a treatment in BMDMs that highly resembles the transcriptomic profile of macrophages of day 4 after CTX-induced injury, we sought to understand if exogenous delivery through intramuscular injection of RvD2, could fine-tune the phenotypic switch from Ly6C^{high} to Ly6C^{low} macrophages, which have been shown to promote tissue's regeneration (Patsalos et al., 2017; Sager, Kessler, & Schunkert, 2017). Bone marrow transplantation (BMT) model was applied, causing a delay in the switch from pro-inflammatory to resolving macrophage immune subsets, obstructing the muscle tissue's regeneration (Patsalos et al., 2017). CD45 recipient congenic murine populations after BMT, were injured through CTX. At days 2 and 3 after injury, recipient mice were injected with RvD2

intramuscularly. An RvD2 concentration of 4μg/kg was applied to mice, reaching an acute intramuscular status that is comparable with its endogenous levels. Its biologically active dose was determined through a deuterated analog of RvD2, to distinguish from endogenous RvD2, showing that the intramuscular in vivo treatment with 4μg/kg is similar to that produced endogenously i.e., 200 pg/g) at 2h post administration). Deuterated RvD2 was no longer detectable after 3h, indicating that the dosing regimen was not supraphysiological (fig. 12a, b).

$CD45^{+}$ cells from RvD2 treated mice were counted at day 4 (fig. 12c) showing that RvD2 didn't affect their total amount, while FACS analysis of $Ly6C^{high}$ $F4/80^{low}$ and $Ly6C^{low}$ $F4/80^{high}$ murine muscle cells was performed at the same time-point (fig. 12d). $Ly6C^{low}$ macrophages constituted a small fraction of 10% of live cell in saline treated mice, while their numbers were greater when treated with RvD2 at day post injury (16% of live cells). Interestingly, when mice were treated with RvD2 at the third day post CTX-induced injury, their proportion at the fourth day was doubled to 20%. By calculating each LyC^{high} and $Ly6C^{low}$ cell population at the indicated time-points, it is shown that RvD2 caused a reduction in the amount of LyC^{high} macrophages in the comparison between saline treated to both treated regimens (fig. 12e).

Figure 12

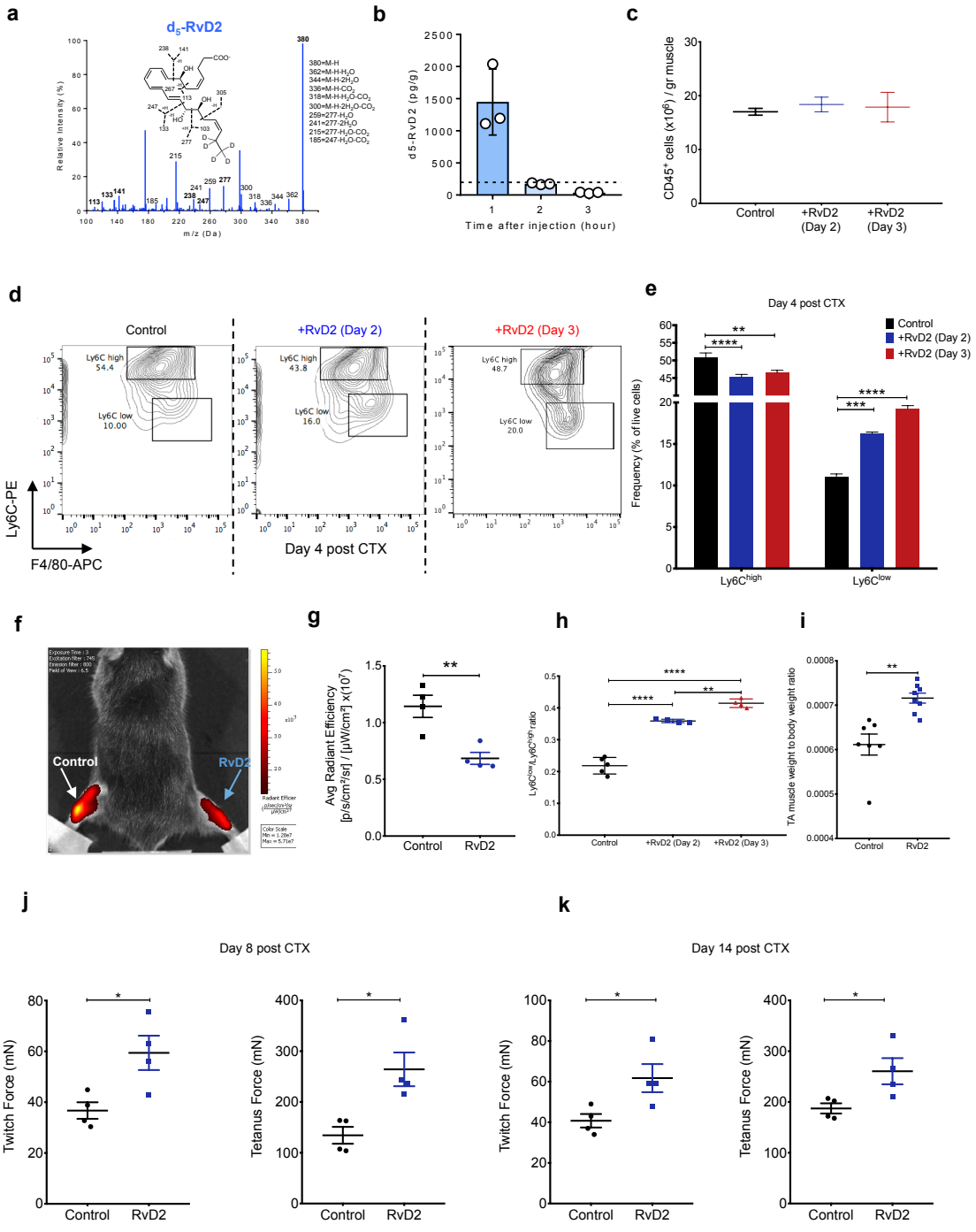

Figure 12: . RvD2 promotes conversion of Ly6C^{high} to Ly6C^{low} macrophages and improves *in vivo* force generation in a model of delayed muscle regeneration. (a) Deuterium-labeled resolvin D2 (d5-RvD2; 4 *µ*g/kg) was injected into the TA muscle of mice. The muscle was then collected at the indicated times and subjected to LC-MS/MS analysis. Representative MS/MS fragmentation spectra of d5-RvD2 identified in the TA muscle, with diagnostic ion assignments. The structure and fragmentation pattern are shown as insets. **(b)** Amount of deuterium labeled resolvin D2 in murine tibialis anterior muscle at 1, 2 and 3 hours after administration (n=3 for every time-point). The dashed line shows the largest amount of endogenous resolvin D2 as detected after LC-MS/MS in whole muscle extracts after

CTX-induced injury (figure 2e). **(c)** Absolute counts of $CD45^{+}$ cells in tibialis anterior muscle in BMT murine samples when administered either with saline or RvD2 at days 2 and 3 post injury. **(d)** Representative flow cytometry contour plots of $Ly6C^{high}$ and $Ly6C^{low}$ macrophage subsets at day 4 from mice administered either with saline or RvD2 at days 2 and 3 post injury. **(e)** Proportion of inflammatory ($Ly6C^{high}$ $F4/80^{low}$) and repair ($Ly6C^{low}$ $F4/80^{high}$) macrophages at day 4 from mice administered either with saline or RvD2 at days 2 and 3 post injury. p<0.05=*, p<0.01=**, p<0.001=***, p<0.0001=**** (Sidak's multiple comparisons test in two-way ANOVA). Data are shown as mean ± SEM, n = 8 mice per group. **(f)** Representative whole body FLI image of BMT mice at day 4 post CTX injury. Tibialis anterior muscles were administered with saline or RvD2 at days 2 and 3 post injury. (n = 4 mice per condition, saline-treated is the contralateral leg). 2-deoxy-glucose was administered intravenously, and images were recorded 3 hours after administration. Image's fluorescence is associated with the degree of ongoing inflammation. **(g)** FLI signals expressed as average radiance efficiency ($[p{\cdot}s^{-1}{\cdot}cm^{-2}{\cdot}sr^{-1}]/[\mu W{\cdot}cm^{-2}]$) (n = 4 mice per group). **(h)** Scatter dot plot displaying the ratio between of inflammatory ($Ly6C^{high}$ $F4/80^{low}$) and repair ($Ly6C^{low}$ $F4/80^{high}$) macrophages at day 4 from mice administered either with saline or RvD2 at days 2 and 3 post injury. p<0.01=**, p<0.0001=**** (Tukey's multiple comparison test in ordinary one-way ANOVA). Data are shown as mean ± SEM, n=4 for the control sample after saline treatment and n=5 for the RvD2 treated samples. **(i)** Scatter dot plot displaying the proportion of tibialis anterior muscle to the whole body weight in RvD2 treated and untreated mice. p<0.01=**, (Tukey's multiple comparison test in ordinary one-way ANOVA). Data are shown as mean ± SEM, n=7 for the control sample and n=8 for the RvD2 treated mice**. (j)** Measure of in vivo muscle twitch and tetanus force (left and right panel, respectively), in RvD2 treated and saline treated mice at day 8 upon CTX-induced injury. **(k)** Measure of in vivo muscle twitch and tetanus force (left and right panel, respectively), in RvD2 treated and saline treated mice at day 14 upon CTX-induced injury. p<0.05=*Mann–Whitney test.

In contrast, $Ly6C^{low}$ macrophage populations were significantly elevated when treated with RvD2 compared to their saline treated counterparts. Taking the ratio between $Ly6C^{low}$ to $Ly6C^{high}$ macrophages as an indicator of the switch from a pro-inflammatory to a repair phenotype, we saw that it increased from 0.22 in saline treated mice, to 0.36 and 0.41 after RvD2 administration at the second and third day post injury, respectively (fig. 12h). All these results suggest an effector role of RvD2 in promoting a phenotypic transition from $Ly6C^{high}$ inflammatory to $Ly6C^{low}$ repair macrophages. To address this claim, to document the effect of RvD2 on immune cell infiltrates, we performed in vivo imaging in samples treated with fluorescently labeled 2-Deoxy-D-glucose (2-DG), which it can be considered as a marker of inflammation (Patsalos et al., 2017). Glucose uptake was significantly higher in murine muscle of untreated samples, when compared to treated ones (fig. 12f, g). The average

radiant efficacy was reduced after administration of resolvin D2, providing evidence that this lipid mediator has an anti-inflammatory resolving effect, supporting muscle tissue's regeneration. To investigate its effect on muscle recovery, we performed three types of functional tests. Firstly, we assessed the proportion of tibialis anterior muscle mass to whole body weight, that was significantly increased in RvD2 treated mice (fig. 12i). Furthermore, we examined the role of RvD2 in improving the muscle force (both twitch and tetanus) recovery at days 8 and 14 upon muscle tissue injury (fig. 12j and 12k, respectively). As can be seen, RvD2 treatment caused an improved increased recovery in both indicated time-points, underscoring the quicker and enhanced regeneration.

5) Discussion

In this study, we elucidated dynamic regulation of the mediator lipidome during sterile skeletal muscle tissue inflammation and regeneration. Our results were consistent between two distinct models of acute muscle injury and the magnitude of the injury was related to the extent of lipid mediator production. Sorted leukocyte populations largely recapitulated temporal profiles obtained from whole muscle and revealed a distinct pro-resolving signature of regenerative macrophages. Integration of transcriptomics and lipidomics results demonstrated that macrophages are both sources and sensors of lipid mediators that facilitate phenotypic transitions.

Using shotgun lipidomics, we observed a marked remodeling of structural lipids in injured muscle that was characterized by a rapid decline in glycerophospholipids and an increase in the formation of LPC. Assessment of PUFA constituents revealed a quantitative decrease in PC species containing PUFA and a concomitant increase in free AA, DHA and EPA that serve as precursors to lipid mediators. Importantly, the time course of these changes closely mirrored the injury/regeneration response in muscle, such that a near restoration of the normal structural lipid architecture was observed when regeneration had taken place. Interestingly, ceramide and sphingomyelin displayed the exact opposite pattern as other phospholipids in that their levels increased after muscle injury and declined back to baseline levels during regeneration. These lipids are associated with apoptosis and metabolic disorders (e.g., muscle insulin resistance), and altered mitochondrial metabolism (Chaurasia & Summers, 2015). The individual contribution of sphingolipids and their metabolites to immunity and tissue regeneration during muscle injury remain of interest.

The liberation of PUFA from phospholipids is classically defined as the rate limiting step in lipid mediator biosynthesis and occurs primarily by activation of cytosolic calcium-dependent phospholipases A_2 ($cPLA_2$) in response to diverse agonists (e.g., pattern recognition receptors, purinergic

receptors), although other enzymes such as secreted forms of PLA_2 can also play a role (Dennis & Norris, 2015). We note that direct delivery of PUFA to inflammatory exudates (e.g., bound to serum proteins) can also facilitate lipid mediator production (Kasuga et al., 2008). Based on our findings that PUFA are rapidly increased during muscle injury, we performed targeted lipidomics analysis to identify specific lipid mediators and to assemble a map of their biosynthetic pathways. The rapid increase in lipid mediator production largely mirrored liberation of PUFA, with distinct temporal regulation observed among pro-inflammatory and pro-resolving mediators. This temporal regulation occurred despite the fact that AA, EPA and DHA levels were all elevated at day 1 post injury and largely remained elevated above baseline through day 4. These results are consistent with the differential expression and regulation of downstream lipid mediator biosynthetic enzymes. Interestingly, we observed that members of the E-series and D-series resolvin families were present in uninjured and regenerated muscle, while leukotrienes and prostaglandins were largely increased during initial phases of acute inflammation. This may indicate distinct roles for some SPM in normal tissue homeostasis. Nonetheless, we did observe rapid lipid mediator class switching, such that levels of pro-inflammatory eicosanoids (e.g. LTB_4) were very transient and were replaced by SPM during later time points. These results are similar to that observed in other models of acute sterile and infectious inflammation, such as peritonitis (Chiang et al., 2012; Dalli et al., 2013; Levy et al., 2001). As a potentially useful index of this response, we measured that ratio of LTB_4 to the total amount of SPM and found a profound decrease from day 2 to day 4 post injury. This ratio has recently been found by us and others to predict chronicity of inflammation in diseases such as atherosclerosis in humans (Fredman et al., 2016; Thul et al., 2017) We used two complementary and well-established models of tissue injury to validate the robustness of the data sets. The CTX-induced muscle injury is characterized by severe damage of the muscle tissue and a relatively short period of an *ad integrum* synchronous regeneration (Arnold et al., 2007), while eccentric exercise-induced injury results in a less severe but similar repair

process and is more physiologically relevant, minimally-invasive and highly reproducible (Kornegay et al., 2012). In both models, we identified a similar profile of AA, DHA and EPA-derived lipid mediators, but with a higher magnitude of change in lipid mediator levels in the CTX model. Moreover, a delay in decline of the of LTB_4 levels together with a delayed transition in SPMs production (i.e., RvD4, 17*R*-RvD1, RvE3) corresponds to a slower lipid mediator class switch in eccentric exercise-induced injury. These results suggest that the lipid mediator profile is closely related to the time course of the inflammation-regeneration response, which is dependent upon the magnitude of the injury. Interestingly, resistance exercise in humans increases serum levels of leukotrienes, prostanoids and SPM, the production of which are negatively impacted by non-steroidal anti-inflammatory drugs (Markworth et al., 2013). The integration of the lipid mediator profiles after CTX-injury in whole muscle and in innate immune cells (i.e., neutrophils and macrophages) showed high overlap between the two datasets indicating the leukocytes are likely the primary source of these lipid mediators in the tissue. As expected, neutrophils were a predominant source of LTB_4 and had the highest expression of *Alox5*; they also expressed *Ptgs1* and *Ptgs2* and produced PGE_2 and $PGF_{2\alpha}$. These mediators were also produced by inflammatory $Ly6C^{hi}$ macrophages at day 2 relative to their $Ly6C^{low}$ counterparts. In contrast, PGD_2 was relatively higher in macrophages that expressed *Hpgds*. While some SPM were also produced by neutrophils, their levels were relatively higher in macrophages, consistent with a recent study demonstrating that macrophage depletion impairs SPM biosynthesis *in vivo* (Halade et al., 2018). Levels of several SPM (e.g., RvD2, LXB_4, LXA_4, RvD5) were higher in $Ly6C^{low}$ macrophages at day 2, while a very distinct SPM cluster was observed in both macrophage subsets at day 4. Expression of *Alox15*, which is a key enzyme in SPM biosynthesis, was observed across all macrophage subsets but was higher in $Ly6C^{low}$ macrophages at day 2 post-injury. These results are consistent with a report demonstrating that expression of *Alox15* is one of the most highly differentially expressed genes characteristic of resolution-phase macrophages (Stables et al., 2011). Along

these lines, polarization of human macrophages to an alternative phenotype increases SPM biosynthesis relative to macrophages polarized with IFNγ/LPS *in vitro* (Dalli & Serhan, 2012). We note that in SPM biosynthesis can also be regulated through transcellular delivery of biosynthetic intermediates during heterotypic leukocyte interactions (e.g., PMN: macrophage) or leukocyte: epithelial/endothelial interactions (Serhan, 2014; Spite et al., 2014). Given the relatively high amounts of biosynthetic precursors to SPM in macrophages isolated at day 4 post-injury (e.g., 17-HDHA, 14-HDHA, 15-HETE, 18-HEPE), it is possible that these intermediates are donated to other tissue cells for conversion to SPM later in the time course.

One particularly intriguing relationship that emerged from our integrated analysis was the production of RvD2 by Ly6C^{low} macrophages at day 2 and expression of its receptor, *Gpr18*, in Ly6C^{hi} macrophages. As a demonstration of how this comprehensive systems-level analysis can generate new hypotheses, we questioned whether RvD2 regulates this temporal macrophage phenotype switch. Our results clearly show that exogenous delivery of RvD2 shifts Ly6C^{hi} macrophages to Ly6C^{low} macrophages *in vivo*. Transcriptomics analysis of naïve macrophages stimulated with RvD2 showed overlap with genes expressed in both subsets *in vivo*, but with more prominent overlap observed at day 4 when Ly6C^{low} macrophages are more prominent. These included genes important in host defense, chemotaxis, and proliferation, the latter of which are characteristic of resolving macrophages (Stables et al., 2011). Interestingly, some of the genes induced by RvD2 in naïve macrophages would be expected to enhance host defense to both viral and bacterial pathogens. Indeed, RvD2 has previously been shown to enhance host defense, reduce inflammation and improve survival in polymicrobial sepsis (Chiang et al., 2017; Spite et al., 2009) These results both confirm and extend the known biological roles of RvD2 and suggest that it uniquely programs macrophages to both facilitate repair and enhance host-defense, even in absence of an active pathogen. Recent studies have shown that RvD2 improves outcomes after tissue injury or after exposure to harmful stimuli. Importantly, we have recently shown that RvD2 both resolves

inflammation and promotes skeletal muscle regeneration and revascularization after ischemia, effects that are dependent upon GPR18 (Zhang et al., 2016). Exogenous treatment with RvD2 reduces tissue necrosis in burn injury and directly stimulates re-epithelialization of cutaneous wounds (Hellmann et al., 2018; Inoue et al., 2017). In macrophages, the RvD2/GPR18 axis is important in mediating the resolution of an inflammatory response and enhancing macrophage phagocytosis via cAMP/PKA signaling and the phosphorylation of STAT3 (Chiang et al., 2017), which is a key process in successful efferocytosis and M2 polarization *in vitro* (Soki et al., 2014).

In addition to RvD2, our analysis revealed dynamic temporal relationships amongst several lipid mediators that could have both overlapping and distinct roles and cellular targets in injured muscle. In addition to the classical roles of eicosanoids mentioned above, recent evidence indicates that prostanoids, such as PGE_2, could potentially target muscle-specific stem cells to promote regeneration (Ho et al., 2017). Along these lines, RvE1 has recently been shown to regulate inflammatory signaling skeletal muscle myotubes, indicating that amongst SPM, distinct cellular targets in muscle could emerge beyond regulating immunity (Baker et al., 2018). Indeed, several SPM directly target fibroblasts, endothelial cells and epithelial cells (Spite et al., 2014). This extends the well-documented actions of SPM in counter-regulating excessive neutrophil recruitment that could promote tissue damage, the clearance of apoptotic cells by macrophages and the counter-regulation of pro-inflammatory mediator production (Serhan, 2014). Thus, the resources generated in the present study could inform new roles of diverse lipid mediators and their receptors in muscle inflammation, fibrosis, angiogenesis and regeneration.

In summary, we demonstrate a multi-omics approach that comprehensively describes muscle inflammation and regeneration after acute sterile injury. We integrated immune cell-specific lipidomics signatures with transcriptomics and epigenomics to provide new insights into the potential effectors of this response, while we highlighted the inflammation dynamics

based on distinct immune cell populations throughout the time course of regeneration.

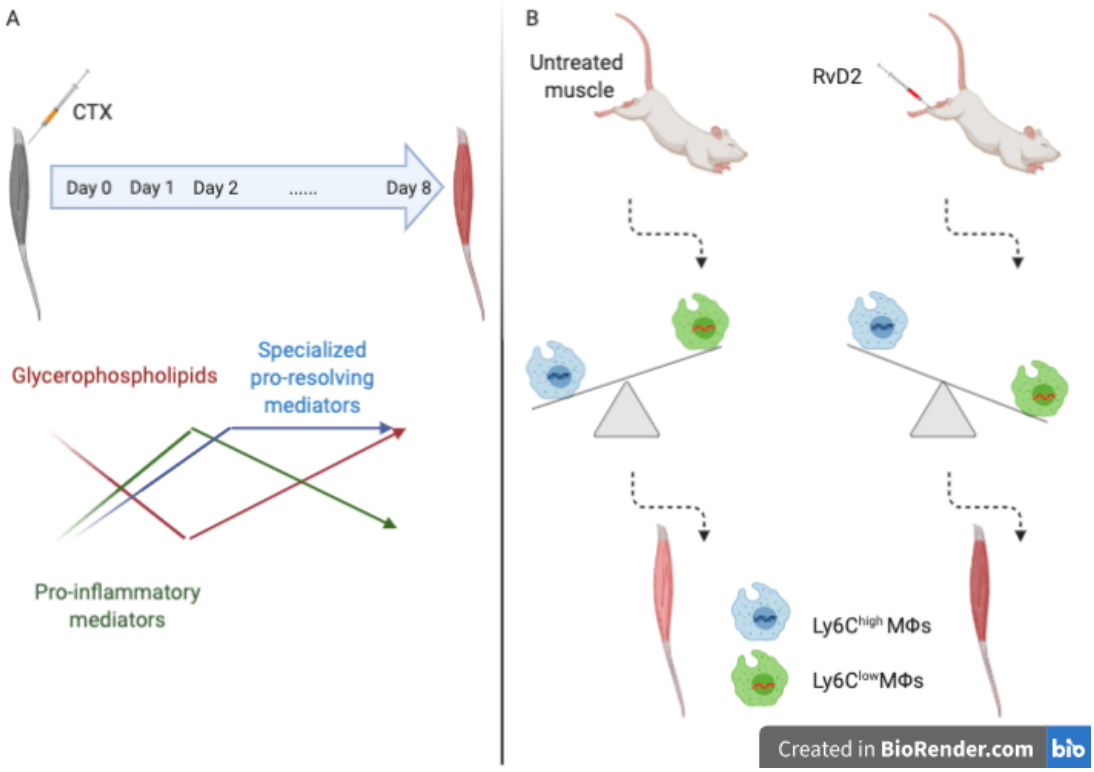

Graphical scheme 7: Findings of this study. **(A)** Temporal regulation of lipids upon CTX injury. **(B)** Effect of RvD2 in the transcription program of naïve macrophages and in the switch from pro-inflammatory to reparative macrophages.

This revealed a striking temporal regulation of lipid mediators throughout the initiation and resolution of inflammation that precipitates tissue regeneration (grapchical scheme 7A). Focusing on RvD2, we showed that it affects the transcription program of naïve macrophages, equipping them with a unique gene signature and promoting their transition from inflammatory to reparatory (graphical scheme 7B). This approach is complementary to the efforts undertaken by us and others (Tidball, 2017; Varga et al., 2016; Varga et al., 2016). to determine the transcriptional changes in the inflammatory components of myeloid cells. Integration of transcriptomic, lipidomic, epigenomic and (phospho)-proteomic landscapes will lead to new directions in our understanding of immune cell function and could identify pathways amenable to the development of novel therapeutics.

6) Summary

Skeletal muscle regeneration upon injury is an active process that is highly orchestrated by immune cells and mechanistically depends on the great level of coordination between biological processes. Indispensable of the regeneration process is the initial inflammation that consists of two phases, initiation and resolution, which are coordinated by metabolites that can mediate it. Lipid mediators have signaling mediated capacities, and here we showed that there is a dynamic regulation of the mediator lipidome, which was consistent in a model of acute sterile injury, and also in a more pathophysiological model upon exercise. We also monitored a marked remodeling of structural lipids, which can act as biosynthetic sources of the lipid mediator pool. Lipid mediators changed dynamically in regard to their biosynthetic sources. We also observed epigenomic alternations during the time course of inflammation. Consistent with these changes was the actively changing transcriptome, which was recapitulated in infiltrating macrophage populations. In conjunction with our observations we asked whether a lipid biomolecule, RvD2, could affect the temporal regulation of macrophage phenotypic switch. Interestingly, we found that RvD2 can facilitate this switch in vivo, enhancing the reparative macrophages populations over their pro-inflammatory counterparts. As a result, through the effector actions of RvD2, regeneration of the injured skeletal muscle tissue was promoted as it was shown through in vivo force measurements in a model of delayed regeneration in mice.

7) List of keywords

macrophages, inflammation dynamics, cardiotoxin, tissue injury, muscle regeneration, tissue repair, inflammation, resolution, lipid mediator, resolvin D2, transcriptomic signature, epigenomic landscape

8) Acknowledgements

First and foremost, I would like to thank my supervisor and mentor Professor Laszlo Nagy for his endless support during my PhD studies. Being professional, serious, motivational and well-organized taught me how research of good quality is achieved, making me a more devoted, more enthusiastic young researcher. He persistently helped me to transform to a person that stands on his own feet.

I am grateful to Professors Fesus and Tozser, former and current head of the Department of Biochemistry and Molecular Biology, Medical School, University of Debrecen.

I would like also to thank Dr. Spite, Dr. Sansbury and Dr. Patsalos for their contribution in wet lab experiments and their scientific input in regard to the publications used in this study.

I am also thankful to our collaborators and all the members of the nlab for the help.

Special thanks go to Mr Petros Tzerpos, whom I consider a good friend, for the long talks and all the support throughout this journey.

Last but not least, I would like to thank my family, Mama, Mpampas, Isidora, Giannis, Konstantinos, Christos, Marielena, Nona Toula, Nona Maria, Anastasia and Vasilis who have been more than supportive during the years of my PhD studies and also my very close friends Vangelis, Matina, Maria, Anna and Ian, who kept me on track, whatever challenges I was facing.

9. Financial support of PhD studies

During my PhD studies I was financially supported by UD-Genomed Ltd through the “Chromatin3D” Innovative Training Network funded by the European Union under the Horizon-2020 Framework Programme (Grant Agreement 622934), a grant from the Higher Education Institutional Excellence Program (NKFIH-1150-6/2019) of the National Research, Development and Innovation Office, a grant about “Harnessing the healing power of macrophages”/ Élvonal Excellence Program (NKFI KKP 129909) of the National Research, Development and Innovation Office and a grant from the Higher Education Institutional Excellence Programme (20428-3/2018/FEKUTSTRAT) of the Ministry of Human Capacities.

10) References

Abbas, A. K., Murphy, K. M., & Sher, A. (1996). Functional diversity of helper T lymphocytes. *Nature, 383*(6603), 787-793. doi:10.1038/383787a0

Adib-Conquy, M., & Cavaillon, J. M. (2007). Stress molecules in sepsis and systemic inflammatory response syndrome. *FEBS Lett, 581*(19), 3723-3733. doi:10.1016/j.febslet.2007.03.074

Anthony, R. M., Rutitzky, L. I., Urban, J. F., Jr., Stadecker, M. J., & Gause, W. C. (2007). Protective immune mechanisms in helminth infection. *Nat Rev Immunol, 7*(12), 975-987. doi:10.1038/nri2199

Arnes, L., Akerman, I., Balderes, D. A., Ferrer, J., & Sussel, L. (2016). betalinc1 encodes a long noncoding RNA that regulates islet beta-cell formation and function. *Genes Dev, 30*(5), 502-507. doi:10.1101/gad.273821.115

Arnold, L., Henry, A., Poron, F., Baba-Amer, Y., van Rooijen, N., Plonquet, A., . . . Chazaud, B. (2007). Inflammatory monocytes recruited after skeletal muscle injury switch into antiinflammatory macrophages to support myogenesis. *J Exp Med, 204*(5), 1057-1069. doi:10.1084/jem.20070075

Ashley, N. T., Weil, Z. M., & Nelson, R. J. (2012). Inflammation: Mechanisms, Costs, and Natural Variation. *Annu. Rev. Ecol. Evol. Syst., 43*, 385-406.

Baker, L. A., Martin, N. R. W., Kimber, M. C., Pritchard, G. J., Lindley, M. R., & Lewis, M. P. (2018). Resolvin E1 (Rv E1) attenuates LPS induced inflammation and subsequent atrophy in C2C12 myotubes. *J Cell Biochem, 119*(7), 6094-6103. doi:10.1002/jcb.26807

Basak, S., Kim, H., Kearns, J. D., Tergaonkar, V., O'Dea, E., Werner, S. L., . . . Hoffmann, A. (2007). A fourth IkappaB protein within the NF-kappaB signaling module. *Cell, 128*(2), 369-381. doi:10.1016/j.cell.2006.12.033

Belcastro, A. N., Arthur, G. D., Albisser, T. A., & Raj, D. A. (1996). Heart, liver, and skeletal muscle myeloperoxidase activity during exercise. *J Appl Physiol (1985), 80*(4), 1331-1335. doi:10.1152/jappl.1996.80.4.1331

Bogdanov, M., Dowhan, W., & Vitrac, H. (2014). Lipids ad topological rules governing membrane protein assembly. *Biochim. Biophys. Acta, 1843*, 1475-1488.

Brigette, M., & al., e. (2010). Muscle resident macrophages control the immune cell reaction in a mouse model of notexin-induced myoinjury. *Arthritis Reum., 62*, 268-279.

Brusselle, G., & Bracke, K. (2014). Targeting immune pathways for therapy in asthma and chronic obstructive pulmonary disease. *Ann Am Thorac Soc, 11 Suppl 5*, S322-328. doi:10.1513/AnnalsATS.201403-118AW

Buenrostro, J. D., Giresi, P. G., Zaba, L. C., Chang, H. Y., & Greenleaf, W. J. (2013). Transposition of native chromatin for fast and sensitive epigenomic profiling of open chromatin, DNA-binding proteins and nucleosome position. *Nat Methods, 10*(12), 1213-1218. doi:10.1038/nmeth.2688

Buenrostro, J. D., Wu, B., Chang, H. Y., & Greenleaf, W. J. (2015). ATAC-seq: A Method for Assaying Chromatin Accessibility Genome-Wide. *Curr Protoc Mol Biol, 109*, 21 29 21-21 29 29. doi:10.1002/0471142727.mb2129s109

Burzyn, D., Kuswanto, W., Kolodin, D., Shadrach, J. L., Cerletti, M., Jang, Y., . . . Mathis, D. (2013). A special population of regulatory T cells potentiates muscle repair. *Cell, 155*(6), 1282-1295. doi:10.1016/j.cell.2013.10.054

Chaurasia, B., & Summers, S. A. (2015). Ceramides - Lipotoxic Inducers of Metabolic Disorders. *Trends Endocrinol Metab, 26*(10), 538-550. doi:10.1016/j.tem.2015.07.006

Chen, A., Chen, D., & Chen, Y. (2018). Advances of DNase-seq for mapping active gene regulatory elements across the genome in animals. *Gene, 667*, 83-94.

Chen, L., Deng, H., Cui, H., Fang, J., Zuo, Z., Deng, J., . . . Zhao, L. (2018). Inflammatory responses and inflammation-associated diseases in organs. *Oncotarget, 9*(6), 7204-7218. doi:10.18632/oncotarget.23208

Cheng, M., Nguyen, M. H., Fantuzzi, G., & Koh, T. J. (2008). Endogenous interferon-gamma is required for efficient skeletal muscle regeneration. *Am J Physiol Cell Physiol, 294*(5), C1183-1191. doi:10.1152/ajpcell.00568.2007

Chertov, O., Yang, D., Howard, O. M., & Oppenheim, J. J. (2000). Leukocyte granule proteins mobilize innate host defenses and adaptive immune responses. *Immunol Rev, 177*, 68-78. doi:10.1034/j.1600-065x.2000.17702.x

Chiang, N., Dalli, J., Colas, R. A., & Serhan, C. N. (2015). Identification of resolvin D2 receptor mediating resolution of infections and organ protection. *J Exp Med, 212*(8), 1203-1217. doi:10.1084/jem.20150225

Chiang, N., de la Rosa, X., Libreros, S., & Serhan, C. N. (2017). Novel Resolvin D2 Receptor Axis in Infectious Inflammation. *J Immunol, 198*(2), 842-851. doi:10.4049/jimmunol.1601650

Chiang, N., Fredman, G., Backhed, F., Oh, S. F., Vickery, T., Schmidt, B. A., & Serhan, C. N. (2012). Infection regulates pro-resolving mediators that lower antibiotic requirements. *Nature, 484*(7395), 524-528. doi:10.1038/nature11042

Childers, M. K., Grange, Robert W., Kornegay, Joe N. (2011). In Vivo Canine Muscle Function Assay. *JoVE,* (50). Retrieved from https://www.jove.com/video/2623 doi:doi:10.3791/2623

Civelek, M., & Lusis, A. J. (2014). Systems genetics approaches to understand complex traits. *Nat Rev Genet, 15*(1), 34-48. doi:10.1038/nrg3575

Claussnitzer, M., Dankel, S. N., Kim, K. H., Quon, G., Meuleman, W., Haugen, C., . . . Kellis, M. (2015). FTO Obesity Variant Circuitry and Adipocyte Browning in Humans. *N Engl J Med, 373*(10), 895-907. doi:10.1056/NEJMoa1502214

Collins, R. A., & Grounds, M. D. (2001). The role of tumor necrosis factor-alpha (TNF-alpha) in skeletal muscle regeneration. Studies in TNF-alpha(-/-) and TNF-alpha(-/-)/LT-alpha(-/-) mice. *J Histochem Cytochem, 49*(8), 989-1001. doi:10.1177/002215540104900807

Consortium, E. P. (2012). An integrated encyclopedia of DNA elements in the human genome. Nature, 489(7414), 57-74. doi:10.1038/nature11247

Dalli, J., Colas, R. A., Walker, M. E., & Serhan, C. N. (2018). Lipid Mediator Metabolomics Via LC-MS/MS Profiling and Analysis. *Methods Mol Biol, 1730*, 59-72. doi:10.1007/978-1-4939-7592-1_4

Dalli, J., & Serhan, C. N. (2012). Specific lipid mediator signatures of human phagocytes: microparticles stimulate macrophage efferocytosis and pro-resolving mediators. *Blood, 120*(15), e60-72. doi:10.1182/blood-2012-04-423525

Dalli, J., & Serhan, C. N. (2018). Identification and structure elucidation of the proresolving mediators provides novel leads for resolution pharmacology. *Br J Pharmacol*. doi:10.1111/bph.14336

Dalli, J., Winkler, J. W., Colas, R. A., Arnardottir, H., Cheng, C. Y., Chiang, N., . . . Serhan, C. N. (2013). Resolvin D3 and aspirin-triggered resolvin D3 are potent immunoresolvents. *Chem Biol, 20*(2), 188-201. doi:10.1016/j.chembiol.2012.11.010

Dennis, E. A., & Norris, P. C. (2015). Eicosanoid storm in infection and inflammation. *Nat Rev Immunol, 15*(8), 511-523. doi:10.1038/nri3859

Dettmer, K., Aronov, P. A., & Hammock, B. D. (2007). Mass spectrometry-based metabolomics. *Mass Spectrom Rev, 26*(1), 51-78. doi:10.1002/mas.20108

Dinarello, C. A., Simon, A., & van der Meer, J. W. (2012). Treating inflammation by blocking interleukin-1 in a broad spectrum of diseases. *Nat Rev Drug Discov, 11*(8), 633-652. doi:10.1038/nrd3800

Dunn, W. B. (2011). Mass spectrometry in systems biology an introduction. *Methods Enzymol, 500*, 15-35. doi:10.1016/B978-0-12-385118-5.00002-5

Dunn, W. B., Broadhurst, D. I., Atherton, H. J., Goodacre, R., & Griffin, J. L. (2011). Systems level studies of mammalian metabolomes: the roles of mass spectrometry and nuclear magnetic resonance spectroscopy. *Chem Soc Rev, 40*(1), 387-426. doi:10.1039/b906712b

Eberwine, R. A., Cort, L., Habib, M., Mordes, J. P., & Blankenhorn, E. P. (2014). Autoantigen-induced focusing of Vbeta13+ T cells precedes onset of autoimmune diabetes in the LEW.1WR1 rat. *Diabetes, 63*(2), 596-604. doi:10.2337/db13-0462

English, J. T., Norris, P. C., Hodges, R. R., Dartt, D. A., & Serhan, C. N. (2017). Identification and Profiling of Specialized Pro-Resolving Mediators in Human Tears by Lipid Mediator Metabolomics. *Prostaglandins Leukot Essent Fatty Acids, 117*, 17-27. doi:10.1016/j.plefa.2017.01.004

Feillet-Coudray, C., Fouret, G., Casas, F., & Coudray, C. (2014). Impact of high dietary lipid intake and related metabolic disorders on the abundance and acyl composition of the unique mitochondrial phospholipid, cardiolipin. *J. Bioenerg. Biomembr., 46*, 447-457.

Ferrero-Miliani L, N. O., Andersen P, Girardin S. . (2007;). Chronic inflammation: importance of NOD2 and NALP3 in interleukin-1β generation. . *Clin Exp Immunol. , 147*, 227–235.

Fielding, R. A., Manfredi, T. J., Ding, W., Fiatarone, M. A., Evans, W. J., & Cannon, J. G. (1993). Acute phase response in exercise. III. Neutrophil and IL-1 beta accumulation in skeletal muscle. *Am J Physiol, 265*(1 Pt 2), R166-172. doi:10.1152/ajpregu.1993.265.1.R166

Flower, R. J. (2006). Prostaglandins, bioassay and inflammation. *Br J Pharmacol, 147 Suppl 1*, S182-192. doi:10.1038/sj.bjp.0706506

Fredman, G., Hellmann, J., Proto, J. D., Kuriakose, G., Colas, R. A., Dorweiler, B., . . . Tabas, I. (2016). An imbalance between specialized pro-resolving lipid mediators and pro-inflammatory leukotrienes promotes instability of atherosclerotic plaques. *Nat Commun, 7*, 12859. doi:10.1038/ncomms12859

Fredman, G., Li, Y., Dalli, J., Chiang, N., & Serhan, C. N. (2012). Self-limited versus delayed resolution of acute inflammation: temporal regulation of pro-resolving mediators and microRNA. *Sci Rep, 2*, 639. doi:10.1038/srep00639

George, R. M., Biressi, S., Beres, B. J., Rogers, E., Mulia, A. K., Allen, R. E., . . . Wilson-Rawls, J. (2013). Numb-deficient satellite cells have regeneration and proliferation defects. *Proc Natl Acad Sci U S A, 110*(46), 18549-18554. doi:10.1073/pnas.1311628110

Gjoneska, B., Markovska-Simoska, S., Hinrikus, H., Pop-Jordanova, N., & Pop-Jordanov, J. (2015). Brain Topography of Emf-Induced Eeg-Changes in Restful Wakefulness: Tracing Current Effects, Targeting Future Prospects. *Pril (Makedon Akad Nauk Umet Odd Med Nauki), 36*(3), 103-112. doi:10.1515/prilozi-2015-0085

Glaudemans, A. W., de Vries, E. F., Galli, F., Dierckx, R. A., Slart, R. H., & Signore, A. (2013). The use of (18)F-FDG-PET/CT for diagnosis and treatment monitoring of inflammatory and infectious diseases. *Clin Dev Immunol, 2013*, 623036. doi:10.1155/2013/623036

Gonzalez-Silva, L., Quevedo, L., & Varela, I. (2020). Tumor Functional Heterogeneity Unraveled by scRNA-seq Technologies. *Trends Cancer, 6*(1), 13-19. doi:10.1016/j.trecan.2019.11.010

Graham, A. L. (2002). When T-helper cells don't help: immunopathology during concomitant infection. *Q Rev Biol, 77*(4), 409-434. doi:10.1086/344414

Griffiths, X. W. (2009). Analysis of neurosterols by GC-MS and LC-MS/MS. *J. Chromatogr. B Analyt*.

Guardiola, O., Andolfi, G., Tirone, M., Iavarone, F., Brunelli, S., & Minchiotti, G. (2017). Induction of Acute Skeletal Muscle Regeneration by Cardiotoxin Injection. *J Vis Exp*(119). doi:10.3791/54515

Gudkov, A. V., & Komarova, E. A. (2016). p53 and the Carcinogenicity of Chronic Inflammation. *Cold Spring Harb Perspect Med, 6*(11). doi:10.1101/cshperspect.a026161

Gupta, R. A., Shah, N., Wang, K. C., Kim, J., Horlings, H. M., Wong, D. J., . . . Chang, H. Y. (2010). Long non-coding RNA HOTAIR reprograms

chromatin state to promote cancer metastasis. *Nature, 464*(7291), 1071-1076. doi:10.1038/nature08975

Gutierrez, J., & Lomonte, B. (2004). Phospholipase A2 myotoxins from Bothrops snake venoms. *Curr. Org. Chem., 8*, 1677-1690.

Halade, G. V., Norris, P. C., Kain, V., Serhan, C. N., & Ingle, K. A. (2018). Splenic leukocytes define the resolution of inflammation in heart failure. *Sci Signal, 11*(520). doi:10.1126/scisignal.aao1818

Halbritter, F., Farlik, M., Schwentner, R., Jug, G., Fortelny, N., Schnoller, T., . . . Hutter, C. (2019). Epigenomics and Single-Cell Sequencing Define a Developmental Hierarchy in Langerhans Cell Histiocytosis. *Cancer Discov, 9*(10), 1406-1421. doi:10.1158/2159-8290.CD-19-0138

Han, J., Zhang, Z., & Wang, K. (2018). 3C and 3C-based techniques: the powerful tools for spatial genome organization deciphering. *Mol Cytogenet, 11*, 21. doi:10.1186/s13039-018-0368-2

Han, X. (2016). Lipidomics for studying metabolism. *Nat Rev Endocrinol, 12*(11), 668-679. doi:10.1038/nrendo.2016.98

Hardy, D., Besnard, A., Latil, M., Jouvion, G., Briand, D., Thepenier, C., . . . Chretien, F. (2016). Comparative Study of Injury Models for Studying Muscle Regeneration in Mice. *PLoS One, 11*(1), e0147198. doi:10.1371/journal.pone.0147198

Hasin, Y., Seldin, M., & Lusis, A. (2017). Multi-omics approaches to disease. *Genome Biol, 18*(1), 83. doi:10.1186/s13059-017-1215-1

Heinz, S., Benner, C., Spann, N., Bertolino, E., Lin, Y. C., Laslo, P., . . . Glass, C. K. (2010). Simple combinations of lineage-determining transcription factors prime cis-regulatory elements required for macrophage and B cell identities. Mol Cell, 38(4), 576-589. doi:10.1016/j.molcel.2010.05.004

Hellmann, J., Sansbury, B. E., Wong, B., Li, X., Singh, M., Nuutila, K., . . . Spite, M. (2018). Biosynthesis of D-series resolvins in skin provides insights into their role in tissue repair. *J Invest Dermatol*. doi:10.1016/j.jid.2018.03.1498

Hishikawa, D., Hashidate, T., Shimizu, T., & Shindou, H. (2014). Diversity and function of membrane glycerophospholipids generated by the remodelling pathway in mammalian cells. *J. Lipid Res., 55*, 799-807.

Ho, A. T. V., Palla, A. R., Blake, M. R., Yucel, N. D., Wang, Y. X., Magnusson, K. E. G., . . . Blau, H. M. (2017). Prostaglandin E2 is essential for efficacious skeletal muscle stem-cell function, augmenting regeneration

and strength. *Proc Natl Acad Sci U S A, 114*(26), 6675-6684. doi:10.1073/pnas.1705420114

Honda, H., Kimura, H., & Rostami, A. (1990). Demonstration and phenotypic characterization of resident macrophages in rat skeletal muscle. *Immunology, 70*, 272-277.

Hotamisligil, G. S. (2006). Inflammation and metabolic disorders. *Nature, 444*(7121), 860-867. doi:10.1038/nature05485

Hunt, S. E., McLaren, W., Gil, L., Thormann, A., Schuilenburg, H., Sheppard, D., . . . Cunningham, F. (2018). Ensembl variation resources. *Database (Oxford), 2018*. doi:10.1093/database/bay119

Inoue, Y., Liu, Y. M., Otawara, M., Chico Calero, I., Stephanie Nam, A., Yu, Y. M., . . . Irimia, D. (2017). Resolvin D2 Limits Secondary Tissue Necrosis After Burn Wounds in Rats. *J Burn Care Res*. doi:10.1097/BCR.0000000000000617

Ishii, N., Ozaki, K., Sato, H., Mizuno, H., Susumu, S., Takahashi, A., . . . Tanaka, T. (2006). Identification of a novel non-coding RNA, MIAT, that confers risk of myocardial infarction. *J Hum Genet, 51*(12), 1087-1099. doi:10.1007/s10038-006-0070-9

Ivashkiv, L. B., & Hu, X. (2003). The JAK/STAT pathway in rheumatoid arthritis: pathogenic or protective? *Arthritis Rheum, 48*(8), 2092-2096. doi:10.1002/art.11095

Jabbour, H. N., Sales, K. J., Catalano, R. D., & Norman, J. E. (2009). Inflammatory pathways in female reproductive health and disease. *Reproduction, 138*(6), 903-919. doi:10.1530/REP-09-0247

Joe, A. W., Yi, L., Natarajan, A., Le Grand, F., So, L., Wang, J., . . . Rossi, F. M. (2010). Muscle injury activates resident fibro/adipogenic progenitors that facilitate myogenesis. *Nat Cell Biol, 12*(2), 153-163. doi:10.1038/ncb2015

Joyce, A. R., & Palsson, B. O. (2006). The model organism as a system: integrating 'omics' data sets. *Nat Rev Mol Cell Biol, 7*(3), 198-210. doi:10.1038/nrm1857

Kaminska, B. (2005). MAPK signalling pathways as molecular targets for anti-inflammatory therapy--from molecular mechanisms to therapeutic benefits. *Biochim Biophys Acta, 1754*(1-2), 253-262. doi:10.1016/j.bbapap.2005.08.017

Kasuga, K., Yang, R., Porter, T. F., Agrawal, N., Petasis, N. A., Irimia, D., . . . Serhan, C. N. (2008). Rapid appearance of resolvin precursors in

inflammatory exudates: novel mechanisms in resolution. *J Immunol, 181*(12), 8677-8687. doi:10.4049/jimmunol.181.12.8677

Kim, D., Langmead, B., & Salzberg, S. L. (2015). HISAT: a fast spliced aligner with low memory requirements. *Nat Methods, 12*(4), 357-360. doi:10.1038/nmeth.3317

Kim, D., Pertea, G., Trapnell, C., Pimentel, H., Kelley, R., & Salzberg, S. L. (2013). TopHat2: accurate alignment of transcriptomes in the presence of insertions, deletions and gene fusions. *Genome Biol, 14*(4), R36. doi:10.1186/gb-2013-14-4-r36

Korn, T., Bettelli, E., Oukka, M., & Kuchroo, V. K. (2009). IL-17 and Th17 Cells. *Annu Rev Immunol, 27*, 485-517. doi:10.1146/annurev.immunol.021908.132710

Kornegay, J. N., Bogan, J. R., Bogan, D. J., Childers, M. K., Li, J., Nghiem, P., . . . Hoffman, E. P. (2012). Canine models of Duchenne muscular dystrophy and their use in therapeutic strategies. *Mamm Genome, 23*(1-2), 85-108. doi:10.1007/s00335-011-9382-y

Krippendorf, B. B., & Riley, D. (1993). <mus.880160116.pdf>. *Distinguishing unloading- versus reloading-induced changes in rat soleus muscle., 16*, 99-108.

Kristiansen, M., Graversen, J. H., Jacobsen, C., Sonne, O., Hoffman, H. J., Law, S. K., & Moestrup, S. K. (2001). Identification of the haemoglobin scavenger receptor. *Nature, 409*(6817), 198-201. doi:10.1038/35051594

Langmead, B. (2010). Aligning short sequencing reads with Bowtie. *Curr Protoc Bioinformatics, Chapter 11*, Unit 11 17. doi:10.1002/0471250953.bi1107s32

Lemos, D. R., Babaeijandaghi, F., Low, M., Chang, C. K., Lee, S. T., Fiore, D., . . . Rossi, F. M. (2015). Nilotinib reduces muscle fibrosis in chronic muscle injury by promoting TNF-mediated apoptosis of fibro/adipogenic progenitors. *Nat Med, 21*(7), 786-794. doi:10.1038/nm.3869

Lepper, C., Partridge, T. A., & Fan, C. M. (2011). An absolute requirement for Pax7-positive satellite cells in acute injury-induced skeletal muscle regeneration. *Development, 138*(17), 3639-3646. doi:10.1242/dev.067595

Levy, B. D., Clish, C. B., Schmidt, B., Gronert, K., & Serhan, C. N. (2001). Lipid mediator class switching during acute inflammation: signals in resolution. *Nat Immunol, 2*(7), 612-619. doi:10.1038/89759

Li, H., Handsaker, B., Wysoker, A., Fennell, T., Ruan, J., Homer, N., . . . Genome Project Data Processing, S. (2009). The Sequence Alignment/Map format and SAMtools. *Bioinformatics, 25*(16), 2078-2079. doi:10.1093/bioinformatics/btp352

Lieber, R. L., Thornell, L., & Friden, J. (1996). Muscle cytoskeletal disruption occurs within the first 15min of cyclic eccentric contraction. *J. Appl. Physiol., 80*, 278-284

Locati, M., Mantovani, A., & Sica, A. (2013). Macrophage activation and polarization as an adaptive component of innate immunity. *Adv Immunol, 120*, 163-184. doi:10.1016/B978-0-12-417028-5.00006-5

Love, M. I., Huber, W., & Anders, S. (2014). Moderated estimation of fold change and dispersion for RNA-seq data with DESeq2. *Genome Biol, 15*(12), 550. doi:10.1186/s13059-014-0550-8

Lu, H., Huang, D., Ransohoff, R. M., & Zhou, L. (2011). Acute skeletal muscle injury: CCL2 expression by both monocytes and injured muscle is required for repair. *FASEB J, 25*, 3344-3355.

Maderna, P., & Godson, C. (2009). Lipoxins: resolutionary road. *Br J Pharmacol, 158*(4), 947-959. doi:10.1111/j.1476-5381.2009.00386.x

Madsen, R., Lundstedt, T., & Trygg, J. (2010). Chemometrics in metabolomics--a review in human disease diagnosis. *Anal Chim Acta, 659*(1-2), 23-33. doi:10.1016/j.aca.2009.11.042

Malawista, S. E., de Boisfleury Chevance, A., van Damme, J., & Serhan, C. N. (2008). Tonic inhibition of chemotaxis in human plasma. *Proc Natl Acad Sci U S A, 105*(46), 17949-17954. doi:10.1073/pnas.0802572105

Markworth, J. F., Vella, L., Lingard, B. S., Tull, D. L., Rupasinghe, T. W., Sinclair, A. J., . . . Cameron-Smith, D. (2013). Human inflammatory and resolving lipid mediator responses to resistance exercise and ibuprofen treatment. *Am J Physiol Regul Integr Comp Physiol, 305*(11), R1281-1296. doi:10.1152/ajpregu.00128.2013

Martinez, C. O., McHale, M. J., Wells, J. T., Ochoa, O., Michalek, J. E., McManus, L. M., & Shireman, P. K. (2010). Regulation of skeletal muscle regeneration by CCR2-activating chemokines is directly related to macrophage recruitment. *Am J Physiol Regul Integr Comp Physiol, 299*(3), R832-842. doi:10.1152/ajpregu.00797.2009

Mayr, J. A. (2015). Lipid metabolism in mitochondrial membranes. *J. Inherit. Metab. Dis., 38*, 137-144.

McLennan, I. S. (1996). Degenerating and regenerating skeletal muscles contain several subpopulations of macrophages with distinct spatial and temporal distributions. *J Anat, 188 (Pt 1)*, 17-28.

McMahon, H. T., & Boucrot, E. (2015). Membrane curvature at a glance. *J. Cell Sci., 128*, 1065-1070.

Medzhitov, R. (2008). Origin and physiological roles of inflammation. *Nature, 454*(7203), 428-435. doi:10.1038/nature07201

Medzhitov, R., Schneider, D. S., & Soares, M. P. (2012). Disease tolerance as a defense strategy. *Science, 335*(6071), 936-941. doi:10.1126/science.1214935

Mehdi Pirooznia, V. N., Youping Deng. (2007). <GeneVenn - A web application for comparing gene lists using Venn diagrams.pdf>. *Bioinformation*, 420-422.

Menon, R. (2012). The effect of resolvins on dermal wound healing. *MS thesis, Rutgers Univ.*

Mills, C. D. (2015). Anatomy of a discovery: m1 and m2 macrophages. *Front Immunol, 6*, 212. doi:10.3389/fimmu.2015.00212

Mills, C. D., Kincaid, K., Alt, J. M., Heilman, M. J., & Hill, A. M. (2000). M-1/M-2 macrophages and the Th1/Th2 paradigm. *J Immunol, 164*(12), 6166-6173. doi:10.4049/jimmunol.164.12.6166

Moestrup, S. K., & Moller, H. J. (2004). CD163: a regulated hemoglobin scavenger receptor with a role in the anti-inflammatory response. *Ann Med, 36*(5), 347-354. doi:10.1080/07853890410033171

Moignard, V., Macaulay, I. C., Swiers, G., Buettner, F., Schutte, J., Calero-Nieto, F. J., . . . Gottgens, B. (2013). Characterization of transcriptional networks in blood stem and progenitor cells using high-throughput single-cell gene expression analysis. *Nat Cell Biol, 15*(4), 363-372. doi:10.1038/ncb2709

Moignard, V., Woodhouse, S., Fisher, J., & Gottgens, B. (2013). Transcriptional hierarchies regulating early blood cell development. *Blood Cells Mol Dis, 51*(4), 239-247. doi:10.1016/j.bcmd.2013.07.007

Montironi, R., Lopez-Beltran, A., & Cheng, L. (2008). Editorial comment on: Prediction of progression of non-muscle-invasive bladder cancer by WHO 1973 and 2004 grading and by FGFR3 mutation status: a prospective study. *Eur Urol, 54*(4), 843-844. doi:10.1016/j.eururo.2007.12.027

Morgenthal, K., Weckwerth, W., & Steuer, R. (2006). Metabolomic networks in plants: Transitions from pattern recognition to biological interpretation. *Biosystems, 83*(2-3), 108-117. doi:10.1016/j.biosystems.2005.05.017

Mosmann, T. R., & Coffman, R. L. (1989). TH1 and TH2 cells: different patterns of lymphokine secretion lead to different functional properties. *Annu Rev Immunol, 7*, 145-173. doi:10.1146/annurev.iy.07.040189.001045

Mounier, R., Theret, M., Arnold, L., Cuvellier, S., Bultot, L., Goransson, O., . . . Chazaud, B. (2013). AMPKalpha1 regulates macrophage skewing at the time of resolution of inflammation during skeletal muscle regeneration. *Cell Metab, 18*(2), 251-264. doi:10.1016/j.cmet.2013.06.017

Murphy, M. M., Lawson, J. A., Mathew, S. J., Hutcheson, D. A., & Kardon, G. (2011). Satellite cells, connective tissue fibroblasts and their interactions are crucial for muscle regeneration. *Development, 138*(17), 3625-3637. doi:10.1242/dev.064162

Nathan, C. (2002). Points of control in inflammation. *Nature, 420*(6917), 846-852. doi:10.1038/nature01320

Nathan C, D. A. (2010). Nonresolving inflammation. *Cell, 140*, 871-882.

Neuschwander-Tetri, B. A. (2010). Hepatic lipotoxicity and the pathogenesis of nonalcoholic steatohepatitis: the central role of nontriglyceride fatty acid metabolites. *Hepatology, 52*, 774-788.

O'Shea, J. J., Schwartz, D. M., Villarino, A. V., Gadina, M., McInnes, I. B., & Laurence, A. (2015). The JAK-STAT pathway: impact on human disease and therapeutic intervention. *Annu Rev Med, 66*, 311-328. doi:10.1146/annurev-med-051113-024537

Ohira, T., Arita, M., Omori, K., Recchiuti, A., Van Dyke, T. E., & Serhan, C. N. (2010). Resolvin E1 receptor activation signals phosphorylation and phagocytosis. *J Biol Chem, 285*(5), 3451-3461. doi:10.1074/jbc.M109.044131

Ozsolak, F., & Milos, P. M. (2011). RNA sequencing: advances, challenges and opportunities. *Nat Rev Genet, 12*(2), 87-98. doi:10.1038/nrg2934

Pasparakis, M., Luedde, T., & Schmidt-Supprian, M. (2006). Dissection of the NF-kappaB signalling cascade in transgenic and knockout mice. *Cell Death Differ, 13*(5), 861-872. doi:10.1038/sj.cdd.4401870

Patsalos, A., Pap, A., Varga, T., Trencsenyi, G., Contreras, G. A., Garai, I., . . . Nagy, L. (2017). In situ macrophage phenotypic transition is affected

by altered cellular composition prior to acute sterile muscle injury. *J Physiol, 595*(17), 5815-5842. doi:10.1113/JP274361

Patti, G. J., Yanes, O., & Siuzdak, G. (2012). Innovation: Metabolomics: the apogee of the omics trilogy. *Nat Rev Mol Cell Biol, 13*(4), 263-269. doi:10.1038/nrm3314

Pearson, G., Robinson, F., Beers Gibson, T., Xu, B. E., Karandikar, M., Berman, K., & Cobb, M. H. (2001). Mitogen-activated protein (MAP) kinase pathways: regulation and physiological functions. *Endocr Rev, 22*(2), 153-183. doi:10.1210/edrv.22.2.0428

Pinot, M. e. a. (2014). Polyunsaturated phospholipids facilitate membrane deformation and fission by endocytic proteins. *Science, 345*, 693-697.

Raberg, L., Sim, D., & Read, A. F. (2007). Disentangling genetic variation for resistance and tolerance to infectious diseases in animals. *Science, 318*(5851), 812-814. doi:10.1126/science.1148526

Raingeaud, J., Whitmarsh, A. J., Barrett, T., Derijard, B., & Davis, R. J. (1996). MKK3- and MKK6-regulated gene expression is mediated by the p38 mitogen-activated protein kinase signal transduction pathway. *Mol Cell Biol, 16*(3), 1247-1255. doi:10.1128/mcb.16.3.1247

Rubartelli, A., & Lotze, M. T. (2007). Inside, outside, upside down: damage-associated molecular-pattern molecules (DAMPs) and redox. *Trends Immunol, 28*(10), 429-436. doi:10.1016/j.it.2007.08.004

Sager, H. B., Kessler, T., & Schunkert, H. (2017). Monocytes and macrophages in cardiac injury and repair. *J Thorac Dis, 9*(Suppl 1), S30-S35. doi:10.21037/jtd.2016.11.17

Sakaguchi, S., Miyara, M., Costantino, C. M., & Hafler, D. A. (2010). FOXP3+ regulatory T cells in the human immune system. *Nat Rev Immunol, 10*(7), 490-500. doi:10.1038/nri2785

Sambasivan, R., Yao, R., Kissenpfennig, A., Van Wittenberghe, L., Paldi, A., Gayraud-Morel, B., . . . Galy, A. (2011). Pax7-expressing satellite cells are indispensable for adult skeletal muscle regeneration. *Development, 138*(17), 3647-3656. doi:10.1242/dev.067587

Schmitz, S. U., Grote, P., & Herrmann, B. G. (2016). Mechanisms of long noncoding RNA function in development and disease. *Cell Mol Life Sci, 73*(13), 2491-2509. doi:10.1007/s00018-016-2174-5

Selvaraj, S., Krishnaswamy, S., Devashya, V., Sethuraman, S., & Krishnan, U. M. (2015). Influence of membrane lipid composition on flavonoid-

membrane interactions: implications on their biological activity. *Prog. Lipid Res., 58*, 1-13.

Serhan, C. N. (2014). Pro-resolving lipid mediators are leads for resolution physiology. *Nature, 510*(7503), 92-101. doi:10.1038/nature13479

Serhan, C. N., & Savill, J. (2005). Resolution of inflammation: the beginning programs the end. *Nat Immunol, 6*(12), 1191-1197. doi:10.1038/ni1276

Shaer, A. J., & Gadegbeku, C. A. (2001). Tsukamurella peritonitis associated with continuous ambulatory peritoneal dialysis. *Clin Nephrol, 56*(3), 241-246.

Shannon, P., Markiel, A., Ozier, O., Baliga, N. S., Wang, J. T., Ramage, D., . . . Ideker, T. (2003). Cytoscape: a software environment for integrated models of biomolecular interaction networks. *Genome Res, 13*(11), 2498-2504. doi:10.1101/gr.1239303

Soki, F. N., Koh, A. J., Jones, J. D., Kim, Y. W., Dai, J., Keller, E. T., . . . McCauley, L. K. (2014). Polarization of prostate cancer-associated macrophages is induced by milk fat globule-EGF factor 8 (MFG-E8)-mediated efferocytosis. *J Biol Chem, 289*(35), 24560-24572. doi:10.1074/jbc.M114.571620

Solon-Biet, S. M., McMahon, A. C., Ballard, J. W., Ruohonen, K., Wu, L. E., Cogger, V. C., . . . Simpson, S. J. (2014). The ratio of macronutrients, not caloric intake, dictates cardiometabolic health, aging, and longevity in ad libitum-fed mice. *Cell Metab, 19*(3), 418-430. doi:10.1016/j.cmet.2014.02.009

Sorci, G., & Faivre, B. (2009). Inflammation and oxidative stress in vertebrate host-parasite systems. *Philos Trans R Soc Lond B Biol Sci, 364*(1513), 71-83. doi:10.1098/rstb.2008.0151

Spite, M., Claria, J., & Serhan, C. N. (2014). Resolvins, specialized proresolving lipid mediators, and their potential roles in metabolic diseases. *Cell Metab, 19*(1), 21-36. doi:10.1016/j.cmet.2013.10.006

Spite, M., Norling, L. V., Summers, L., Yang, R., Cooper, D., Petasis, N. A., . . . Serhan, C. N. (2009). Resolvin D2 is a potent regulator of leukocytes and controls microbial sepsis. *Nature, 461*(7268), 1287-1291. doi:10.1038/nature08541

Stables, M. J., Shah, S., Camon, E. B., Lovering, R. C., Newson, J., Bystrom, J., . . . Gilroy, D. W. (2011). Transcriptomic analyses of murine resolution-phase macrophages. *Blood, 118*(26), e192-208. doi:10.1182/blood-2011-04-345330

Stark, R., and G. Brown. 2011. DiffBind: differential binding analysis of ChIPSeq peak data. Bioconductor. Available at: http://bioconductor.org/packages/release/bioc/vignettes/DiffBind/inst/doc/DiffBind.pdf

Steuer, R. (2006). Review: on the analysis and interpretation of correlations in metabolomic data. *Brief Bioinform, 7*(2), 151-158. doi:10.1093/bib/bbl009

Tabas, I., & Glass, C. K. (2013). Anti-inflammatory therapy in chronic disease: challenges and opportunities. *Science, 339*(6116), 166-172. doi:10.1126/science.1230720

Takeuchi O, A. S. (2010). Pattern Recognition Receptors and Inflammation. *Cell, 140*, 805-820.

Tang, L. (2019). Bisulfite-free epigenetic sequencing. *Nat Methods, 16*(4), 286. doi:10.1038/s41592-019-0387-x

Teixeira, C. F., Landucci, E. C., Antunes, E., Chacur, M., & Cury, Y. (2003). Inflammatory effects of snake venom myotoxic phospholipases A2. *Toxicon, 42*, 947-962.

Thorvaldsdottir, H., Robinson, J. T., & Mesirov, J. P. (2013). Integrative Genomics Viewer (IGV): high-performance genomics data visualization and exploration. Brief Bioinform, 14(2), 178-192. doi:10.1093/bib/bbs017

Thul, S., Labat, C., Temmar, M., Benetos, A., & Back, M. (2017). Low salivary resolvin D1 to leukotriene B4 ratio predicts carotid intima media thickness: A novel biomarker of non-resolving vascular inflammation. *Eur J Prev Cardiol, 24*(9), 903-906. doi:10.1177/2047487317694464

Tidbal, J. G. (2017). Regulation of muscle growth and regeneration by the immune system. *Nature Reviews Immunology, 17*, 165-178.

Tidbal, J. G., & Wehling-Henricks, M. (2007). Macrophages promote muscle membrane repair and muscle fibre frowth and regeneration during modified muscle loading in mice in vivo. *J. Physiol., 578*, 327-336.

Tidball. (2017). Regulation of muscle growth and regeneration by the immune system. *NATURE REVIEWS IMMUNOLOGY, 17*.

Unger, R., & Scherer, P. E. (2010). Gluttony, sloth and the metabolic syndrome: a roadmap to lipotoxicity. *Trend Endocrinol. Metab., 21*, 345-352.

Varga, T., Mounier, R., Horvath, A., Cuvellier, S., Dumont, F., Poliska, S., . . . Chazaud, B. (2016). Highly Dynamic Transcriptional Signature of Distinct Macrophage Subsets during Sterile Inflammation, Resolution, and Tissue Repair. *J Immunol, 196*(11), 4771-4782. doi:10.4049/jimmunol.1502490

Varga, T., Mounier, R., Patsalos, A., Gogolak, P., Peloquin, M., Horvath, A., . . . Nagy, L. (2016). Macrophage PPARgamma, a Lipid Activated Transcription Factor Controls the Growth Factor GDF3 and Skeletal Muscle Regeneration. *Immunity, 45*(5), 1038-1051. doi:10.1016/j.immuni.2016.10.016

Villalta, S. A., Rosenthal, W., Martinez, L., Kaur, A., Sparwasser, T., Tidball, J. G., . . . Bluestone, J. A. (2014). Regulatory T cells suppress muscle inflammation and injury in muscular dystrophy. *Sci Transl Med, 6*(258), 258ra142. doi:10.1126/scitranslmed.3009925

Walker, J., Dichter, E., Lacorte, G., Kerner, D., Spur, B., Rodriguez, A., & Yin, K. (2011). Lipoxin a4 increases survival by decreasing systemic inflammation and bacterial load in sepsis. *Shock, 36*(4), 410-416. doi:10.1097/SHK.0b013e31822798c1

Walker, J. G., & Smith, M. D. (2005). The Jak-STAT pathway in rheumatoid arthritis. *J Rheumatol, 32*(9), 1650-1653.

Wang, H., Melton, D. W., Porter, L., Sarwar, Z. U., McManus, L. M., & Shireman, P. K. (2014). Altered macrophage phenotype transition impairs skeletal muscle regeneration. *Am J Pathol, 184*(4), 1167-1184. doi:10.1016/j.ajpath.2013.12.020

Wang, M., & Han, X. (2014). Multidimensional mass spectrometry-based shotgun lipidomics. *Methods Mol Biol, 1198*, 203-220. doi:10.1007/978-1-4939-1258-2_13

Wang, M., Huang, Y., & Han, X. (2014). Accurate mass searching of individual lipid species candidates from high-resolution mass spectra for shotgun lipidomics. *Rapid Commun Mass Spectrom, 28*(20), 2201-2210. doi:10.1002/rcm.7015

Wang, M., Wang, C., Han, R. H., & Han, X. (2016). Novel advances in shotgum lipidomics for biology and medicine. *Progr. Lipid. Res., 61*, 83-108.

Wang, Z., Gerstein, M., & Snyder, M. (2009). RNA-Seq: a revolutionary tool for transcriptomics. *Nat Rev Genet, 10*(1), 57-63. doi:10.1038/nrg2484

Warren, G. L., Hulderman, T., Jensen, N., McKinstry, M., Mishra, M., Luster, M. I., & Simeonova, P. P. (2002). Physiological role of tumor necrosis

factor alpha in traumatic muscle injury. *FASEB J, 16*(12), 1630-1632. doi:10.1096/fj.02-0187fje

Xia, J., Sinelnikov, I. V., Han, B., & Wishart, D. S. (2015). MetaboAnalyst 3.0--making metabolomics more meaningful. *Nucleic Acids Res, 43*(W1), W251-257. doi:10.1093/nar/gkv380

Yang, K., Cheng, H., Gross, R. W., & Han, X. (2009). Automated lipid identification and quantification by multidimensional mass spectrometry-based shotgun lipidomics. *Anal Chem, 81*(11), 4356-4368. doi:10.1021/ac900241u

Yao, B., Christian, K. M., He, C., Jin, P., Ming, G. L., & Song, H. (2016). Epigenetic mechanisms in neurogenesis. *Nat Rev Neurosci, 17*(9), 537-549. doi:10.1038/nrn.2016.70

Zerbino, D. R., Achuthan, P., Akanni, W., Amode, M. R., Barrell, D., Bhai, J., . . . Flicek, P. (2018). Ensembl 2018. *Nucleic Acids Res, 46*(D1), D754-D761. doi:10.1093/nar/gkx1098

Zhang, M. J., Sansbury, B. E., Hellmann, J., Baker, J. F., Guo, L., Parmer, C. M., . . . Spite, M. (2016). Resolvin D2 Enhances Postischemic Revascularization While Resolving Inflammation. *Circulation, 134*(9), 666-680. doi:10.1161/CIRCULATIONAHA.116.021894

Zhang, Y., Liu, T., Meyer, C. A., Eeckhoute, J., Johnson, D. S., Bernstein, B. E., . . . Liu, X. S. (2008). Model-based analysis of ChIP-Seq (MACS). Genome Biol, 9(9), R137. doi:10.1186/gb-2008-9-9-r137

Zhou, Y., Hong, Y., & Huang, H. (2016). Triptolide Attenuates Inflammatory Response in Membranous Glomerulo-Nephritis Rat via Downregulation of NF-kappaB Signaling Pathway. *Kidney Blood Press Res, 41*(6), 901-910. doi:10.1159/000452591

Zuliani, J. P., Fernandes, C. M., Zamuner, S. R., Gutierrez, J. M., & Teixeira, C. F. (2005). Inflammatory events induced by Lys-49 and Asp-49 phospholipases A2 isolated from Bothrops asper snake venom: role of catalytix activity. *Toxicon, 45*, 335-346.

11) List of publications related to the dissertation

UNIVERSITY AND NATIONAL LIBRARY
UNIVERSITY OF DEBRECEN
H-4002 Egyetem tér 1, Debrecen
Phone: +3652/410-443, email: publikaciok@lib.unideb.hu

Registry number: DEENK/145/2020.PL
Subject: PhD Publikációs Lista

Candidate: Nikolas Giannakis
Neptun ID: YXG51K
Doctoral School: Doctoral School of Molecular Cellular and Immune Biology

List of publications related to the dissertation

1. Giannakis, N., Sansbury, B. E., Patsalos, A., Hays, T. T., Riley, C. O., Han, X., Spite, M., Nagy, L.: Dynamic changes to lipid mediators support transitions among macrophage subtypes during muscle regeneration.
   Nat. Immunol. 20 (5), 626-636, 2019.
   DOI: http://dx.doi.org/10.1038/s41590-019-0356-7
   IF: 23.53 (2018)
2. Patsalos, A., Tzerpos, P., Halász, L., Nagy, G., Pap, A., Giannakis, N., Lyroni, K., Koliaraki, V., Pintye, É., Dezső, B., Kollias, G., Spilianakis, C. G., Nagy, L.: The BACH1-HMOX1 Regulatory Axis Is Indispensable for Proper Macrophage Subtype Specification and Skeletal Muscle Regeneration.
   J. Immunol. 203 (6), 1532-1547, 2019.
   DOI: http://dx.doi.org/10.4049/jimmunol.1900553
   IF: 4.718 (2018)

DEBRECENI EGYETEM Egyetemi és Nemzeti Könyvtár

12) List of other publications

UNIVERSITY AND NATIONAL LIBRARY
UNIVERSITY OF DEBRECEN
H-4002 Egyetem tér 1, Debrecen
Phone: +3652/410-443, email: publikaciok@lib.unideb.hu

List of other publications

3. Horváth, A., Dániel, B., Széles, L., Cuaranta-Monroy, I., Czimmerer, Z., Ozgyin, L., Steiner, L., Kiss, M., Simándi, Z., Póliska, S., Giannakis, N., Raineri, E., Gut, I. G., Nagy, B., Nagy, L.: Labelled regulatory elements are pervasive features of the macrophage genome and are dynamically utilized by classical and alternative polarization signals.
Nucleic Acids Res. 47 (6), 2778-2792, 2019.
DOI: http://dx.doi.org/10.1093/nar/gkz118
IF: 11.147 (2018)

4. Czimmerer, Z., Horváth, A., Dániel, B., Nagy, G., Cuaranta-Monroy, I., Kiss, M., Kolostyák, Z., Póliska, S., Steiner, L., Giannakis, N., Varga, T., Nagy, L.: Dynamic transcriptional control of macrophage miRNA signature via inflammation responsive enhancers revealed using a combination of next generation sequencing-based approaches.
Biochim. Biophys. Acta. Gene Regul. Mech. 1861 (1), 14-28, 2018.
DOI: http://dx.doi.org/10.1016/j.bbagrm.2017.11.003
IF: 4.599

Total IF of journals (all publications): 43,994
Total IF of journals (publications related to the dissertation): 28,248

The Candidate's publication data submitted to the iDEa Tudóstér have been validated by DEENK on the basis of the Journal Citation Report (Impact Factor) database.

13 May, 2020